# DEVELOPMENT OF UNFIRED BRICK THROUGH ALKALI ACTIVATION USING WASTE FROM AGGREGATE RECYCLING FACILITY AS AN ALTERNATIVE TO CONVENTIONAL FIRED CLAY BRICK

**ALI ABDULHUSSEIN FADHIL SHUBBAR**

**A thesis submitted in partial fulfilment**

**of the requirements of Liverpool John Moores University**

**for the degree of Doctor of Philosophy**

**July 2020**

# DECLARATION

The research reported in this thesis was conducted at Liverpool John Moores University, Department of Civil Engineering, between December 2017 and July 2020. I declare that the work is my own and has not been submitted for a degree at another university.

Ali Abdulhussein Fadhil Shubbar

Liverpool John Moores University

July 2020

# ABSTRACT

Bricks have been playing a significant role in building and construction for thousands of years for their outstanding properties such as good durability, strength and low costs. In the UK, fired clay bricks are one of the main elements needed to fuel the construction industry in the country with annual production of more than 2 billion bricks. However, the production of fired clay bricks is energy intensive and considered one of the main producers of carbon dioxide ($CO_2$). Therefore, searching for alternative techniques in the production of bricks is becoming essential in order to develop environmentally friendly bricks to replace fired clay bricks and reduce their negative environmental impact. One of the alternative techniques in the production of bricks is the alkali activation technique (geopolymerisation) that depends on the poly-condensation of the raw materials normally containing silica and alumina in the presence of an alkali solution to produce amorphous to semi-crystalline geopolymer. This technique is very attractive relative to firing of brick as the final products can provide structural strength in a very short time, they are sufficiently durable and $CO_2$ emissions are reduced significantly. This research reports the development of a Novel Alkali-Activated Unfired Brick (NAAUB) using clay filter cake (CFC) waste produced during the washing of recycled construction and demolition materials. Comparisons of strength (compressive strength), durability (water absorption and freeze and thaw cycle effect), thermal properties (thermal conductivity) and $CO_2$ emissions during the manufacturing and operational processes of the NAAUB and the conventional fired clay brick have been carried out. The results indicated that the NAAUB showed comparable compressive strength (25.8 MPa) relative to conventional fired brick (25.7 MPa) after 7 days of water curing. Regarding the limited durability properties studied of the NAAUB, the results indicated that the water absorption rate of the NAAUB was very low and was significantly lower than that of the conventional fired brick. Additionally, the results of the freezing and thawing cycles showed that the NAAUB has no physical damage after 180 cycles of freezing and thawing and it can be classified as a frost resistant brick. Furthermore, the results of thermal properties of the NAAUB indicated good thermal behaviour that will help in increasing indoor comfort and reducing the overall consumption of energy required for heating/cooling of any structure that is using this brick relative to conventional fired bricks. The results of the $CO_2$ emissions indicated that replacing the conventional fired brick with the NAAUB could reduce the $CO_2$ emissions by about 51.4% and 5.65% during the manufacturing process and operational process, respectively. The comparison between the cost of the NAAUB and conventional fired brick indicated that the NAAUB is cheaper than the conventional fired brick by about 5%. The overall results indicated that the NAAUB is a successful alternative to conventional fired bricks in different applications with the benefits of decreasing the $CO_2$ emissions and decreasing the overall cost of bricks. .

# ACKNOWLEDGEMENTS

This research could not have been completed without the support, guidance and help of many people. I can safely say that I would not have been successful without their precious support. First of all, I would like to thank the Faculty of Engineering and Technology, Liverpool John Moores University for funding this project. In addition, I would like to express my sincere gratitude and appreciation to the following persons; if any have been forgotten, please accept my sincerest of apologies:

- I owe my deepest gratitude to my Director of Studies, Dr. Monower Sadique, for his excellent supervision, guidance and encouragement throughout this study without which this project would never have been completed.

- I would like to express my sincere thanks to my second supervisor, Dr. Patryk Kot, and my third supervisor, Dr. William Atherton, for their expert advice and support.

- A big thank you goes to CCC Waste Management, Kirkby, UK, Hanson Heidelberg Cement group, Scunthorpe, UK and Cenin Ltd, Bridgend, UK, for the supply of materials, free of charge, during the course of the research. Their support is kindly acknowledged.

- I also would like to acknowledge the assistance and friendship of all current and past lecturers, researchers, technicians and administrative staff in the Department of Civil Engineering, Faculty of Engineering and Technology, Liverpool John Moores University, especially those involved with this research. Their enthusiasm and encouragement have made my research enjoyable and memorable. The author appreciates the efforts of Dr. Nicola Dempster, Mrs. Elizabeth Hoare, Miss Alexia Montaubin, Mr Mal Feegan, Mr. Alan Jones, Mr. Chris Byrne, Mr. Paul Gibbons and Mr. David Williams, for their assistance.

- The author has had numerous productive discussions and many enjoyable times with past and present fellow students in the Research Hub. The author would like to thank them for their kindness and friendship: Alaa Abbas, Layth Kraidi, Hayder Shanbara, Ali Al-Attabi, Muhammad Abdulredha, Salah Zubaidi and Hayder Al-Hawesah.

- The author would like to express his extreme gratitude to his Father and Mother for their unending support, unstinting sacrifice and great love throughout the research duration.

- Last but not least, I am particularly grateful to my wife Mrs. Shahad Al-Mamoori and my son Yousif and my sister Raghad, for providing tremendous and continuous support and encouragement and for their unconditional patience throughout the research period.

# DEDICATION

This thesis is dedicated specially to:

Allah, the most Gracious and the most Merciful.

Prophet Mohammed and his household.

My Father and Mother, the most precious persons in my life. You have sacrificed so much for us and I hope that this work will be of benefit for humanity; the reward will be for you. I hope you are proud of me.

My lovely wife Mrs. Shahad Al-Mamoori, my son Yousif and my sister Raghad.

# TABLE OF CONTENTS

DECLARATION ..... i
ABSTRACT ..... ii
ACKNOWLEDGEMENTS ..... iii
DEDICATION ..... v
TABLE OF CONTENTS ..... vi
LIST OF TABLES ..... x
LIST OF FIGURES ..... xi
LIST OF ACRONYMS AND ABBREVIATIONS ..... xiii
CHAPTER 1 ..... 1
INTRODUCTION ..... 1
**1.1 Problem Statement** ..... 1
**1.2 State of the art** ..... 4
**1.3 Aim of the research** ..... 10
**1.4 Objectives** ..... 10
**1.5 Novelty Statement** ..... 10
**1.6 Overview of the Thesis** ..... 11
CHAPTER 2 ..... 13
LITERATURE REVIEW ..... 13
**2.1. Introduction** ..... 13
**2.2 Alternative techniques for brick production** ..... 14
***2.2.1 Production of unfired building materials through solidification*** ..... 15
***2.2.1.1 Critical evaluation of using the technique of solidification in the production of unfired building materials*** ..... 22
***2.2.2. Production of unfired building materials through alkali activation (Geopolymerisation)*** ..... 24
***2.2.2.1 Critical evaluation of using the technique of alkali activation (Geopolymerisation) in the production of unfired building materials*** ..... 35
**2.3. *Comparative assessment of the techniques used in the production of unfired building materials*** ..... 40
***2.3.1 Technical Assessment*** ..... 40
***2.3.2 Environmental assessment*** ..... 41
**2.4 Summary** ..... 43
CHAPTER 3 ..... 44

RESEARCH METHODOLOGY AND MATERIALS ..... 44
**3.1 Research Methodology** ..... 44
**3.2 Materials** ..... 44
***3.2.1 Clay Filter Cake (CFC) Waste*** ..... 44
***3.2.2 Potential Candidate Materials*** ..... 45
***3.2.3 Alkali Activators*** ..... 46
***3.2.4. Sand*** ..... 46
***3.2.5 Water*** ..... 46
**3.3 Programme of Laboratory works and Testing Equipment** ..... 46
***3.3.1 Moisture content (%)*** ..... 48
***3.3.2 Loss on Ignition (LoI)*** ..... 48
***3.3.3 pH Measurements*** ..... 48
***3.3.4 Specific surface area (SSA)*** ..... 49
***3.3.5 Particle size distribution (PSD)*** ..... 50
***3.3.6 Particle Density (Specific Gravity, Gs)*** ..... 51
***3.3.7 Compressive strength*** ..... 52
***3.3.8 Flexural strength*** ..... 53
***3.3.9 Water absorption*** ..... 54
***3.3.10 Freeze and thaw*** ..... 54
***3.3.11 Thermal Properties*** ..... 55
***3.3.12 Energy Dispersive X-Ray Fluorescence (EDXRF) spectrometer*** ..... 56
***3.3.13 Microstructural analysis*** ..... 57
**3.4 Sample preparation for different tests** ..... 57
***3.4.1 Compressive Strength and flexural strength of the unfired brick with dimensions of (160 x 40 x 40 mm)*** ..... 57
***3.4.2 Compressive strength, water absorption, freeze and thaw, thermal of the NAAUB with dimensions of (215 x 102.5 x 65 mm)*** ..... 58
***3.4.3 Microstructural analysis (SEM/EDS)*** ..... 59
**3.5 $CO_2$ calculations of the NAAUB during the manufacturing and operational processes** ..... 61
**3.6 Summary** ..... 62
CHAPTER 4 ..... 64
RESULTS AND DISCUSSION ..... 64
**4.1 Introduction** ..... 64
**4.2 Section (1): Materials Characterization** ..... 64

*4.2.1 Introduction* ..... 64
*4.2.2 Properties of the clay filter cake (CFC)* ..... 64
*4.2.3 Comparison between the chemical and physical properties of the candidate materials* ..... 67
*4.2.4 Summary of section (1)* ..... 71
**4.3 Section 2: Candidate Mix Design** ..... 72
*4.3.1 Introduction* ..... 72
*4.3.2 Selection of binder materials* ..... 73
*4.3.3 Selected Candidate Binder Material* ..... 76
*4.3.4 Effect of sand to binder ratio on strength development of alkali activated brick* 78
*4.3.5 Effect of liquid to binder ratio on the compressive strength of alkali activated brick* ..... 80
CHAPTER 1 ..... 82
*4.3.6 Effect of $Na_2SiO_3$/NaOH ratio on the compressive strength of alkali activated brick* ..... 83
*4.3.7 Effect of NaOH concentration on the compressive strength of alkali activated brick* ..... 84
*4.3.8 Summary of section (2)* ..... 86
**4.4. Section 3: Effect of different curing methods on the mechanical performance of the NAAUB** ..... 87
*4.4.1 Introduction* ..... 87
*4.4.2 Effect of different water curing temperatures* ..... 88
*4.4.3 Effect of different methods of curing on long term strength of the NAAUB.* ..... 89
*4.4.4 Summary of section (3)* ..... 93
**4.5 Section 4: Physical, Chemical and Microstructural properties of the NAAUB** ..... 94
*4.5.1 Introduction* ..... 94
*4.5.2 Physical and chemical Properties* ..... 94
*4.5.3 Microstructural properties* ..... 96
**4.5.3.1 SEM analysis of the NAAUB paste under different curing methods** ..... 96
**4.5.3.2 SEM/EDS analysis of the NAAUB paste under different curing methods** ..... 104
*4.5.4 Summary of section (4)* ..... 107
**4.6 Section 5: Comparative Performance of the NAAUB against standards specifications** ..... 109
*4.6.1 Introduction* ..... 109
*4.6.2 Compressive strength* ..... 109

*4.6.3 Dry Density* ..... 111
*4.6.4 Durability* ..... 112
**4.6.4.1 Water absorption** ..... 112
**4.6.4.2 Freezing and thawing** ..... 113
*4.6.5 Thermal Properties* ..... 115
*4.6.7 Summary of section (5)* ..... 120
**4.7 Section 6: A comparison between $CO_2$ emission of the NAAUB and conventional fired brick.** ..... 121
*4.7.1 Introduction* ..... 121
*4.7.2 $CO_2$ emission during the manufacturing process* ..... 121
*4.7.3 $CO_2$ emissions during the operational process* ..... 124
*4.7.4 Summary of section (6)* ..... 128
**4.8 Section 7: A comparison between the cost of NAAUB and conventional fired brick.** ..... 129
*4.8.1 Introduction* ..... 129
*4.8.2 Breakdown of the costs associated with production of NAAUB.* ..... 129
**4.9 Summary of the chapter** ..... 132
CHAPTER 5 ..... 135
CONCLUSIONS AND RECOMMENDATIONS ..... 135
**5.1 Conclusions** ..... 135
**5.2 Research Limitations** ..... 138
**5.3 Recommendations for future work** ..... 138
**REFERENCES** ..... 140
APPENDIX A: PATENT APPLICATION ..... 150

# LIST OF TABLES

Table 1-1. A summary of the current state of the art regarding the use of CFC in the construction industry .....7
Table 2-1. Studies on production of unfired building materials through solidification .....16
Table 2-2. Studies on production of unfired clay-based building materials through alkali activation (geopolymerisation) .....26
Table 2-3. Principal chemical composition of clays used in previous studies listed in Table 2-2 .....36
Table 3-1. Description and sources of the identified candidate materials .....45
Table 3-2. CFC and candidate materials identification tests. .....62
Table 3-3. Test method used for analysis of samples. .....63
Table 4-1. The chemical properties and EDXRF analysis of the CFC .....65
Table 4-2. The Physical properties of the CFC. .....66
Table 4-3. Comparative chemical properties of candidate materials. .....68
Table 4-4. The Physical properties of the candidate materials. .....69
Table 4-5. Mixing proportions of different candidate materials. .....74
Table 4-6. Mixing proportion of the binder materials. .....77
Table 4-7. Mixing proportions of various S/B ratios .....79
Table 4-8. Mixing proportions of various L/B ratios .....81
Table 4-9. Mixing proportions of various $Na_2SiO_3$/NaOH ratios .....83
Table 4-10. Mixing proportions of various NaOH concentrations. .....85
Table 4-11. Selected candidate synthesis parameters of the NAAUB. .....86
Table 4-12. The Physical properties of the NAAUB. .....94
Table 4-13. The chemical properties and EDXRF analysis of the NAAUB. .....96
Table 4-14. Element analysis of NAAUB paste by EDS under air curing (NAAUB-A) .....104
Table 4-15. Element analysis of NAAUB paste by EDS under water curing (NAAUB-W) 105
Table 4-16. Element analysis of NAAUB paste by EDS under water curing temperature (NAAUB-H50) .....106
Table 4-17. Dry density of the NAAUB and conventional fired brick .....111
Table 4-18 Assessment of physical damage of the NAAUB and conventional fired brick at the end of the 180th freezing and thawing cycle .....115
Table 4-19. Mechanical, durability and thermal properties of the NAAUB against conventional fired brick .....119
Table 4-20. Quantification for $CO_2$ emission for the NAAUB and conventional fired brick. .....123
Table 4-21. The geometric features and design parameters of the office building .....126
Table 4-22. Characteristics of the conventional fired brick and the NAAUB used for the simulation .....127
Table 4-23. Breakdown of production costs of NAAUB and conventional fired bricks. .....131
Table 4-24. Summary of Chapter 4 .....133

# LIST OF FIGURES

Figure 1-1. The annual production of bricks in the UK from 2013 to 2018 (Statista, 2019) 2
Figure 1-2. The breakdown of $CO_2$ emissions of brick production by process (Carbon Trust, 2012) 3
Figure 1-3. Clay filter cake waste produced during washing of recycled C&D wastes. 5
Figure 3-1. Particle size distribution of the sand 46
Figure 3-2. LoI test for CFC and other candidate materials 48
Figure 3-3. pH measurement test apparatus 49
Figure 3-4. Blaine air-permeability apparatus 50
Figure 3-5. Laser Diffraction Particles Analyser 51
Figure 3-6. Multi-pycnometer used for density measurement of powders. 52
Figure 3-7. Control Automax 5 compressive strength machine 53
Figure 3-8. Flexural strength testing of prism mortar. 54
Figure 3-9. Temperature Chamber TC-ME-025/065/100 for freeze and thaw testing 55
Figure 3-10. ISOMET 2114 meter 56
Figure 3-11. EDXRF spectrometer 56
Figure 3-12. The mortar specimens with the dimensions of (160 x 40 x 40 mm) 58
Figure 3-13. Preparation of the brick sample with dimensions of (215 x 102.5 x 65 mm) 59
Figure 3-14. The aluminium stub 60
Figure 3-15. The gold coating of the samples. 60
Figure 3-16. Placing the samples inside the SEM/EDS machine and starting the test 61
Figure 4-1. Particle size distribution of the CFC 66
Figure 4-2. The SEM image of the CFC (dry powder) 67
Figure 4-3. Comparative PSD of the candidate materials 69
Figure 4-4. SEM imaging of the candidate materials (dry powder) 70
Figure 4-5. Development of compressive strength of different blends 75
Figure 4-6. Compressive strength development of different alkali activated blends in different curing conditions 77
Figure 4-7. Compressive strength of FCW50 bricks with different S/B ratio in different curing conditions 79
Figure 4-8. Compressive strength of alkali activated bricks with different L/B ratio in different curing conditions 82
Figure 4-9. Compressive strength of alkali activated bricks with different $Na_2SiO_3$/NaOH ratio in different curing conditions 84
Figure 4-10. Effect of NaOH concentration upon the compressive strength of the alkali activated brick. 85
Figure 4-11. Effect different water curing temperatures on compressive strength development of the NAAUB. 88
Figure 4-12. Effect of curing method on compressive strength development of the NAAUB. 90
Figure 4-13. Effect of curing method on flexural strength development of the NAAUB 91
Figure 4-14. Particle size distribution of the NAAUB 95
Figure 4-15. SEM micrographs of the NAAUB paste from 3 days to 7 days of air curing 97

Figure 4-16. SEM micrographs of the NAAUB paste from 28 days to 180 days of air curing 98
Figure 4-17. SEM micrographs of the NAAUB paste from 3 days to 7 days of water curing 99
Figure 4-18. SEM micrographs of the NAAUB paste from 28 days to 180 days of water curing 100
Figure 4-19. SEM micrographs of the NAAUB paste from 3 days to 7 days of water curing temperature 101
Figure 4-20. SEM micrographs of the NAAUB paste from 28 days to 180 days of water curing temperature 102
Figure 4-21. The NAAUB with dimensions 215mm x 102.5mm x 65mm. 109
Figure 4-22. Compressive strength of the standard size NAAUB 110
Figure 4-23. Compressive strength of conventional fired brick and NAAUB 111
Figure 4-24. Water absorption rate of conventional fired brick and NAAUB. 113
Figure 4-25. Percentage weight loss for the conventional fired brick and NAAUB. 114
Figure 4-26. Thermal conductivity against temperature of the NAAUB 116
Figure 4-27. Thermal conductivity of the conventional fired brick and NAAUB 117
Figure 4-28. Volume heat capacity against temperature of the NAAUB. 118
Figure 4-29. Specific heat capacity against temperature of the NAAUB 119
Figure 4-30. Embedded kg $CO_2$ - per tonne of conventional fired brick and NAAUB. 124
Figure 4-31. The studied office building 125
Figure 4-32. $CO_2$ emissions for conventional fired brick and NAAUB during the operational phase. 127

# LIST OF ACRONYMS AND ABBREVIATIONS

| | |
|---|---|
| ***BS*** | British Standard |
| ***CFA*** | Cenin Fly Ash |
| ***CFC*** | Clay Filter Cake |
| ***C–A–S–H*** | Calcium-Silicate-Aluminate-Hydrate |
| ***C-S-H*** | Calcium-Silicate-Hydrate |
| ***EDX*** | Energy Dispersive X-Ray Spectroscopy |
| ***EDXRF*** | Energy Dispersive X-Ray Florescence |
| ***GGBS*** | Ground Granulated Blast Furnace Slag |
| ***GHGs*** | Greenhouse Gases |
| ***LOI*** | Loss on Ignition |
| ***MK*** | Metakaolin |
| ***OPC*** | Ordinary Portland Cement |
| ***PFA*** | Pulverised Fuel Ash |
| ***PSD*** | Particle Size Distribution |
| ***RHA*** | Rice Husk Ash |
| ***SCMs*** | Supplementary Cementitious Materials |
| ***SEM*** | Scanning Electronic Microscopy |
| ***SSA*** | Specific Surface Area |
| ***UCS*** | Unconfined Compressive Strength |
| ***XRD*** | X-Ray Diffraction |
| ***XRF*** | X-Ray Florescence |
| ***%*** | Percentage |
| ***µm*** | Micrometre, Dimension unit ($10^{-6}$ Metre) |
| ***Λ*** | Thermal conductivity |
| $Al_2O_3$ | Aluminium oxide (chemical compound) |
| ***BCE*** | Before the Current Era |
| $Ca^{2+}$ | Calcium ione |
| ***CaO*** | Calcium oxide (chemical compound) |
| $CO_2$ | Carbon dioxide (chemical compound) |
| ***c*** | Specific heat capacity |
| ***Cp*** | Volumetric heat capacity |
| $d_{50}$ | The median particle size |
| $Fe_2O_3$ | Iron oxide (chemical compound) |
| ***g*** | Gram, Weight unit ($10^{-3}$ kilogram) |
| ***GJ*** | Gigajoule, Energy unit ($10^{9}$ Joules) |
| ***Gs*** | Specific gravity |
| $K_2O$ | Potassium oxide (chemical compound) |
| ***kg*** | Kilograms, Weight unit (kilograms) |
| ***kWh*** | Kilowatts per hour, electricity consumption unit. |
| ***MgO*** | Magnesium oxide (chemical compound) |
| ***min.*** | Minute, time unit |
| ***mm*** | Millimetre, Dimension unit ($10^{-3}$ metre) |
| ***MN*** | Mega newton, load unit ($10^{6}$ Newtons) |
| ***MnO*** | Manganese (II) oxide (chemical compound) |
| $Na_2O$ | Sodium oxide (chemical compound) |
| ***NaOH*** | Sodium hydroxide |

| | |
|---|---|
| $Na_2SiO_3$ | Sodium silicate |
| ***NOx*** | Nitrogen oxides |
| ***SOx*** | Oxides of sulphur |
| $P_2O_5$ | Phosphorus pentoxide (chemical compound) |
| ***pH*** | Measure of acidity or basicity of an aqueous liquid |
| ***S/B*** | Sand to binder ratio |
| ***Si/Al*** | Silica to alumina ratio |
| $SiO_2$ | Silicon dioxide (chemical compound) |
| $SO_3$ | Sulphur trioxide (chemical compound) |
| ***SPM*** | Suspended Particulate Matters |
| ***SrO*** | Strontium oxide (chemical compound) |
| $TiO_2$ | Titanium oxide (chemical compound) |
| ***Tonne*** | Weight unit (1000 kilograms) |
| ***UK*** | United Kingdom |
| ***w/b*** | Water/binder ratio |

# CHAPTER 1: INTRODUCTION

## 1.1 Problem Statement

Bricks have been playing a significant role in building and construction for thousands of years for their outstanding properties such as good durability, strength and low costs. The first brick produced by humans can be traced back to 8,000 BCE (Smith et al., 2016, Zhang, 2013). Clay bricks and blocks were hand-moulded and sun-dried at that time. Dating back to 4500 BCE, there have been some records on using fire to produce clay bricks for yielding better performance (Smith et al., 2016). Since then, the brick industry has developed and evolved enormously especially benefiting from modern machinery, such as powerful excavation equipment, mixers, tunnel kilns and so forth (Zhang et al., 2018). These significantly stimulated the capacity and quality of brick production (Zhang et al., 2018).

In 2013, the annual production of bricks was about 1,391 billion units worldwide (Zhang, 2013). This number was increased to about 1,500 billion pieces in 2015 and it is expected to further growth through the rapid development of the construction industry globally, together with an expected increase in the world population (Zhang et al., 2018, Climate and Clean Air Coalition, 2016, Department of Energy & Climate Change, 2015). In the UK, bricks are one of the main elements needed to fuel the construction industry in the country (Statista, 2019). The annual production of bricks in the UK from 2013 to 2018 is presented in Figure 1-1. It can be seen from Figure 1-1 that in 2018, the brick industry produced about 2.025 billion bricks (Statista, 2019). This was the peak since the beginning of the reporting period in 2013 and the first time figures exceeded two billion units (Statista, 2019). Conventional fired bricks account for 95% of all the bricks, while the remaining 5% is for unfired bricks (Smith et al., 2016).

Figure 1-1. The annual production of bricks in the UK from 2013 to 2018

Source: (Statista, 2019). The diagram originally presented here cannot be made freely available via LJMU Digital Collections because of 'copyright'

The production of fired clay brick has always been associated with many negative environmental impacts (Lozano-Miralles et al., 2018). For example, the firing of clay bricks emits huge quantity of toxic elements that are responsible for many serious health hazards (Skinder et al., 2014, Orion et al., 2011). Some of the toxic elements emitted during the firing process are suspended particulate matters (SPM), oxides of sulphur (SOx), nitrogen oxides (NOx) and carbon monoxides that are harmful to lungs, eyes and throat (Skinder et al., 2014, Orion et al., 2011). According to Orion et al. (2011), brick production is the second main producer of SOx and NOx after road traffic. Additionally, the production of fired clay brick is one of the main producers of carbon dioxide ($CO_2$). In 2017, the brick manufacturing in the UK emitted about 312,000 tonnes of $CO_2$ into the atmosphere (Turtle et al., 2019). The breakdown of $CO_2$ emissions shows that about 87.5% of the brick manufacturing is attributed to the drying and firing processes as shown in Figure 1-2 (Carbon Trust, 2012). Furthermore, the manufacturing of fired brick is an energy and resource intensive process. For example, the annual consumption of clay used by the brick industry is about 4.5 million tonnes (Smith et al.,

2016) and each brick requires about 2.0 kWh of energy (Muñoz Velasco et al., 2014). Therefore, developing new technologies in the production of bricks to cut the negative environmental impacts of the brick industry is crucial as this will help in:

- Increase in the pace of $CO_2$ reduction
- Cost savings as a result of energy savings
- Increased revenues or decreased costs from carbon trading
- Lower dependency on fossil fuels

Figure 1-2. The breakdown of $CO_2$ emissions of brick production by process

Source: (Carbon Trust, 2012) The diagram originally presented here cannot be made freely available via LJMU Digital Collections because of 'copyright'

## 1.2 State of the art

Considering the environmental issues associated with the production of conventional fired clay bricks, a wide range of studies has been conducted into producing unfired bricks; trying to minimize the large carbon footprint of the brick industry. New techniques have been employed in the production of unfired bricks as an alternative to conventional fired bricks. It is worth mentioning that the production of unfired bricks has only recently been introduced to the UK and it is still at the developmental stage (Smith et al., 2016). One of the oldest techniques is the solidification of clay with cementing binders such as cement and/or lime (Seco et al., 2017, Muñoz Velasco et al., 2014, Oti et al., 2009). This technique does not need any firing as the mechanical and durability performance of the produced bricks relies mainly on the formation of hydration products such as C–S–H gel and C–A–S–H gel produced from the chemical reaction between the silica sources (mainly the clay) and the CaO from the binders (Seco et al., 2017, Nagaraj et al., 2014). However, the production of cement clinker is highly energy intensive and releases a significant amount of greenhouse gases. Production of 1 kg of clinker requires approximately 1.5 kg of raw materials and releases about 0.9 kg of $CO_2$ into the atmosphere (Jafer et al., 2018a, O'Rourke et al., 2009). Worldwide, production of Portland cement is responsible for about 7% of all $CO_2$ generated (Hawileh et al., 2017). Similar to cement, the production of lime is associated with many negative environmental impacts such as the high $CO_2$ emissions, consuming a large amount of energy and the high level of water pollution (Prétot et al., 2014). Therefore, the production of cement/lime-based building bricks/blocks also consumes a large amount of energy and releases a substantial quantity of $CO_2$.

Another technique in the production of unfired brick is the employment of the alkali activation technique (geopolymerisation). This technique depends on the poly-condensation of the raw materials normally containing silica and alumina in the presence of an alkali solution to produce amorphous to semi-crystalline geopolymer (Yun-Ming et al., 2016). This technique is very attractive relative to other techniques (firing of brick or solidified clay brick) as the final products can provide structural strength in a very short time, they are sufficiently durable and $CO_2$ emissions are reduced significantly (Qian et al., 2017, McLellan et al., 2011). Different waste and/or by-product materials have been utilised as raw materials in the production of alkali activated bricks including volcanic ash (Lemougna et al., 2020), red mud and metakaolin (He et al., 2012), Fly ash and mine tailings (Zhang et al., 2011), type F Fly ash (Arıöz et al.,

2010), copper mine tailings (Ahmari and Zhang, 2012), Fly ash and blast furnace slag (Nath and Kumar, 2013). Recently, the possibility of employing different construction and demolition (C&D) wastes in the production of low carbon construction materials using alkali activation techniques has been investigated (Amin et al., 2017, Oti et al., 2014, Robayo et al., 2016, Robayo-Salazar et al., 2017a, Sivrikaya et al., 2013). In 2016, the C&D wastes generated within the UK was about 66.2 million tonnes (Government Statistical Service, 2019). It has been estimated that the global population will increase, this will create a substantial expansion of infrastructure and that inevitably will be associated with an increase in the production of C&D wastes (Aprianti et al., 2015, Department of Energy & Climate Change, 2015).

The recycling of different C&D wastes such as concrete, brick and ceramic tiles involves screening, breaking and crushing these materials to extract recycled construction materials such as sand and aggregate with specified size and quality. Washing of the produced materials is part of the recycling process to remove clay and other fine particles to improve the quality of the secondary aggregates. In doing this, an enormous amount of clay waste is generated that is usually filter-pressed and the final product is clay filter cake (CFC) waste as shown in Figure 1-3.

Figure 1-3. Clay filter cake waste produced during washing of recycled C&D wastes.

CFC waste is produced at C&D waste washing plants with the range of between 5 and 80 tonnes per hour depending on the size of plant and the amount of materials being processed (Lupo and Cheeseman, 2008). Owing to the lack of suitable low energy treatment techniques

in the market, CFC waste clay is currently disposed to land fill sites. The disposal of CFC is becoming a substantial issue as the CFC is being produced in enormous quantities and the disposal process is associated with transportation and diminishing of landfill space (Lupo and Cheeseman, 2008).

The UK has set a strategy with a target of recovering at least 70% of non-hazardous C&D wastes by 2020 (Government Statistical Service, 2016). The main theme of the strategy is: where waste is created it must be reused through recycling, composting or using it as a fuel. Therefore, in order to comply with the strategy there is a need to recover such waste and put it to good use. Currently, there are limited studies about using CFC in the construction industry although there are huge quantities of CFC waste, which is sent directly to landfill. A summary of the current state of the art regarding the use of CFC in the construction industry can be seen in Table 1-1.

Table 1-1. A summary of the current state of the art regarding the use of CFC in the construction industry

| Reference | Material used | Produced material | Method | Main findings | Advantages | Limitations |
|---|---|---|---|---|---|---|
| **(Lupo and Cheeseman, 2008).** | CFC, PC and polyvinyl alcohol (PVA) | Aggregate | Extruder was used to manufacture aggregates and some samples were moulded to form cylindrical samples that could be tested for unconfined compressive strength (UCS). | The UCS of the selected candidate mixture was about 15 MPa and the UCS of fully saturated samples (samples submersed in water for 24 hours) was reduced to approximately 30% of the dry UCS. The proposed application of the product was to produce aggregate for bound applications where aggregate is used in concrete or asphalt. It was found that a blend of 10% dry CFC aggregate with 90% normal aggregate could be used for unbound engineering fill applications. However, in wet condition the properties were potentially problematic due to deformation and crushing of CFC aggregate particles, rather than excessive fines production. | The positive environmental impacts are diverting waste from landfill and saving natural resources. There were also positive social impacts due to reduced traffic near landfill and recycling sites. | The process was more expensive than landfill due to the high cost of PC and PVA. Additionally, $CO_2$ emissions from the CFC aggregate process were much higher than landfill due to the significant $CO_2$ of PC production, thus creating a negative environmental impact. |

| Reference | Material used | Produced material | Method | Main findings | Advantages | Limitations |
|---|---|---|---|---|---|---|
| **(Lampris et al., 2009)** | CFC, fly ash and metakaolin | Aggregate | Samples were moulded to form cylindrical samples (22mm diameter and 20mm height) that tested for unconfined compressive strength (UCS). | Samples cured at room temperature had average 7-day compressive strengths of 18.7 MPa, while partial substitution (20%) of CFC by metakaolin or fly ash increased average compressive strengths to 30.5 and 21.9 MPa, respectively. | The positive environmental impacts are diverting waste from landfill and saving natural resources. There were also positive social impacts due to reduced traffic near landfill and recycling sites. | Compressive strength was the only test that was conducted in this study with no durability and environmental investigations of the final products. Authors aimed to produce aggregate from this research, however, aggregate was not produced and proposed application of their product (using the aggregate for unbound engineering filling) was not investigated. |

Table 1.1 presented the only available studies in the literature concerning the use of CFC in the construction industry. As can be seen from Table 1.1, Lupo and Cheeseman (2008), have used CFC in the production of aggregate where CFC was blended with carbon intensive Portland cement (PC) using the technique of solidification that is associated with many environmental and economic issues. On the other hand, (Lampris et al., 2009), have proposed the use of CFC in the production of aggregate for unbound engineering filling using the technique of geopolymerisation. Lampris et al. (2009) , justified the employment of the geopolymerisation technique in the production of aggregate for its attractive characteristics such as high compressive strength and durability. However, during that research only the unconfined compressive strength test was conducted for cylindrical samples that were not represent the proposed aggregate. Additionally, durability and environmental performance of the developed product was not investigated which are crucial characteristics for the final product in order to for it to be used as an alternative to normal aggregate in different applications. According to Table 1.1, the two available studies investigated the use of CFC in the production of aggregate and there is no study that investigated the utilisation of CFC in the production of unfired brick and comprehensively investigated its properties as an alternative to conventional fired clay brick. In order to produce environmentally friendly unfired brick, the technique of alkali activation (Geopolymerisation) could be used as it is of great research interest in the field of sustainable building materials due to its characteristics such as developing high mechanical strength within a very short time, enhanced durability and considerably decreased greenhouse gas emissions and energy consumption (Murmu and Patel, 2018, Sore et al., 2018, Slaty et al., 2015)

### 1.3 Aim of the research

The aim of this research is to develop unfired brick through alkali activation of waste from the aggregate recycling facility as an alternative to conventional fired clay brick.

### 1.4 Objectives

The objectives of this research project to achieve the aim above are:

1. To characterise the properties of CFC through chemical and physical analyses. Then carry out a review on different available candidate waste/by-product materials within the UK, which can be used in combination with the CFC to act as a binder for the unfired brick and characterise the properties of these materials.
2. To investigate the performance of different candidate materials to activate the CFC and identify the best candidate material that can be utilised in the formation of binder material for the unfired brick.
3. To study the mechanical and microstructural performance of the developed brick (produced by activating the CFC with selected candidate material) under different methods of curing and for different curing ages.
4. To investigate the limited durability and thermal properties of the developed brick under the selected candidate method of curing.
5. To provide quantitative comparison in terms of carbon footprint of the developed brick against conventional fired brick.
6. To provide a cost analysis of the developed brick and compare it against the conventional fired brick.

### 1.5 Novelty Statement

Using waste from the aggregate recycling facility in the production of unfired brick through geopolymerisation will meet the needs of recovering valuable waste materials along with developing a business-oriented disposal route for these wastes by providing a fully characterised brick for use in commercial scale. This is very timely with respect to the ongoing debate about moving to a low carbon economy and the current discussions regarding the future of the $CO_2$ allowances currently allocated to the construction sector. Unlike conventional fired clay brick, using waste from the aggregate recycling facility in the production of unfired alkali activated (Geopolymer) brick will not require any energy for drying and firing and will not

consume natural clay or any other virgin mineral materials. Therefore, developing low carbon brick, with validated characteristics, will be highly attractive to construction companies as this cannot currently be provided with existing bricks.

### 1.6 Overview of the Thesis

This thesis has been organised as follows:

- **Chapter 1** presents a general overview of the brick production, problems associated with conventional brick production and other alternative methods of brick production. Additionally, this chapter presents the aim and novelty statement, objectives and the structure of the thesis.
- **Chapter 2** provides a brief background about various techniques used for the manufacture of unfired building materials (bricks, blocks or solidified brick) Additionally, this chapter also provides a comprehensive comparisons regarding the technical and environmental aspects associated with different production techniques, along with selecting the best technique to improve the sustainability of the final product that will be employed in this study.
- **Chapter 3** presents detailed descriptions of the experimental works conducted, the equipment and apparatus, different procedures that have been followed for preparation and testing of different samples, along with the research methodology followed to achieve the aim of this research.
- **Chapter 4** presents the results obtained from the experimental works and gives a reasonable explanation for these data. Generally, this chapter will be divided into seven main parts, the characterization of the physical and chemical properties of the CFC and the candidate materials, selected candidate mix design and selected candidate of different methods of curing. Then, the physical, chemical and microstructural properties of the selected candidate mixture and the production of unfired brick using the selected candidate mix design with the same dimensions (215mm x 102.5mm x 65mm) of building bricks and evaluate its performance against standards specifications. Furthermore, conducting a comparison between $CO_2$ production of the new brick and conventional fired brick during manufacturing and operational processes. The final part will be a cost analysis of the developed brick and compare it against the conventional fired brick.

- **Chapter 5** starts with a conclusion for the main findings of this study, then the limitations of this study. Additionally, this chapter provides the recommendations and suggestions for future works.

# CHAPTER 2: LITERATURE REVIEW

## 2.1. Introduction

For thousands of years, clay has been widely used as an integral part of construction materials and products. Examples of the main structural clay products are bricks, blocks and roof tiles. Floor and wall tiles are examples of non-structural products made from clay. Buildings made from clay materials date back to the earliest periods of civilized development (Gillott, 2000, El-Mahllawy and Kandeel, 2014).

The desirable properties of clay-based products such as the durability, strength, heat and sound insulation along with fire-resistance mean that there is still considerable demand for them in a variety of sectors, despite the availability of modern alternative materials such as concrete, glass-fibre/resin composites, steel and plastics (Reeves et al., 2006).

Sun-baked clay bricks are thought to have been first used circa 8000 B.C while fired clay bricks were used circa 4500 B.C (Smith et al., 2016, Zhang, 2013). In Europe, the Romans introduced clay-based brick during the $9^{th}$ and $10^{th}$ centuries and thousands of churches and cathedrals were built in masonry during the middle Ages (Smith et al., 2016). The oldest skyscraper buildings in the world are located in the city of Shibam in Yemen (Aubert et al., 2013). These 500 huddled buildings, ranging from 5 to 11 stories high, reaching about 30m, were built with clay blocks (Atlas Obscura, 2017, Aubert et al., 2013).

In the UK, brick manufacturing was introduced from the Netherlands during the $12^{th}$ and $13^{th}$ centuries (Smith et al., 2016). The demand for bricks increased significantly after the Great Fire of London in 1666 (Smith et al., 2016). Additionally, bricks became the dominant construction material in the UK during the Industrial Revolution in the $19^{th}$ century (Smith et al., 2016).

The annual production of conventional fired brick reached about 1,500 billion pieces worldwide in 2015 (Zhang et al., 2018, Climate and Clean Air Coalition, 2016). This number is expected to increase through the rapid development of the construction industry globally, together with an expected increase in the world population (Department of Energy & Climate Change, 2015). In the UK, the annual production of fired clay brick is exceeding 2 billion bricks with a market value of about £550 million (Statista, 2019, Smith et al., 2016). Apart

from that, the annual consumption of clay used by the brick industry is about 4.5 million tonnes (Smith et al., 2016).

The conventional process of converting clay into brick involves firing the brick at temperatures ranging between 900 and 1300°C, depending on the type of clay (Akinshipe and Kornelius, 2017, Muñoz Velasco et al., 2014, Carbon Trust, 2010). During this process, clay minerals break down and sinter forming a glassy bond with other minerals and materials in the brick (Smith et al., 2016). The main purpose of the firing process is to transform the porous and weak dried clay into strong, dense bricks with low porosity (Brick Development Association, 2017, Reeves et al., 2006). This process requires high levels of energy consumption and a resulting release of greenhouse gases into the atmosphere (Zhang et al., 2018). The production of one brick requires some 2.0 kWh of energy and the release of approximately 0.665 kg of $CO_2$ (Department for Business; Energy & Industrial Strategy, 2018, Muñoz Velasco et al., 2014). The UK's industrial strategy for construction 2025 sets a range of targets, such as reducing emissions of greenhouse gasses by 50% and reducing the initial construction and whole life cost of assets along with reducing the trade gap between total exports and total imports for construction products and materials (British Standards Institution, 2016). Therefore, the main driving force behind research into more sustainable alternatives is to to comply with these targets and help in reducing the undesirable features of the manufacturing process along with conservation of the clay resource and the environment.

## 2.2 Alternative techniques for brick production

Considering the environmental issues associated with the production of conventional fired bricks such as $CO_2$ emissions and consumption of energy and natural resources, new methods have been developed to produce alternative building products with better performance and properties than those created in the firing process. Unfired building materials (bricks and blocks) have been recently introduced to the UK and are still at the development stage as an alternative to fired bricks (Smith et al., 2016). As the production of unfired building materials excludes the utilisation of kilns for firing, therefore, their embodied energy and $CO_2$ emissions are very low relative to fired bricks (Smith et al., 2016). The techniques used in the production of unfired building materials are divided into two groups: solidification and alkali activation.

### *2.2.1 Production of unfired building materials through solidification*

One of the oldest techniques in the production of unfired building materials is the solidification of clay with other cementing materials such as cement, lime and/or other waste materials with the aim of enhancing their strength, durability and volume stability (Seco et al., 2017, Muñoz Velasco et al., 2014, Nagaraj et al., 2014, Oti et al., 2009). Solidification of clays with other waste or by-product materials has many benefits such as reducing landfill, solving the issues of waste management, protecting the environment and saving energy, which in turn, reduces the cost of the final product (Muñoz Velasco et al., 2014).

The performance of different solidified building materials is dependent upon the characteristics of soil, binder and the mix design. The binder is any substance that is used for construction that sets, hardens, and adheres to other materials to bind them together (Hasan, 2019). This technique relies mainly on the formation of hydration products such as C–S–H gel and C–A–S–H gel produced from the chemical reaction between the silica sources (mainly the clay) and the CaO from the binders.

A brief summary of key experimental research work on using different binders for the solidification of building materials is presented in Table 0-1. In the reviewed studies (Table 0-1), most of the clays have high percentages of $SiO_2$ and $Al_2O_3$, while having only small CaO content. Therefore, cement, lime and other binders with high CaO content are added in small dosages to form C–S–H gel and C–A–S–H gel that enhance the mechanical and durability performance of the final product. The development of unfired building products with comparable or better performance than fired products significantly reduces $CO_2$ emissions and reduces consumption of energy that in turn leads to cheaper products with reduced environmental impact.

Table 0-1. Studies on production of unfired building materials through solidification

| **Reference** | **Clay type** | **Solidification material** | **Building product** | **Curing condition** | **Tests conducted** | **Findings** |
|---|---|---|---|---|---|---|
| (El-Mahllawy et al., 2018) | Kafr Homied clay | Marble Cutting Waste (0%, 10%, 15% and 20%), Hydrated lime (0%, 10%, 15% and 20%) and 5% Portland cement | Brick | Cured in a humidity chamber at 40$^{o}$C±2 for 14 and 28 days | Compressive strength, water absorption, bulk density, and XRD | The results indicated that the water absorption decreased while the bulk density and compressive strength increased with extended curing time and increase of the marble cutting waste content in the presence of hydrated lime. The maximum achieved compressive strength was 16.4 MPa and minimum water absorption was 10.1% obtained after 28 days of curing. |
| (Sekhar and Nayak, 2018) | Lithomargic clay | GGBS 25% and Cement (0, 6, 8, 10 and 12 %) | Solidified earth blocks (SEB) | Cured in water and air for 28 days | Compressive strength and water absorption | The results indicated a reduction in the water absorption and an increase in the compressive strength with the increase in the cement dosage and the air cured SEB provided higher strength than water cured SEB. The maximum achieved compressive strength was 5.5 MPa and 4.19 MPa for air curing and water curing, respectively with a minimum water absorption of 10.9%. |

| Reference | Clay type | Solidification material | Building product | Curing condition | Tests conducted | Findings |
|---|---|---|---|---|---|---|
| (Sitton et al., 2018) | Silty-clayey soil | Cement (3.6, 5.5, 9.1 and 10.9 %) | Solidified earth blocks | Cured in water and air for 7 and 28 days | Compressive strength and flexural strength | The results showed that strength of the SEB increased with the increase in the cement content. Additionally, the SEB under water curing exhibited lower strength (10.89 MPa) than that under air curing (15.72 MPa) after 28 days of curing. |
| (Saidi et al., 2018) | Sidi Amor soil | Cement (0, 5, 8, 10 and 12%) or lime (0, 5, 8, 10 and 12%) | Solidified earth blocks (SEB) | Cured in a humid atmosphere for 28 days at temperature of 20±2$^{o}$C | Thermal conductivity | The results indicated that with increased binder content, the thermal conductivity increased, which in turns resulted in decreasing the thermal insulation. The results also indicated that lime SEB exhibited lower thermal conductivity relative to cement SEB at the same levels of solidification. |
| (Nshimiyimana et al., 2018) | Reddish clayey soil | Calcium carbide residue (0, 5, 8, 10 and 15 %) or calcium carbide residue and rice husk ash (RHA) (0, 5, 8, 10 and 15 %) | Solidified earth blocks | Cured in ambient condition (30 ± 5°C) for 45 days. | Compressive strength and SEM | The results indicated that the highest compressive strength of 3.4 MPa was achieved with calcium carbide residue (CCR) content of 8% that was about 180% the compressive strength of the control SEB (100% reddish clayey soil). Additionally, the compressive strengths were significantly improved by the addition of RHA along with the CCR. |

| Reference | Clay type | Solidification material | Building product | Curing condition | Tests conducted | Findings |
|---|---|---|---|---|---|---|
| (Espuelas et al., 2017) | Spanish clay soil | Magnesium oxide rich kiln dust (PC-8) (0, 3, 6, 9, 12, 15 and 18%) | Brick | Cured in wet chamber | Compressive strength and water absorption | The results indicated that the compressive strength increased and water absorption decreased with both the curing time and increased PC-8 dosage. The selected candidate dosage of PC-8 was 15% that provided a compressive strength of 9.9 MPa and a water absorption value of about 5% after 90 days of curing. |
| (Abdullah et al., 2017) | Laterite Soil or clay | Cement (10%) or (20%) | Solidified earth brick | Spraying the samples with water every day up to 7 or 28 days. | Compressive strength and water absorption | The effect of compaction on compressive strength for clay and laterite soil was contradictory as the best strength was achieved by the samples subjected to compaction of 14 MPa and 28 MPa for laterite soil and clay, respectively. The highest compressive strength was 9 MPa for laterite soil and 5.1 MPa for clay soil. Additionally, water absorption was decreased through increased compaction resulting in denser samples with fewer voids. The minimum water absorption was 14.5% and 18.5% for laterite soil and clay soil, respectively. |

| Reference | Clay type | Solidification material | Building product | Curing condition | Tests conducted | Findings |
|---|---|---|---|---|---|---|
| (Zhang et al., 2017) | Local soil in Xinjiang | Cement (3, 5, 7 and 9 %) | Solidified earth blocks | Samples wrapped with plastic foils and placed in the laboratory for 28 days at temperature of 20 ± 1°C | Compressive strength and thermal conductivity | The results indicated a significant improvement in the strength of SEB by increasing the cement dosage. The highest compressive strength achieved was 9 MPa recorded with 9% cement content. The results also indicated that by increasing the bulk density, the thermal conductivity and compressive strength of the SEB increased. |
| (Taallah and Guettala, 2016) | Biskra soil | Quicklime (8, 10 and 12%) | Solidified earth blocks | Cured in water and air for 28 days | Compressive strength and tensile strengths. | The results indicated higher compressive and tensile strengths of the SEB under air curing relative to water curing. The results also showed an increased strength with increasing the quicklime content until the best dosage of 10%, however, below this level the strength tends to decrease. The highest compressive strength was 7.9 MPa and 6.4 MPa for samples subjected to air curing and water curing, respectively. |

| Reference | Clay type | Solidification material | Building product | Curing condition | Tests conducted | Findings |
|---|---|---|---|---|---|---|
| (Rahmat et al., 2016) | Lower Oxford Clay | PFA (50%), Lime-GGBS (30:70) and cement-GGBS (40:60) (10%) | Brick | Curing in humidity chamber at 20$^{o}$C for 7 and 28 days | Compressive Strength, Water Absorption, thermal conductivity freeze and thaw, and environmental performance. | The results of compressive strength and water absorption tests indicated that blending GGBS with lime or cement provided maximum compressive strength of 2.5 MPa and minimum water absorption of 8% which was better than using only cement or Lime. In addition, the results of thermal conductivity testing indicated that bricks solidified with cement-GGBS provided the lowest thermal conductivity value. Moreover, the results of the freezing and thawing at the end of the 30$^{th}$ cycle indicated that the weight loss of the bricks increased with increasing the freezing and thawing cycles and the bricks solidified with cement-GGBS achieved the lowest percentage of weight loss. |

| Reference | Clay type | Solidification material | Building product | Curing condition | Tests conducted | Findings |
|---|---|---|---|---|---|---|
| (Oti et al., 2014) | Mercia mudstone clay | Brick dust waste (BDW) (5%, 10%, 15% and 20%), GGBS (11%) and lime (11%) | Mortar, block and brick | The samples were moist-cured for 3, 7, 14, 28 and 56 days at room temperature of about 20°C. | Compressive Strength, water absorption and freeze and thaw | The results indicated an increase in compressive strength with increased percentages of BDW in the mixtures with a maximum value of 2.1 MPa. The results also showed that the water absorption rate for all the mixtures was extremely low (about 2.7%). Additionally, the results of the weight loss of samples after 7, 28, 56 and 100 cycles of freezing and thawing indicated an increase in the weight loss with increasing BDW content |
| (Nagaraj et al., 2014) | Red soil | Cement (4, 6 and 8%) and lime (0%, 2% and 4%) | Solidified earth blocks (CSEBs) | Cured in water for 7, 15, 30, 60, 120, 180 days; 1, 2 and 5 years | Compressive strength and water absorption | The results indicated that the compressive strength increased and water absorption decreased with the increase in the period of curing. The results also showed that up to 120 days, the strength of the SEBs solidified with cement alone was higher than that solidified with cement and lime. The maximum compressive strength of 7 MPa and minimum water absorption of 7% was achieved after 5 years of curing. |

2

#### *2.2.1.1 Critical evaluation of using the technique of solidification in the production of unfired building materials*

The technique of producing unfired building materials by the solidification of clay is considered an important step in the fabrication of different unfired building materials. The main aim of this technique (that depends mainly on the production of hydration products such as C–S–H and C–A–S–H phases) is enhancing the mechanical and durability performance of the produced product.

According to the reviewed studies (Table 0-1) and amongst the variety of binders utilised, cement and lime have been the most popular binders in the production of solidified building materials. Cement and/or lime were used either alone (Sekhar and Nayak, 2018, Sitton et al., 2018, Saidi et al., 2018, Zhang et al., 2017, Abdullah et al., 2017, Taallah and Guettala, 2016, Lupo and Cheeseman, 2008), in combination with each other (El-Mahllawy et al., 2018, Nagaraj et al., 2014) or in combination with other binders such as GGBS or PFA (Rahmat et al., 2016, Oti et al., 2014). However, two of the reviewed studies used different binders such as calcium carbide residue with rice husk ash (Nshimiyimana et al., 2018) and magnesium oxide rich kiln dust (Espuelas et al., 2017).

The dosage of the binders in the reviewed studies varied depending on the type of binder. For example, the cement dosage was ranging between 3% and 12% (Sekhar and Nayak, 2018, Sitton et al., 2018, Saidi et al., 2018, Zhang et al., 2017) and only two research studies have shown the usage of 20% (Abdullah et al., 2017) and 50% (Lupo and Cheeseman, 2008) cement as binder. The dosage of lime as the binder was similar to that of the cement (ranging between 2% and 12%). Additionally, the lime and cement were blended with other by-product binders such as GGBS or PFA to boost the hydration process of these materials by the highly alkali environment (pH > 12) and accelerate the production of cementitious compound that binds the soil together (Rahmat et al., 2016, Oti et al., 2014). The dosage of binder for the research with calcium carbide residue and rice husk ash (Nshimiyimana et al., 2018) was in the range of 5-12%, while the magnesium oxide rich kiln dust (Espuelas et al., 2017) was in the range of 3-18%.

The reviewed studies (Table 0-1) indicated that the production of C–S–H and C–A–S–H gel phases increased with the increase in the amounts of binder in the mixture (El-Mahllawy et al., 2018, Nshimiyimana et al., 2018, Sekhar and Nayak, 2018, Saidi et al., 2018, Rahmat et al.,

2016). This was due to the chemical reaction occurring between the CaO from the cement, lime and other binders and amorphous silica provided by clay, together with the high alkalinity environment of cement or lime (Sekhar and Nayak, 2018, Saidi et al., 2018, Rahmat et al., 2016, Oti et al., 2014). These gels tend to fill pores and grow into capillary spaces, resulting in a more impermeable, dense and higher-strength structure (Jafer et al., 2018a). However, a high dosage of binder with high CaO content negatively affected the performance of the product because this resulted in free CaO that led to expansion and cracks in the final product (Muñoz Velasco et al., 2014, Lupo and Cheeseman, 2008).

Curing is a very important process for solidified building materials, especially when cement or lime is used in preparation of these products as a solidification agent. Water curing would aid in enhancing the hydration process of the cement/lime, as this process can take place more efficiently in the presence of water that results in hardening the materials treated with cement/lime. Table 0-1 shows the methods of curing that were used for each of the solidified building materials. According to the reviewed studies (El-Mahllawy et al., 2018, Sekhar and Nayak, 2018, Sitton et al., 2018, Saidi et al., 2018, Abdullah et al., 2017, Taallah and Guettala, 2016, Rahmat et al., 2016), the produced building materials that incorporated cement and/or lime were kept moist for 28 days by immersing in water, spraying with water or placed in a humidity chamber at ambient temperature that ranged between 20-40$^{o}$C, according to the weather conditions in the country where the experiments were conducted. This is because the presence of moisture will allow unreacted cement or/and lime particles to hydrate further, producing additional cementing gel as reported by Joel and Edeh (2013). Additionally, increasing the period of curing to 28 days or even longer (Oti et al., 2014, Nagaraj et al., 2014) in the presence of moisture will aid the formation of secondary cementing gel that is formed due to the chemical reaction between calcium from the portlandite phase (CH) and silicates from the clays (El-Mahllawy and Kandeel, 2014).

### *2.2.2. Production of unfired building materials through alkali activation (Geopolymerisation)*

In addition to the use of solidification techniques in the production of unfired building materials, researchers have investigated the use of alkali activation techniques (geopolymerisation). Generally, geopolymer is formed by mixing an alumina-silicate precursor with an alkali solution (Yun-Ming et al., 2016, Ahmari and Zhang, 2013, Tennakoon et al., 2015, Robayo et al., 2016, Rakhimova and Rakhimov, 2015). This technique relies on the chemical reaction between the alumina-silicate precursor and a high alkali solution to produce amorphous to semi-crystalline geopolymer (Phummiphan et al., 2018, Yun-Ming et al., 2016, Slaty et al., 2015, Rakhimova and Rakhimov, 2015). The three-dimensional alumina-silicate structures consist of linked $SiO_4$ and $AlO_4$ tetrahedra by sharing all the oxygen atoms (Davidovits, 1991, Dimas et al., 2009). According to Davidovits (1994) the chemical reaction comprises the following steps:

i) Dissolution of Si and Al atoms from the source material through the action of OH- ions.
ii) Transportation or orientation or condensation of precursor ions into monomers.
iii) Setting or polycondensation/polymerisation of monomers into polymeric structures.

However, these three steps can overlap with each other and occur almost simultaneously, thus making it difficult to isolate and examine each of them separately (Palomo et al., 1999).

During the development of building materials using the technique of geopolymerisation, the most important chemical compounds that should be available in high quantities are the $SiO_2$ and $Al_2O_3$ because they react with a high alkali solution to produce amorphous to semi-crystalline geopolymer materials (Yun-Ming et al., 2016, Zhang, 2013). Preferably, the total composition of the $SiO_2$ and $Al_2O_3$ compounds should be more than 70% (Yun-Ming et al., 2016). Yun-Ming et al. (2016) stated that the raw materials with an abundant amount of $SiO_2$ and $Al_2O_3$, that is suitable for the production of geopolymer materials, can be found in different types of clay. Additionally, any other material that principally contains Silicon (Si) and Aluminium (Al) in amorphous form is a potential source material for the production of geopolymer. Minerals and industrial by-products have been considered as source materials in the past, including volcanic ash (Lemougna et al., 2020), red mud and metakaolin (He et al., 2012), Fly ash and mine tailings (Zhang et al., 2011), type F Fly ash (Arıöz et al., 2010), copper

mine tailings (Ahmari and Zhang, 2012), Fly ash and blast furnace slag (Nath and Kumar, 2013), metakaolin or calcined kaolin (Palomo et al., 1999, Davidovits, 1994) low-calcium Class F fly ash, natural Al-Si minerals, and metakaolin and combination of granulated blast furnace slag and metakaolin (Cheng and Chiu, 2003).

This technique is of great research interest in the field of sustainable building materials due to its characteristics such as developing high mechanical strength within a very short time, enhanced durability, abundant raw material resources, high fire resistance and considerably decreased greenhouse gas emissions and energy consumption (Murmu and Patel, 2018, Sore et al., 2018, Slaty et al., 2015). Table 2-2 presents a summary of the main findings of researchers that have investigated the production of unfired clay-based building materials using the technique of alkali activation (geopolymerisation).

Table 2-2. Studies on production of unfired clay-based building materials through alkali activation (geopolymerisation)

| Reference | Clay type | Blended material | Alkali activator | Clay-based product | Curing condition | Tests conducted | Results |
|---|---|---|---|---|---|---|---|
| (Faqir et al., 2019) | Kaolin clay | - | NaOH (13, 16.3, 17, 17.8 and 19.7 M) | Mortar and brick | Cured in oven at 80$^{o}$C for 24 hours then at air or in water for 7 days | Compressive strength and water absorption | The results indicated that with decreasing the sand to kaolin clay ratio and increasing both the concentration and the amount of the NaOH, the compressive strength increased for both curing methods. The maximum achieved compressive strength in this study was 27.1 MPa for air curing and 18.1 MPa for water curing. Additionally, the results indicated that the geopolymer mortar and bricks exhibit lower water absorption rate with the increase in the concentration of the NaOH. The lowest water absorption rate was 3.7%. |

| Reference | Clay type | Blended material | Alkali activator | Clay-based product | Curing condition | Tests conducted | Results |
|---|---|---|---|---|---|---|---|
| (Dassekpo et al., 2018) | Clay waste from construction site | Class F fly ash (0, 10, 20 and 30%) | $Na_2SiO_3$ and NaOH (14M) | Paste, brick | Cured in a humidity chamber at 75$^{o}$C±2 for 24 hours then at ambient temperature for 7, 14 and 28 days | Compressive strength, SEM/EDX | The results indicated an increase in the compressive strength with the increase in the curing period and the FA content. The Maximum compressive strength of 20.849 MPa was achieved after 28 days of curing for the mixture incorporating 30% FA. The SEM images showed an increase in the degree of compaction and formation of a denser microstructure as the amount of FA in the mixes increased. |
| (Sore et al., 2018) | Laterite clay | Metakaolin (MK) (0, 5, 10, 15 and 20%) | NaOH (12M) | Compressed earth blocks (CEB) | Cured at ambient temperature of (30$^{o}$C ± 5$^{o}$C) for 7 days and then placed in oven for another 7 days at 60$^{o}$C ± 2$^{o}$C | Weight loss after curing, porosity, apparent density, compressive strength, flexural strength, thermal diffusivity and thermal conductivity. | The results indicated that with increased MK content, the weight loss and porosity increased, while the apparent density decreased. In addition, the compressive and flexural strength of geopolymer CEB improved with increased MK content with a maximum value of 8.95 MPa and 1.68 MPa for samples incorporated 20% MK. The results also indicated low thermal diffusivity and thermal conductivity with all MK percentages. |

| Reference | Clay type | Blended material | Alkali activator | Clay-based product | Curing condition | Tests conducted | Results |
|---|---|---|---|---|---|---|---|
| (Phummiphan et al., 2018) | Lateritic soil (LS) | Class C fly ash (30%) and Granulated Blast Furnace Slag (10, 20 and 30%) | $Na_2SiO_3$ and NaOH (5M) | Pavement base material | Wrapped with plastic sheets and cured at room temperature between (27–30)˚C for 7, 28 and 60 days | Compressive Strength, SEM and XRD | The results indicated that the highest compressive strength values after 28 and 60 days were 16 MPa and 20 MPa obtained at LS: FA: GBFS = 60:30:10 and $Na_2SiO_3$: NaOH of 90:10. The results of SEM and XRD tests indicated that the geopolymerisation products increased in volume as the curing time increased. |
| (Miranda et al., 2017) | Granitic residual soil | Fly ash (5% and 15%) | $Na_2SiO_3$ and NaOH (5M and 12.5M) | Mortar and brick | Cured at ambient temperature for 30, 60 and 90 days | Compressive strength and flexural strength | The results indicated an improvement in the compressive and flexural strengths with the increase in the curing time and FA content. The highest compressive strength and flexural strength achieved was 5.6 MPa and 2.8 MPa, respectively after 90 days of curing. |
| (Leitão et al., 2017) | Granitic residual soil | Fly ash (15%) | $Na_2SiO_3$ and NaOH (12.5M) | Compressed earth block | Cured at ambient temperature for 28 days | Compressive strength and thermal conductivity | The results indicated a compressive strength of 3 MPa after 28 days of curing. The results of the thermal conductivity of the masonry wall suggested that the use of alkali activators in the presence of 15% FA improved the thermal properties of the wall with respect to heat transference. |

| Reference | Clay type | Blended material | Alkali activator | Clay-based product | Curing condition | Tests conducted | Results |
|---|---|---|---|---|---|---|---|
| (Messina et al., 2017) | Calcined clay sediments | Calcined water potabilization sludge (30, 50 and 70 %) | $Na_2SiO_3$ and NaOH (14 M) | Paste, mortar and paving brick | Cured for 24h either at 20°C or 60°C and then in climatic chamber operating at 20°C for 7 days. | Compressive strength, splitting tensile strength, SEM, XRD and visual assessment. | The results indicated that the compressive strength of the developed pastes and mortars were very similar and were in the range between 17-23 MPa. The developed paving bricks have showed splitting tensile strength between 0.82-2.01 MPa. The durability assessment of the developed bricks after 180 days of exposure to room conditions showed that there was no cracking and no efflorescence was formed on the surface of the developed paving brick. |

| Reference | Clay type | Blended material | Alkali activator | Clay-based product | Curing condition | Tests conducted | Results |
|---|---|---|---|---|---|---|---|
| (Slaty et al., 2015) | Jordanian Hiswa kaolinite clay | - | NaOH | Mortar, paste and brick | Cured for 24h or 48h at 80 °C and then for 7, 30, 60, 90 and 180 days at ambient temperature. | Compressive strength, drying shrinkage, wetting and drying conditions, sea water attack and alkali-silica reaction | The results indicated a very low drying shrinkage for all samples and the presence of sand in mortar significantly reduced the shrinkage relative to geopolymer paste. The results also indicated that the compressive strength achieved was about 40 MPa after 28 days of curing and there was a 50% reduction in the compressive strength of specimens subjected to 100 cycles of wetting and drying conditions relative to geopolymer specimens cured under dry conditions. In addition, the results indicated a very good mechanical performance for geopolymer bricks immersed in sea water with a small formation of efflorescent material on the external surface of the samples. |

| Reference | Clay type | Blended material | Alkali activator | Clay-based product | Curing condition | Tests conducted | Results |
|---|---|---|---|---|---|---|---|
| (Poowancum and Horpibulsuk, 2015) | Dan Kwian sedimentary clay (DKSC) | - | $Na_2SiO_3$ and NaOH (8 M) | Paste and brick | Cured at 60°C for 7 days | Setting time, compressive strength and Porosity. | The results indicated that for a fixed $Na_2SiO_3$/NaOH ratio, the setting time of the paste calcined for 1 and 2 h was about 55 min and was about 60 min for the paste calcined for 5 h. The results also showed that the compressive strength of the geopolymer brick decreased with the increase in the $Na_2SiO_3$/NaOH ratio and the lowest compressive strength was recorded for $Na_2SiO_3$/NaOH ratio of 1. The highest compressive strength of 27 MPa and lowest porosity of 35% was achieved with calcination of the DKSC for 2 h and $Na_2SiO_3$/NaOH ratio of 0.5. |
| (Silva et al., 2015) | Granitic residual soil | Fly ash (10% and 15%) | $Na_2SiO_3$ and NaOH (12.5M) | Compressed earth blocks | Cured at ambient temperature for 180 days | Compressive strength and flexural strength | The results showed superior compressive and flexural strengths of CEBs incorporating 15% FA relative to the CEBs with 10% FA. The highest recorded compressive strength of 12 MPa was achieved for mixtures incorporating 15% FA. |

| Reference | Clay type | Blended material | Alkali activator | Clay-based product | Curing condition | Tests conducted | Results |
|---|---|---|---|---|---|---|---|
| (Ferone et al., 2015) | Sabetta clay sediments (SCS) | GGBS (0 and 17 %) | $Na_2SiO_3$ and NaOH (5, 7 and 10 M) | Paste and brick | Cured for 3 days at 60°C in an oven, then at room temperature for 28 days. | Compressive strength, SEM, EDX and XRD. | The results indicated that compressive strength of the geopolymer products was significantly enhanced with the increase in the calcination temperature from 400ºC to 750ºC. Additionally, the results showed that the compressive strength was improved with the increase in the concentration of the NaOH and when the SCS was activated by a mixture of NaOH and $Na_2SiO_3$. The compressive strength was further enhanced by the addition of 17 % GGBS. The highest compressive strength value was 38.9 MPa achieved with SCS treated at 750ºC mixed with 17% GGBS and activated by a mixture of NaOH and $Na_2SiO_3$. |
| (Phetchuay et al., 2014) | Silty clay soil | Fly ash (0, 5, 10, 15, and 20 %) and 7% Calcium Carbide Residue | $Na_2SiO_3$ | Pavement subgrade material | Cured either at ambient temperature (27–30)ºC or at 40ºC for 7, 14, 28 and 60 days | Unconfined Compressive Strength and SEM | The results indicated that the selected candidate FA replacement level was 15% that achieved a maximum compressive strength of 3.8 MPa. Regarding the effect of $Na_2SiO_3$/water ratio, the results showed that it was 0.6 for samples under water curing and 1.4 for samples under air curing. |

| Reference | Clay type | Blended material | Alkali activator | Clay-based product | Curing condition | Tests conducted | Results |
|---|---|---|---|---|---|---|---|
| (Molino et al., 2014) | Occhito clay sediments | - | NaOH (5 M), sodium aluminate (8.5, 11, 13 and 17 M) and potassium aluminate (8.5, 11, 13 and 17 M) | Paste and brick | Cured for 3 days at 60°C in an oven, then kept in air for 11 days | Unconfined Compressive Strength and SEM | At 3 days, the results indicated an improvement in the compressive strength with the increase in the temperature of calcination from 650°C to 750°C for the samples activated with either NaOH solution or sodium aluminate solution, while it decreased for samples activated with potassium aluminate solution. After 14 days of curing, the results indicated higher compressive strength with the increase in the temperature of calcination for all the used activators with the highest compressive strength of 7.7 MPa achieved at the temperature of calcination 750°C. |
| (Slaty et al., 2013) | Kaolinitic clay | Silica sand (25, 50, 100 and 150%) | NaOH | Mortar and brick | Cured at temperature (50, 60, 70 and 80°C) for curing period (6, 12, 18, 24, 48 and 72h) | Workability, compressive strength, wetting and drying, SEM and XRD | The results showed that by increasing the sand content, the workability of mortar and brick improved and the highest compressive strength value was achieved when the sand to clay ratio was 1. The results also indicated that with the increase in the curing temperature from 50°C to 80°C, the compressive strength increased from 14 MPa to 32 MPa after 24h of curing. |

| Reference | Clay type | Blended material | Alkali activator | Clay-based product | Curing condition | Tests conducted | Results |
|---|---|---|---|---|---|---|---|
| (Sukmak et al., 2013) | Silty clay soil | Fly ash (30, 50 and 70%) | $Na_2SiO_3$ and NaOH (10M) | Brick | Cured at ambient temperature for 7, 14, 28, 60, and 90 days | Compressive strength | The results indicated that for different liquid/FA and FA/clay ratios, the best compressive strength was 12 MPa for the mixtures with $Na_2SiO_3$/NaOH ratio of 0.7. The results also indicated that the compressive strength increased with increases in the FA content |
| (Mohsen and Mostafa, 2010) | White clay | - | NaOH alone or Na2SiO3 and NaOH | Brick | Cured at (i) room temperature for 3 days, (ii) 75°C for 24 h and (iii) 150°C for 24 h | Compressive strength, Water absorption, SEM and XRD. | The results indicated that the compressive strength of the developed bricks with NaOH alone was improved from 19.8 MPa to about 22 MPa with the increase in the curing temperature from room temperature to 75°C. Additionally, the compressive strength results of the geopolymer bricks activated with $Na_2SiO_3$ and NaOH improved from 44 MPa to about 79 MPa with the increase in the curing temperature. The results of water absorption test indicated that increasing the curing temperature reduced the water absorption of the produced bricks for both activators. The minimum water absorption of 4.7% was obtained with curing temperature of 150°C. |

### *2.2.2.1 Critical evaluation of using the technique of alkali activation (Geopolymerisation) in the production of unfired building materials*

It is well understood that the chemical composition of raw materials has a significant influence upon the properties of the alkali activated building materials (Muñoz Velasco et al., 2014). Therefore, the chemical composition of raw materials should be tested to elucidate the performance of these materials when they are chemically activated by different activators. The chemical composition of different types of clay as collected from the Energy Dispersive X-ray Florescence Spectrometer (EDXRF) test for all the reviewed studies that provide such information are presented in Table 2-3

Table 2-3 presents the results of the most common chemical compounds ($SiO_2$, $Al_2O_3$ and CaO) of the clay powder materials used for the preparation of different alkali activated building materials. It can be seen from Table 2-3 that about 67% of the clays used in the production of different alkali activated building materials have $SiO_2$ content in the range between 40% and 60%. Additionally, 20% of the clays have showed $SiO_2$ content in the range of 70-80 % and the other 13% have $SiO_2$ content in the range of 20-30%. The second chemical compound that is essential for the geopolymerisation reaction and can be found in abundance in different types of clay is the $Al_2O_3$. Table 2-3 shows that the $Al_2O_3$ content collected from different types of clay ranges from 4.42% to 29% and the majority of the observations lie between 13% and 25%. Another important compound is the CaO content. Table 2-3 indicated that 67% of the clays have relatively small CaO content (below 5%), while 20% of the clays have a CaO content in the range of 5-15% and the other 13% have a CaO content of 26.16%. As observed from Table 2-3 most of the clays utilised in the production of alkali activated building materials displayed similar ranges of $SiO_2$, CaO and $Al_2O_3$, although they came from different origins and places around the world.

Table 2-3. Principal chemical composition of clays used in previous studies listed in Table 2-2

| Reference | $SiO_2$% | $Al_2O_3$% | CaO% |
|---|---|---|---|
| **(Faqir et al., 2019)** | 45.7 | 25.1 | 1.1 |
| **(Sore et al., 2018)** | 50.9 | 29 | 0.19 |
| **(Phummiphan et al., 2018)** | 77.81 | 4.42 | 1.13 |
| **(Miranda et al., 2017)** | 48.81 | 21.77 | 3.85 |
| **(Leitão et al., 2017)** | 48.81 | 21.77 | 3.85 |
| **(Messina et al., 2017)** | 50.95 | 16.86 | 7.9 |
| **(Slaty et al., 2015)** | 48.92 | 25.16 | 0.68 |
| **(Poowancum and Horpibulsuk, 2015)** | 72.95 | 18.76 | 0.38 |
| **(Silva et al., 2015)** | 48.81 | 21.77 | 3.85 |
| **(Ferone et al., 2015)** | 50.0 | 15.9 | 6.9 |
| **(Phetchuay et al., 2014)** | 20.1 | 7.55 | 26.15 |
| **(Molino et al., 2014)** | 57.13 | 16.33 | 12.5 |
| **(Slaty et al., 2013)** | 49.0 | 25.0 | 0.7 |
| **(Sukmak et al., 2013)** | 20.1 | 7.55 | 26.15 |
| **(Mohsen and Mostafa, 2010)** | 70.23 | 11.79 | 1.13 |

In some of the reviewed studies (Table 2-2), the clay materials were blended with different materials such as FA (Dassekpo et al., 2018, Miranda et al., 2017, Leitão et al., 2017, Silva et al., 2015, Phetchuay et al., 2014, Sukmak et al., 2013), GGBS (Ferone et al., 2015), metakaolin (Sore et al., 2018) and calcined water potabilization sludge (Messina et al., 2017). The main reason behind blending the clay with the alkali activators and the aforementioned materials was to induce the geopolymerisation products that in turn resulted in enhanced mechanical and durability performance (Yun-Ming et al., 2016). In the reviewed studies (Table 2-2), both class C and class F fly ash types were used. The reaction between alkali activator and class C fly ash forms Calcium Silicate Hydrate (C-S-H) gel in addition to the geopolymerisation products that is normally formed during the activation of class F fly ash (Phummiphan et al., 2018). This behaviour is similar to the alkali activation of GGBS and is attributed to the adequate calcium content in class C fly ash and GGBS (Rakhimova and Rakhimov, 2015, Ghosh and Subbarao, 2007). The amount of fly ash blended with different types of clay that have high $SiO_2$ and $Al_2O_3$ content was in the range of 5-30% (Dassekpo et al., 2018, Phummiphan et al., 2018, Miranda et al., 2017, Leitão et al., 2017, Silva et al., 2015, Phetchuay et al., 2014). However, the amount of blended fly ash reached about 70% in the case of clay with total $SiO_2$ and $Al_2O_3$ content of about 28% (Sukmak et al., 2013).

According to the reviewed studies, the most commonly used alkali activator solutions were sodium hydroxide (NaOH) and sodium silicate ($Na_2SiO_3$). Sodium hydroxide was used alone as an activator (Faqir et al., 2019, Sore et al., 2018, Slaty et al., 2015, Slaty et al., 2013) or in combination with sodium silicate (Dassekpo et al., 2018, Phummiphan et al., 2018, Miranda et al., 2017, Leitão et al., 2017, Messina et al., 2017, Poowancum and Horpibulsuk, 2015, Silva et al., 2015, Ferone et al., 2015, Sukmak et al., 2013, Mohsen and Mostafa, 2010). The utilisation of both activators together in the production of unfired alkali activated products was vital because NaOH is required for the dissolution of alumina-silicate precursor, while $Na_2SiO_3$ acts as a binder or alkali reactant (Yun-Ming et al., 2016, Feng et al., 2012, Xu et al., 2002, Wang et al., 2005). Therefore, the final product will have better mechanical and durability performance (Ferone et al., 2015, Mohsen and Mostafa, 2010).

In many of the reviewed studies that utilised NaOH with different concentrations (Faqir et al., 2019, Ferone et al., 2015), the results indicated an improvement in the strength and reduction in the water absorption with the increase in the NaOH concentration. This enhancement in the strength and durability perfomance of the geopolymer materials is believed to be due to the formation of a denser microstructure that bonds the particles of the raw materials, thus resulting in fewer pores (Faqir et al., 2019, Yun-Ming et al., 2016).

Generally, the $Na_2SiO_3$/NaOH ratio in the preparation of unfired alkali activated products is important (Yun-Ming et al., 2016, Wang et al., 2005). Based on the reviewed studies, the $Na_2SiO_3$/NaOH ratios were in the range of 0.25 to 9. The optimum $Na_2SiO_3$/NaOH ratio in the reviewed studies varied significantly according to the type of clay, blended materials, methods of curing, etc. In general, increasing the $Na_2SiO_3$/NaOH ratio resulted in improved strength and durability of the final product. This was attributed to the increased (Si) content that aids in the production of more Si-O-Si bonds, and significantly enhanced the compressive strength of the unfired alkali activated materials (Hameed et al., 2017a, Sukmak et al., 2013). However, the strength started to decrease after reaching the optimum $Na_2SiO_3$/NaOH ratio. This was due to the excess Si content that hinders water evaporation and structure formation and negatively affects the geopolymerisation rate (Hameed et al., 2017a, Sukmak et al., 2013).

In addition to the aforementioned alkali activators, sodium aluminate and potassium aluminate activators were used by Molino et al. (2014) with the aim of improving the performance of the raw materials with low $Al_2O_3$ content (16.33%). The results indicated an improvement in the

performance of geopolymer material with the use of alkali aluminate solutions relative to NaOH solution.

Researchers also investigated the utilisation of waste and/or by product materials as alternatives to NaOH and $Na_2SiO_3$. This including; paper sludge (Adesanya et al., 2018) , maize cobsand maize stalk ashes (Peys et al., 2016), lime kiln dust (Kadhim et al., 2020) , sugar cane straw ash (Moraes et al., 2018), desulphurization dust that generated during the process of steel making (Adesanya et al., 2020), industrial cleaning solution (Cristelo et al., 2019), glass waste (Puertas et al., 2015) and bayer process liquor (Van Riessen et al., 2013) proven their potential to be used as an alternative to conventional alkali activators.

It is worth mentioning that the PAS 8820:2016 did not specify any limits for the content of alkali activators, however, it has clearly stated that the activators should be as minimal as required, and they should not be used to indefinitely enhance the mechanical performance (British Standards Institution, 2016). The main reason for this limitations is that the excessive usage of alkali activators doses could induce problematic efflorescence for the final product (British Standards Institution, 2016).

In some of the reviewed studies (Table 2-2), the raw materials (clays) were calcined at different temperatures and times (Messina et al., 2017, Poowancum and Horpibulsuk, 2015, Ferone et al., 2015, Molino et al., 2014, Mohsen and Mostafa, 2010), while the other studies used non-calcined clays. Ferone et al. (2015) stated that calcined clay could provide better performance than non-calcined clay. This is because heat treatment helps to transform the crystalline phases into reactive amorphous raw materials that leads to enhance the strength of geopolymers (Yun-Ming et al., 2016, Ferone et al., 2015, Xu and Van Deventer, 2002). Additionally, the reviewed studies showed that the temperature at which the clays were calcined was in the range of 400$^{o}$C to 750$^{o}$C, while the calcination time was between 1-5 hours. Generally, the strength of different calcined clay-based building materials has improved with the increase in the temperature of calcination (Ferone et al., 2015, Mohsen and Mostafa, 2010) and the selected candidate calcination time was 2 hours (Messina et al., 2017, Poowancum and Horpibulsuk, 2015, Ferone et al., 2015, Mohsen and Mostafa, 2010). The improvement in the strength with the increase in the calcination temperature is due to the increased surface area of raw materials that dissolves more quickly in the alkali solution and consequently improves the geopolymerisation reaction (Yun-Ming et al., 2016). On the other hand, the reduction in strength with the increase in the time of calcination to more than two hours is attributed to the over calcination that leads to the

transformation of the reactive amorphous phase into mullite crystalline phases that are dead burnt and not reactive (Yun-Ming et al., 2016).

The method and period of curing can significantly affect the properties of the alkali activated unfired clay-based building materials (Hameed et al., 2017a, Yun-Ming et al., 2016). Alkali activated unfired clay-based building materials are usually cured at ambient or slightly higher temperature after mixing. Normally, the curing temperature is preferable to be less than 100$^{o}$C (Yun-Ming et al., 2016). Based on the reviewed studies (Table 2-2), different curing temperatures with various periods of time were employed in the production of different alkali activated building materials.

According to the reviewed studies (Table 2-2), air curing was considered by many of the researchers under ambient temperatures that ranged between 20-35$^{o}$C. For the alkalie activated building materials under air curing, the period of curing was a minimum of 7 days and some of the studies extended the time to 28 days (Leitão et al., 2017), 60 days (Phummiphan et al., 2018, Phetchuay et al., 2014), 90 days (Miranda et al., 2017, Sukmak et al., 2013) and even 180 days (Silva et al., 2015). This is because the geopolymerisation reaction is very slow at ambient temperature and extending the period of curing is essential to produce materials with enhanced strength and reduced water absorption due to the formation of additional geopolymerisation products (Phummiphan et al., 2018, Miranda et al., 2017, Yun-Ming et al., 2016, Silva et al., 2015, Zuhua et al., 2009).

In addition, oven curing was one of the techniques used in the curing of alkali activated unfired clay-based building materials due to the fact that heat is essential to improve the reaction by accelerating the dissolution of silica and alumina species from the raw materials (He et al., 2013, Kong et al., 2007b, Perera et al., 2006). According to the reviewed studies, the curing temperatures were reported in the range between 40$^{o}$C and 150$^{o}$C and the period under oven curing ranged between 6 hours and 7 days. Slaty et al. (2013) reported that increasing the temperature to (50$^{o}$C, 60$^{o}$C, 70$^{o}$C and 80$^{o}$C) improved the strength gain after 6-72 hours. However, a high curing temperature (150$^{o}$C) resulted in reduced compressive strength due to the formation of large pores (Mohsen and Mostafa, 2010).

## 2.3. *Comparative assessment of the techniques used in the production of unfired building materials*

Sustainable development in the construction industry required evaluating different parameters of the production techniques. The criteria considered in this study for the assessment are technical and environmental aspects for the production of different unfired building materials. The technical aspects considered in this study are compressive strength, durability and thermal performances of different techniques used in the production of unfired building materials. The study also presents comprehensive evaluation of environmental impacts associated with different techniques to produce unfired building materials.

### *2.3.1 Technical Assessment*

A range of tests were carried out on the resulting products to evaluate their performance following different standards. Compressive strength was the common test considered by most of the studies as the compressive strength is considered a basic and universally acceptable measurement to specify the quality of building materials as stated by common standards (Nagaraj et al., 2014). According to the reviewed studies (Table 0-1 and Table 2-2) there was a substantial difference in the compressive strengths for alkali activated building materials relative to that of solidified building materials. The compressive strength of the alkali activated building materials was between 3 MPa and 79 MPa with the majority ranging between 12 MPa and 30 MPa. On the other hand, the compressive strength for the solidified building materials were in the range of 2.1 MPa to 16.4 MPa with the dominant value between 5 MPa and 10 MPa. For both techniques there is a wide range of difference in the obtained results for the compressive strength tests. This was because researchers have tested samples with different sizes and shapes by following different standards. For example, the lowest compressive strength for the solidification technique was 2.1 MPa obtained by testing cylindrical samples (38mm in diameter and 76mm in height) in according with BS 1924-2:1990 (Oti et al., 2014). On the other hand, the maximum compressive strength of 79 MPa was obtained using the technique of alkali activation for cylindrical samples with dimensions 20.15 mm in diameter and 20 mm in height (Mohsen and Mostafa, 2010). Furthermore, samples with rectangular shapes were considered by different researchers. For example, (Sekhar and Nayak, 2018) tested samples with dimensions of 355 x 180 x 110 mm for compressive strength according to ASTM

C140, while Sore et al. (2018) followed the XP P13-901 standards for testing the compressive strength of samples with dimensions of 140 x 140 x 95 mm.

Regarding the durability assessment, most of the unfired building materials considered the water absorption test as a durability measurement (Murmu and Patel, 2018). According to Table 0-1 and Table 2-2, the water absorption values for solidified building materials was in the range of 2.7% to 18.5% with an average value of about 10% and was significantly higher than the water absorption values for alkali activated building materials (3.7% to 4.7%).

Since clay-based building materials are recognised as materials which contribute towards the thermal insulation of buildings and consequently increase indoor comfort, some of the research projects (Saidi et al., 2018, Zhang et al., 2017, Rahmat et al., 2016, Sore et al., 2018, Leitão et al., 2017) investigated this property. The results indicated that the thermal insulation of the clay-based units has been reduced slightly with the increase in the binder content (Saidi et al., 2018, Zhang et al., 2017, Rahmat et al., 2016), however, the use of alkali activators and especially in the presence of FA improved the thermal insulation of the clay-based units (Sore et al., 2018, Leitão et al., 2017).

### *2.3.2 Environmental assessment*

From an environmental point of view, the construction industry is responsible for about 40% of the energy consumption worldwide, nearly 30% of the global greenhouse gas emissions, generation of solid waste, depletion of natural resources and environmental damage (Joglekar et al., 2018). Therefore, the construction industry is looking for alternative techniques and materials with the aim of moving towards more sustainable development. The main advantages of using sustainable techniques and materials are to protect the environment and ecology, reduce the depletion of natural resources, energy efficiency and healthy outdoor and indoor environments (Joglekar et al., 2018, Chong et al., 2009).

The main goal of this study is to assess the environmental impact of different techniques used in the production of unfired building materials, and to compare them with traditional fired building materials. The assessment criteria include quantifying the consumption of energy, consumption of natural resources, consumption of fossil fuel and production of greenhouse gases.

The production of building materials through firing is considered the most significant impact on the environment. This is because of the high temperature kiln firing needed that consumes significant amounts of energy, along with releasing large quantities of greenhouse gases including $CO_2$ (attributed to the utilisation of coal for the firing process) (Joglekar et al., 2018, Zhang, 2013). Additionally, in some cases where the coal used for firing is of low quality, this could significantly contribute to the acidification due to the release of $SO_2$ emissions and the formation of NOx (Joglekar et al., 2018, Sunil Kumar et al., 2016). Furthermore, the production of fired building materials contributes considerably to the depletion of fossil fuels as firing is obtained mainly from coal (Joglekar et al., 2018).

On the other hand, the production of unfired building materials through solidification seem to be the trend to follow to achieve sustainable development in the construction industry in terms of environmental concerns. However, the solidification technique involves the addition of cementing material(s) such as lime or/and cement, whose manufacture requires intensive energy, consumes huge quantities of natural resources along with releasing huge quantities of $CO_2$ emissions (Joglekar et al., 2018, Marcelino-Sadaba et al., 2017, Zhang, 2013). The manufacture of Portland cement consumes about 5.6 GJ of energy and requires approximately 1.5 tonnes of raw materials along with the production of about 7% of $CO_2$ emission in the atmosphere (Jafer et al., 2018b). Additionally, the production of solidified building materials contributes to greater water depletion that is needed for the curing process and lower consumption of fossil fuels relative to fired building materials (Joglekar et al., 2018).

In comparison with the aforementioned production techniques, the production of building materials through alkali activation (geopolymerisation) consumes much less energy and releases considerably lower quantities of greenhouse gases (Zhang, 2013). Therefore, the environmental burden of the alkali activated building materials is generally lower than fired or solidified building materials (Poinot et al., 2018). However, the production of alkali activated building materials is also associated with some environmental impacts that are mainly attributed to the utilisation of alkali activators (Turner and Collins, 2013). The manufacture of the alkali activators requires intensive energy. Additionally, in order to achieve reasonable strength for alkali activated building materials, there is a need for curing at elevated temperatures ($40^oC$-$80^oC$), that means extra energy consumption (Turner and Collins, 2013, Zhang, 2013).

## 2.4 Summary

This chapter provided a detailed review regarding the environmental issues associated with the production of building materials through firing. Additionally, it presented a detailed review about the alternative methods in the production of building materials. The reviewed techniques in the production of unfired building materials were: solidification and alkali activation. According to the reviewed studies, cement and/or lime are the preferable binders to improve the technical performance of the solidified building materials. However, the use of cement and/or lime is characterised with negative environmental impacts specifically the $CO_2$ emissions. The literature also revealed that although the production of unfired building materials through alkali activation (geopolymerisation) is associated with some negative environmental impacts, it has a lower environmental impact and relatively superior mechanical and durability performance. According to the comparative assessment of the techniques used in the production of unfired building materials (Section 2.3), the production of unfired building materials through alkali activation (geopolymerisation) is seen to be the best production technique, as it has shown better technical and environmental performance relative to the solidification technique. According to the available literature, there was no study conducted that employed the technique of alkali activation in the production of unfired brick using CFC. Therefore, this research was conducted with the aim of developing a novel alkali activated brick using CFC as an alternative to conventional fired bricks.

# CHAPTER 3: RESEARCH METHODOLOGY AND MATERIALS

## 3.1 Research Methodology

This chapter presents a description of the materials, equipment and methods of testing that were used to achieve the objectives of this research project. The experimental work for this research was conducted in seven stages in order to achieve the corresponding aim of this project. These stages are the characterization of the physical, chemical and microstructural properties of the CFC and the candidate materials, selected candidate mix design, selected candidate of different methods of curing, the physical, chemical and microstructural properties of the selected candidate mixture, the production of unfired brick using the selected candidate mix design with the same dimensions (215mm x 102.5mm x 65mm) of building bricks and to evaluate its performance against standard specifications, a comparison between $CO_2$ production of the new brick and conventional fired brick during the manufacturing and operational processes and finally a cost analysis of the developed brick and compare it against the conventional fired brick.

## 3.2 Materials

### *3.2.1 Clay Filter Cake (CFC) Waste*

The Clay Filter Cake (CFC) waste is produced during the washing of recycled C&D wastes at washing plants to produce recycled sand and aggregate with specified size and quality. The CFC was supplied by CCC Waste Management, Kirkby, UK. The CFC has been supplied within heavy duty plastic bags with around 20 kg in each. Upon the arrival of CFC at the laboratory, representative samples were taken from different bags directly to calculate the moisture content of the CFC according to the BS EN ISO 17892-1:2014 (European Committee for Standardization, 2014). The remaining samples were oven dried at 105$^{o}$C for 24 hours, to be prepared for the required experimental works at later stages. Experimental investigations were carried out to identify physical, chemical, and microstructural properties of the CFC.

### *3.2.2 Potential Candidate Materials*

In order to improve the performance of the CFC during the alkali activation, different by-product materials were identified from the literature review that can be blended with CFC in the production of unfired alkali activated brick. Four different by-product materials, which are produced from different industrial sectors within the UK were identified in this study. The materials were Ground Granulated Blast Furnace Slag (GGBS), Pulverised Fuel Ashes (PFA) (Class F fly ash), Cenin Fly Ash (CFA) (Class C fly ash) and Metakaolin (MK). There were many aspects that were taken into consideration in selecting the potential candidate materials including that these materials were the main materials that blended with clay in the production of alkali activated building materials according to the literature review. Additionally, all the candidate materials were produced within the UK to reduce the cost and environmental impact of the transportation of these materials. Moreover, the availability of such materials in huge quantities, so that there will be sufficient supply for potential commercialisation of the unfired brick that will be developed from the current research, was an important consideration. The description and source of each of the identified candidate materials are presented in Table 0-1.

Table 0-1. Description and sources of the identified candidate materials

| Material | Description and Source |
|---|---|
| **GGBS** | A white sample of GGBS that classified under BS EN 15167-1 standard was supplied by Hanson Heidelberg Cement group, Scunthorpe, UK. |
| **PFA** | A dark grey sample of PFA was collected from Cemex Ltd company, Warwickshire, UK. The sample is fly ash type 450-S according to the British Standard. |
| **CFA** | Cenin Fly Ash is a formulation predominantly consisting of a fine powder of mainly spherical, glassy particles, derived from burning of pulverised coal with a combination of supplementary hydraulic cementitious materials. The CFA was supplied by Cenin Ltd, Bridgend, UK. |
| **MK** | MK is an artificial pozzolana obtained by calcining and micronising a kaolinic clay from the Charentes basin. The MK was supplied by Mike Wye & Associates Ltd, Buckland Filleigh, UK. |

### *3.2.3 Alkali Activators*

According to the literature review, the most common alkali activators are sodium hydroxide (NaOH) and sodium silicate ($Na_2SiO_3$). Therefore, these two alkali activators were used in this research.

- Sodium hydroxide (NaOH): it was obtained as pellets from Fisher Scientific, Leicestershire, UK.
- Sodium silicate solution ($Na_2SiO_3$): it was obtained as a solution from Fisher Scientific, Leicestershire, UK.

### *3.2.4. Sand*

The sand used in this investigation was Tarmac Maxipack Kiln Dried Paving Sand. The particle size distribution of the sand is shown in Figure 3-1.

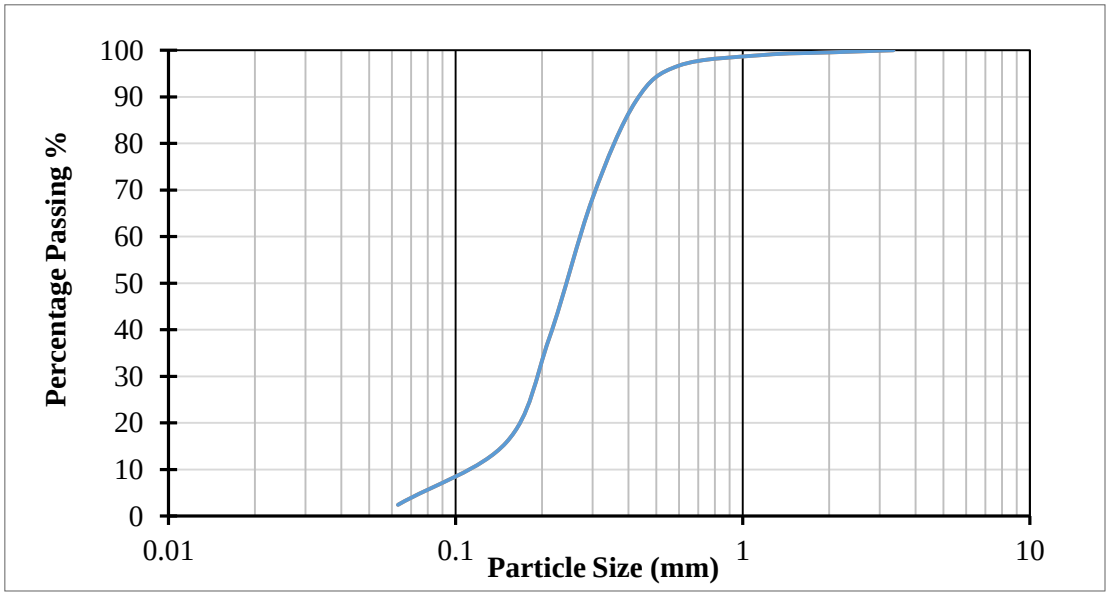


Figure 3-1. Particle size distribution of the sand

### *3.2.5 Water*

The water used in this research was tap water supplied by United Utilities (City of Liverpool).

## 3.3 Programme of Laboratory works and Testing Equipment

The laboratory work consisted of the following work packages

- Characterising the physical, chemical and microstructural properties of CFC and other by-product materials (GGBS, PFA, CFA and MK) using different identification techniques. For example, moisture content, particle size distribution (PSD), specific surface area (SSA), pH, Loss on Ignition (LoI), specific gravity, energy dispersive X-ray fluorescence (EDXRF), and scanning electron microscopy (SEM).
- Activating the CFC using alkali activation solution and blending with the selected by-product materials to develop unfired brick. Then the effect of each of the selected materials on the performance of brick was evaluated by testing compressive strength using different curing methods and at different curing periods.
- Identifying the best candidate material that provided the highest compressive strength upon blending with CFC and using it in combination with CFC for further investigations.
- Investigating the properties of the developed bricks in terms of mix design and methods of curing.
- Identifying the selected candidate mix design and curing method that provides acceptable compressive strength.
- Evaluating the microstructural performance of the selected candidate blend of the binder materials using Scanning Electron Microscopy (SEM) with Energy Dispersive X-ray Spectroscopy (EDS) analysis.
- Using the selected candidate mix design in the production of alkali activated unfired bricks with similar sizes (215 x 102.5 x 65 mm) to commercially available fired bricks.
- Evaluating the durability of the developed alkali activated unfired bricks under various types of exposure such as water absorption and freezing and thawing.
- Evaluating the thermal properties of the developed product by determining thermal conductivity, specific heat capacity and volume heat capacity.
- Conducting a comparison between $CO_2$ production during the manufacturing and operational processes of the new brick and conventional fired brick
- Conducting a cost analysis of the developed brick and compare it against the conventional fired brick.

The methods and equipment of testing that have been used during this study alongside the details for preparing the samples for different testes are explained as follows:

### *3.3.1 Moisture content (%)*

The moisture content of the CFC was investigated directly upon the arrival of the CFC at the laboratory. This test was conducted according to the BS EN ISO 17892-1:2014 (European Committee for Standardization, 2014).

### *3.3.2 Loss on Ignition (LoI)*

The loss of ignition is a method to find the content of the organic matter in CFC and other binder materials (GGBS, PFA, CFA and MK); the adopted procedure is described in BS EN 196-2:2005 (British Standard, 2005a). Figure 3-2 shows the CFC and other binder materials after the LoI testing.

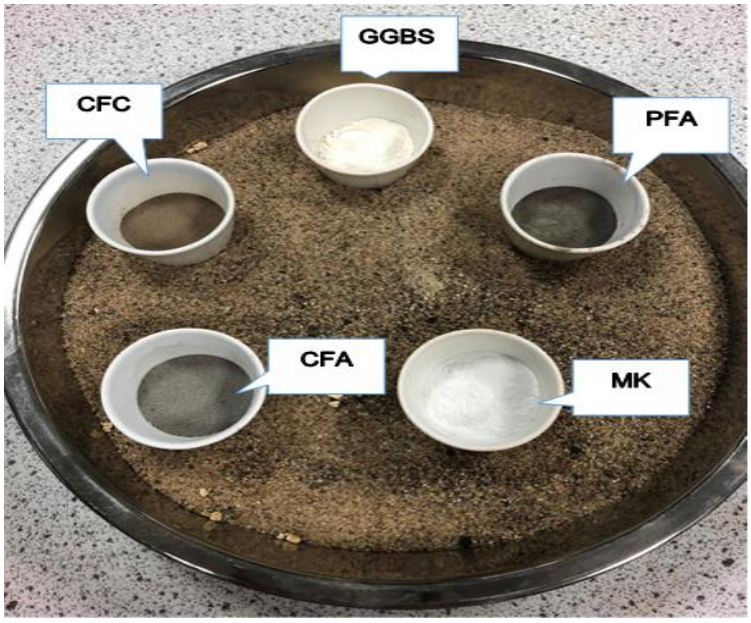


Figure 3-2. LoI test for CFC and other candidate materials

### *3.3.3 pH Measurements*

Solutions of dried and pulverised materials with water (1 part by mass with 5 parts distilled water) were made to identify the pH value of the CFC and all other candidate materials. This method of measuring the pH is according to BS EN 450:1995 (British Standard, 1999) using the pH meter as shown in Figure 3-3.

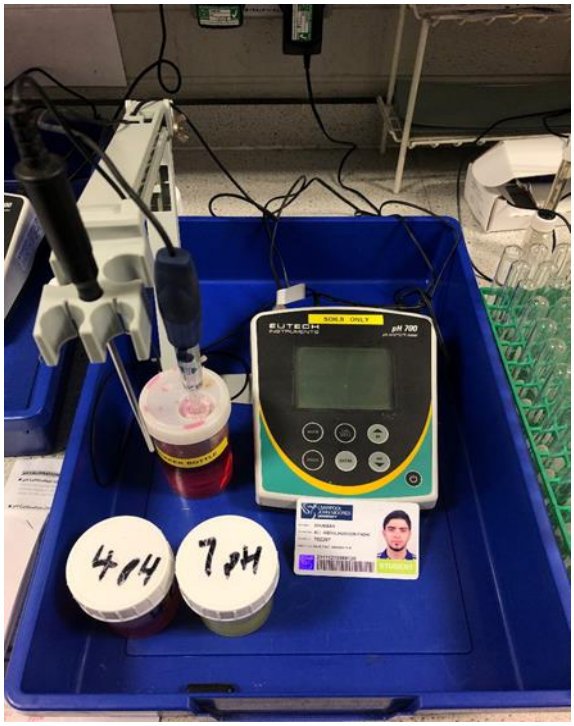


Figure 3-3. pH measurement test apparatus

### *3.3.4 Specific surface area (SSA)*

For measuring the SSA of the CFC, the CFC was firstly dried in the oven for 24 hours at 105 $^{o}$C and then the CFC was crushed manually using a hammer. After that the crushed CFC was ground using a pestle and mortar grinder for 3 minutes to form a fine powder. The SSA of the produced fine powder along with the candidate materials were determined using the Blaine air-permeability apparatus (Figure 3-4) in accordance with BS EN 196-6:2018 (British Standard, 2018).

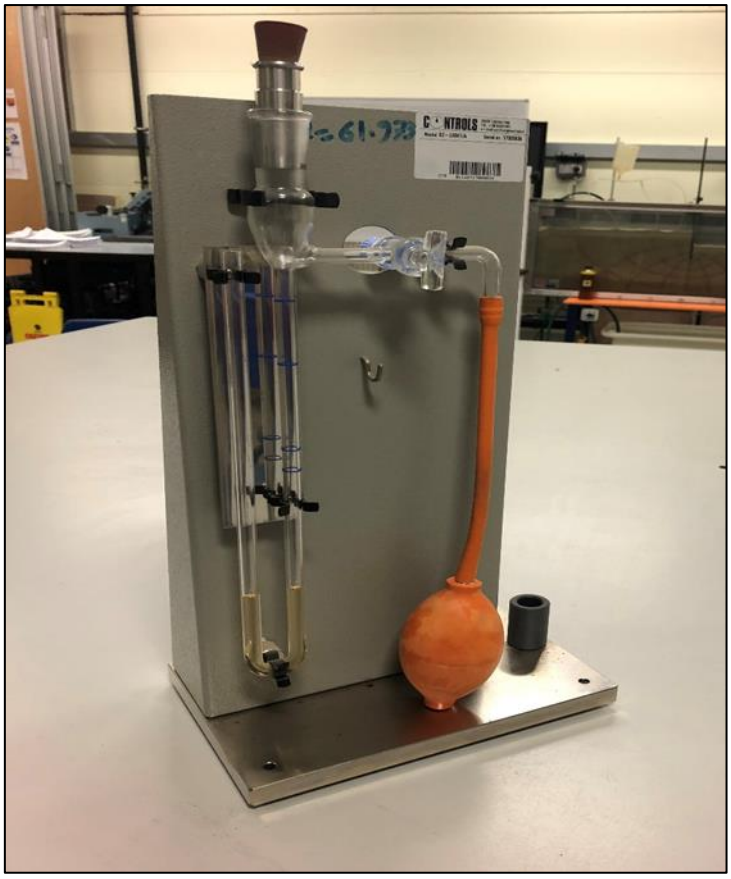

Figure 3-4. Blaine air-permeability apparatus

### *3.3.5 Particle size distribution (PSD)*

To determine the PSD of the CFC, the same method for sample preparation as mentioned in section 3.3.4 was adopted. The PSD of the CFC and the other candidate materials were determined using Laser Diffraction Particles Analyser (brand - Beckman Coulter) as shown in Figure 3-5. The Beckman Coulter LS 13 320 uses reverse Fourier optics incorporated in a patented fibre optic spatial filter system and a binocular lens system. Consequently, the LS 13 320 is enabled to optimize light scattering measurement across the widest dynamic range, from 40nm to 2000µm, in a single scan with no extrapolation (Beckman Coulter, 2009).

Figure 3-5. Laser Diffraction Particles Analyser

### *3.3.6 Particle Density (Specific Gravity, Gs)*

The particle density of the CFC and the other candidate materials was determined using an automatic gas expansion multi-pycnometer as shown in Figure 3-6. A dry sample was placed in the sample cell and degassed by purging with a flow of dry helium gas by vacuum. The test was conducted by pressurizing the sample cell to about 17 psi and recoding the value. The selector valve was then rotated so the gas expanded into the reference and that lower pressure of less than 7 psi was recorded. From the obtained two values, the volume of the sample was calculated using the volume-pressure relationship (Equation (1)),known as Boyle's Law. As the volume was determined from this relationship and the corresponding weight of each sample was recorded at the start of the test, then the particle density was calculated accurately by using Equation (1).

$$e = \frac{m}{v} \quad \text{.....(1)}$$

Figure 3-6. Multi-pycnometer used for density measurement of powders.

### *3.3.7 Compressive strength*

Compression testing was performed in accordance with BS EN 196-1 (BSI, 2005) using a compression machine (brand Control Automax 5) (Figure 3-7). This machine is featured with an accurate application of loading rate and the failure data can be obtained and downloaded to a computer connected to the machine. The data are presented in both loads and stresses directly. The rate of loading used during this investigation for the compressive testing machine was (0.4 MPa/s). Samples from each of the investigated stages were tested after 7, 14 and 28 days of both air curing and water curing. Two specimens of dimensions 40 x 40 x 160 mm, were prepared for each mixing proportion, curing age and curing method. Each specimen was broken into two halves using three-point loading of the prism samples and averages of four halves were taken to represent the final values for compressive strength. The compressive strength testing was also performed on the selected candidate mix design named as the Novel Alkali Activated Unfired Brick (NAAUB) at 1, 3, 7, 14 and 28, 56, 90 and 180 days of curing under different curing methods (water curing, air curing and water curing temperatures). The compressive strength test was also performed for the NAAUB with dimensions of (215 x 102.5 x 65 mm) after 7, 14 and 28 days of curing using the selected candidate method of curing in order to make a direct comparison with commercially available fired bricks according to BS

EN 772-1:2011+A1:2015 (British Standard, 2015). Five samples of the NAAUB with the size of 215 x 102.5 x 65 mm and tested for compressive strength.

Figure 3-7. Control Automax 5 compressive strength machine

### *3.3.8 Flexural strength*

Flexural testing was conducted after finding the NAAUB. Three prism specimens of dimensions 40 x 40 x 160 mm, were prepared and tested for flexural strength after 1, 3, 7, 14 and 28, 56, 90 and 180 days of curing under different curing methods. The flexural strength of the NAAUB was determined by three-point loading of the prism specimens (Figure 3-8) and averages of the three samples were taken to represent the final values for flexural strength according to BS EN 196-1(BSI, 2005).

Figure 3-8. Flexural strength testing of prism mortar.

### *3.3.9 Water absorption*

The water absorption test was conducted for the NAAUB specimens according to BS EN 771-1:2003+A1:2005 (British Standard, 2005b). After the required time of curing has been obtained (7 days in this research), ten bricks were dried in an oven at 105 ± 5 °C for 24 hours and then the dry mass ($m_d$) of samples was recorded. Then each sample was submerged in a water tank (the samples were resting on small pads to allow water to be in contact with all faces) at room temperature for 24 hours. After that, the samples were taken out from the tank and any surplus water from their surfaces was removed using a damp cloth. The wet mass ($m_w$) of each sample was recorded. Then the mean water absorption (W***m***) was determined using Equation (2):

$$W\mathrm{m} = \frac{m_w - m_d}{m_d} \times 100\ \% \quad \text{.....(2)}$$

### *3.3.10 Freeze and thaw*

The freeze-thaw testing was conducted for the NAAUB samples in accordance with DD CEN/TS 12390-9:2006 (British Standard, 2006). This test was preformed using Temperature Chamber TC-ME-025/065/100 (Figure 3-9). The apparatus consisted of refrigerating and heating units, with continuous freeze and thaw cycles at chamber temperatures in the range of ±20$^{o}$C. Wet freezing-thawing test was conducted for the NAAUB after 7 days of curing using the selected candidate curing method in order to evaluate the performance of the developed

NAAUB after 7, 14, 21, 28, 42, 56, 90 and 180 cycles of freeze and thaw. Three samples with the dimensions of (215 x 102.5 x 65 mm) were subjected to the freeze and thaw cycles and the weight loss after 7, 14, 21, 28, 42, 56, 90 and 180 cycles of freeze and thaw was recorded and compared with that of the conventional fired brick.

Figure 3-9. Temperature Chamber TC-ME-025/065/100 for freeze and thaw testing

### *3.3.11 Thermal Properties*

Thermal conductivity, specific heat capacity and volume heat capacity tests were used to evaluate the ability of different materials to transfer heat by conduction. The thermal conductivity, specific heat capacity and volume heat capacity measurements of the developed NAAUB were conducted using ISOMET 2114 meter. This meter can provide information about thermal conductivity ($\lambda$), volume heat capacity (*cp*) and temperature of the tested material. This method of testing the thermal properties of the bricks is a transient method not steady state method and only used for comparison between developed brick and conventional fired brick. The test specimen of dimensions (215 x 102.5 x 65 mm) with a density of 2300 kg/m$^3$ was prepared and tested using the 60 mm diameter circular contact probe (Figure 3-10). Thermal measurements were carried out at a range of temperatures ranging between -5$^o$C and 40$^o$C taking into consideration the temperature profile in the UK.

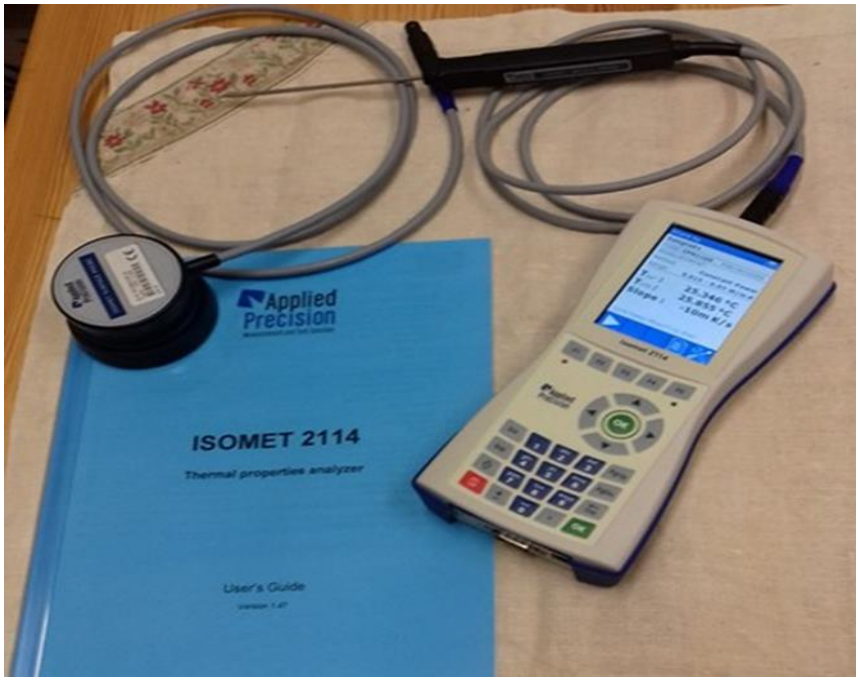


Figure 3-10. ISOMET 2114 meter

### *3.3.12 Energy Dispersive X-Ray Fluorescence (EDXRF) spectrometer*

A Shimadzu EDX-720, EDXRF, was used in this study to identify the elemental compositions of the CFC alongside the candidate materials. EDXRF (Figure 3-11) is one of the non-destructive applications that have been used for analysing the elemental compositions (major oxides and trace elements content) of the CFC and candidate materials quantitatively.

Figure 3-11. EDXRF spectrometer

### *3.3.13 Microstructural analysis*

Scanning Electron Microscopy (SEM) with Energy Dispersive X-ray Spectroscopy (EDS) testing were used for evaluating the morphology of each of the CFC and the other candidate binder materials, along with the morphology and the atomic changes in elemental composition of the NAAUB paste, after 3, 7, 28 and 180 days of curing using different curing methods. This testing was conducted using an EDX Oxford Inca x-act detector, an FEI SEM model Inspect S and a Quanta 200 with an accelerating voltage of 5–20 kV. In order to increase the visibility of the samples, the samples were coated with a layer of gold using a sputter coater before starting the SEM/EDS testing.

## 3.4 Sample preparation for different tests

For different experimental investigations, the CFC was firstly dried in the oven for 24 hours at 105$^{o}$C and then the CFC was crushed manually using a hammer. After that the crushed CFC was ground using a pestle and mortar grinder for 3 minutes to form a fine powder. The prepared CFC was used for material identification purposes (LoI, pH, SSA, PSD, specific gravity, EDXRF and SEM testes) while the candidate materials were subjected directly to the aforementioned tests.

### *3.4.1 Compressive Strength and flexural strength of the unfired brick with dimensions of (160 x 40 x 40 mm)*

During all the investigated stages, bricks were cast as small prisms with dimensions of 160 x 40 x 40 mm for many reasons including that these prisms required a small amount of materials for preparations of samples and there were sufficient prism moulds in the lab to investigate different parameters such as different methods of curing at the same time that in turn positively affected the progress of the project. The following steps were followed in the preparation of unfired brick samples with dimensions of (160 x 40 x 40 mm).

1. The NaOH has been initially prepared by dissolving the NaOH pellets in distilled water then the NaOH solution was left to cool down at room temperature for 24 hours before using.

2. Prepare all the material needed for the mix, this starts with weighing the sand, CFC, candidate materials, NaOH, $Na_2SiO_3$ and the water.

3. Initially, the sand, CFC and candidate material were mixed together for 3 minutes, and then a mixture of the liquid materials (NaOH, $Na_2SiO_3$ and water) was added to the mix and mixed for 2 minutes.

4. Then the mixture was cast inside the steel prism moulds with dimensions of (160mm x 40mm x 40mm) and according to BS EN 196-1 (BSI, 2005) as shown in Figure 3-12.

5. The prisms were demoulded after 24 hours from the start of the casting process and the samples were cured using different methods of curing.

Figure 3-12. The mortar specimens with the dimensions of (160 x 40 x 40 mm)

### *3.4.2 Compressive strength, water absorption, freeze and thaw, thermal of the NAAUB with dimensions of (215 x 102.5 x 65 mm)*

The same (first 3 steps) procedure in section 3.4.1 was adopted in the preparation of the NAAUB for preparing the NAAUB with dimensions of (215 x 102.5 x 65 mm). After that the NAAUB was moulded using a hydraulic pressure of 1.5 MPa. The hydraulic pressure was applied using a Clark manual hydraulic jack. The samples were demoulded after 24 hours from the start of the casting process and cured using the selected candidate curing method. Preparation of the brick sample with dimensions of (215 x 102.5 x 65 mm) is shown in Figure 3-13. The depth of the mould was 100 mm and in order to obtain the required depth of brick

(65mm) to steel bars were fixed at the top of the compression plate. The function of these steel bars is to stop the compression plate upon reaching the required depth of brick (65mm).

Figure 3-13. Preparation of the brick sample with dimensions of (215 x 102.5 x 65 mm)

### *3.4.3 Microstructural analysis (SEM/EDS)*

Before starting the SEM/EDS test there were some steps that were followed for achieving the purpose of the test. The following are the steps that were followed in this test:

- Preparing a paste from the NAAUB without sand then casting in small containers for 24 hours to set.
- Demoulding the sample and curing it using different methods of curing until the time of testing.
- One day before the test, the samples from different methods of curing were broken into small pieces and placed in the oven at 40$^{o}$C to dry.

- At the time of testing, in order to observe a clear image, the samples should not move. For that reason, samples were attached to the aluminium stub by using a small sticky carbon tab that stuck to the surface of the stub, and following this, the specimen can be stuck down, as shown in Figure 3-14. This in turns reduces damage to the specimens by reducing the number of times the specimens are being touched, as the stub can be picked up instead.

Figure 3-14. The aluminium stub

- To improve the quality of the image, the samples were coated with gold (Figure 3.15). The coating should be thin so that details of the surface are not covered.

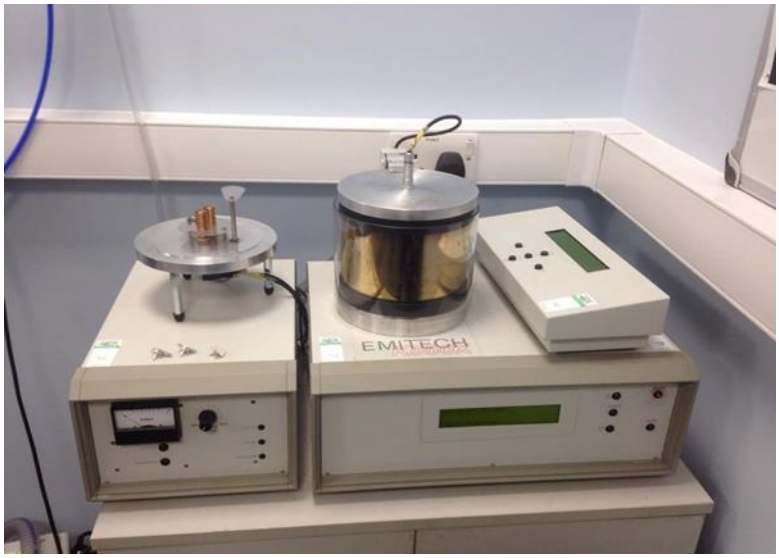


Figure 3-15. The gold coating of the samples.

- The final step in this test was inserting the samples inside the SEM/EDS machine and starting the test. Figure 3.16 shows the machine of the SEM/EDS test.

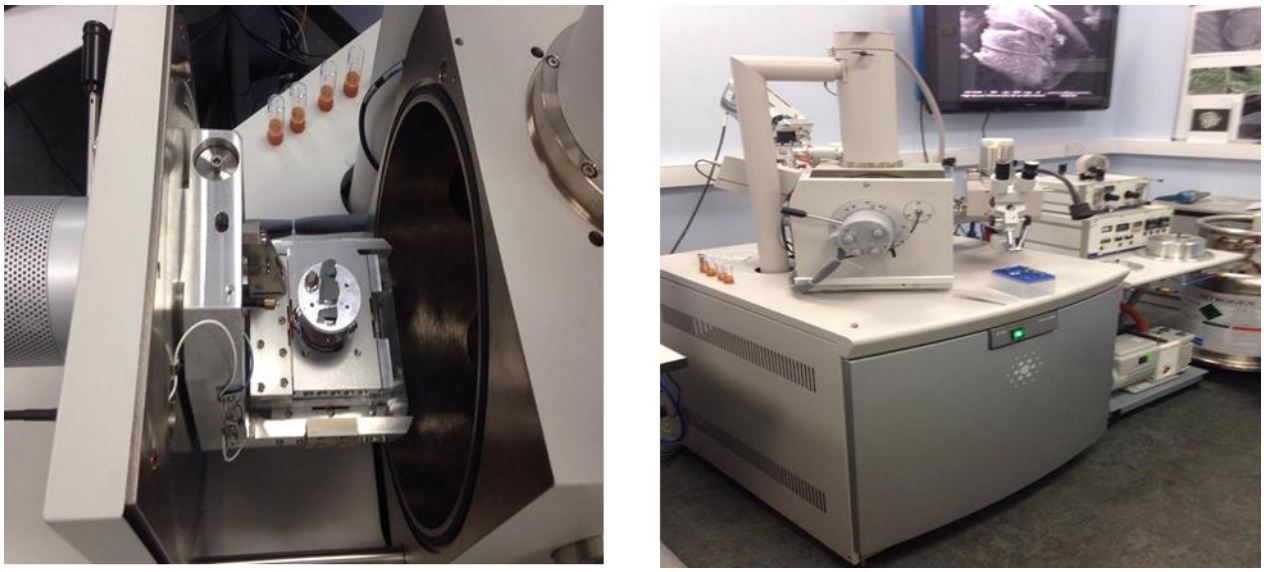

Figure 3-16. Placing the samples inside the SEM/EDS machine and starting the test

### 3.5 $CO_2$ calculations of the NAAUB during the manufacturing and operational processes

For calculating the $CO_2$ emissions of the NAAUB during the manufacturing process, the $CO_2$ emissions for each of the raw materials used in the production of the NAAUB, along with the electricity needed for the preparation of the brick (crushing, grinding and mixing of the raw materials) were obtained from the available literature. Additionally, in this study, energy simulation software "Design Builder" was used to model an office building in Liverpool, UK to evaluate the $CO_2$ emissions of conventional fired brick against the NAAUB during the operational phase. Design Builder is one of the most comprehensive user interfaces for the EnergyPlus dynamic thermal simulation engine (Ramesh et al., 2012). Design Builder generates detailed $CO_2$ emissions data for 1 year by simulation using real weather data (Ramesh et al., 2012). Hourly weather files of Liverpool from Design Builder database were used for the simulation.

### 3.6 Summary

A summary for the tests that were used to characterise the physical, chemical and microstructural properties of the CFC and the candidate materials is presented in Table 0-2. Additionally, Table 3-3 presents the summary for the specifications that were followed in this research for different tests.

Table 0-2. CFC and candidate materials identification tests.

| Test/Analysis | CFC | GGBS | PFA | CFA | MK |
|---|---|---|---|---|---|
| **Moisture content (%)** | * | | | | |
| **Loss on Ignition (%)** | * | * | * | * | * |
| **pH value** | * | * | * | * | * |
| **SSA** | * | * | * | * | * |
| **PSD (laser particle analyser)** | * | * | * | * | * |
| **Particle density (Specific gravity),Gs** | * | * | * | * | * |
| **EDXRF** | * | * | * | * | * |
| **SEM** | * | * | * | * | * |

Table 3-3. Test method used for analysis of samples.

| Property tested | Test/Technique used |
|---|---|
| **Moisture content** | BS EN ISO 17892-1:2014 |
| **Loss on Ignition** | BS EN 196-2:2005 |
| **pH value** | BS EN 450:1995 |
| **Specific surface area (Blaine)** | BS EN 196-6:2018 |
| **Particle size distribution** | Laser particle analyser |
| **Particle Density (Specific Gravity)** | Gas pycnometer |
| **Compressive Strength** | BS EN 196-1 and BS EN 772-1:2011+A1:2015 |
| **Flexural strength** | BS EN 196-1 |
| **Water absorption** | BS EN 771-1:2003+A1:2005 |
| **Freeze and thaw** | DD CEN/TS 12390-9:2006 |
| **Thermal properties** | ISOMET 2114 |
| **Oxide composition** | EDXRF |
| **Morphology** | SEM/EDS |
| **$CO_2$ emissions** | Excel and Design Builder software |
| **Cost Analysis** | Excel |

# CHAPTER 4: RESULTS AND DISCUSSION

## 4.1 Introduction

This chapter presents the results obtained from the all the experimental works and gives reasonable explanations for these data. Generally, this chapter has been divided into seven main sections in order to present the results of the experimental works in a clear and understandable way.

## 4.2 Section (1): Materials Characterization

### *4.2.1 Introduction*

This part of Chapter 4 presents the results of the experimental works regarding the characterisation of the physical, chemical and microstructural properties of the CFC along with the candidate materials used in this research project. For each of the physical and chemical properties investigated in this section, the test was repeated three times and the average value was considered and presented in Tables 4.1- 4.4 and Figures 4.1 and 4.3.

### *4.2.2 Properties of the clay filter cake (CFC)*

The CFC has a moisture content in the range between (39%-41%). The chemical compositions, pH value and LoI of the CFC used in this research project are presented in Table 4-1. It can be seen from Table 4-1 that the CFC has high silica oxide with high calcium oxide and moderate content of $Al_2O_3$. The nature of the chemical composition present in the CFC is appropriate for the application of geopolymerisation as reported by Lampris et al. (2009). As CFC has a high content of calcium oxide alongside the content of silicates and aluminates, calcium silicate hydrates (C-S-H) gel will be formed in conjunction with geopolymeric gel within the hydration products, that in turn contribute to enhance the strength and durability performance of the final product (Yun-Ming et al., 2016, Yunsheng et al., 2007, Yip and Van Deventer, 2003).

Table 4-1. The chemical properties and EDXRF analysis of the CFC

| Item | CFC 1 | CFC 2 | CFC 3 | CFC 4 | CFC 5 | Ava |
|---|---|---|---|---|---|---|
| **CaO %** | 18.1 | 16.9 | 17.1 | 17.5 | 17.9 | 17.5 |
| **$SiO_2$ %** | 53.1 | 52.8 | 56.2 | 57.4 | 56.8 | 55.3 |
| **$Al_2O_3$ %** | 6.4 | 6.5 | 6.9 | 6.3 | 7.2 | 6.7 |
| **$Fe_2O_3$ %** | 6.7 | 6.7 | 6.8 | 6.4 | 6.8 | 6.7 |
| **MgO %** | 5.2 | 5.5 | 5.3 | 4.9 | 5.6 | 5.3 |
| **$Na_2O$ %** | 2.3 | 2.3 | 2.4 | 2.4 | 2.4 | 2.4 |
| **$K_2O$ %** | 4.2 | 4.7 | 4.9 | 4.2 | 4.5 | 4.5 |
| **$TiO_2$ %** | 0.7 | 0.8 | 0.8 | 0.8 | 0.9 | 0.8 |
| **MnO %** | 0.1 | 0.1 | 0.1 | 0.1 | 0.1 | 0.1 |
| **LoI** % | 15.4 | 15.4 | 15.6 | 15.1 | 14.9 | 15.3 |
| **pH** | 8 | 7.9 | 8.1 | 8.1 | 8 | 8.0 |

The particle size distribution of the processed fine powder of the CFC is presented in Figure 4-1. The Physical properties such as the Blain Specific Surface Area (SSA), specific gravity (Gs), mean PSD, and the median ($d_{50}$) PSD of the CFC are presented in Table 4-2. The shape of the particles of the raw materials has an influence on fresh and hardened properties of the produced materials, thus SEM images of the raw materials can aid to elucidate the behaviour of these materials when they were blended to produce alkali-activated Materials (Wattimena et al., 2017). The SEM image of the CFC in its dry state is shown in Figure 4-2. This figure shows that the CFC has coagulated particles with irregular shapes that could reduce the workability due to the absorption of more liquid by the large open areas of high porosity (Jafer et al., 2018a).

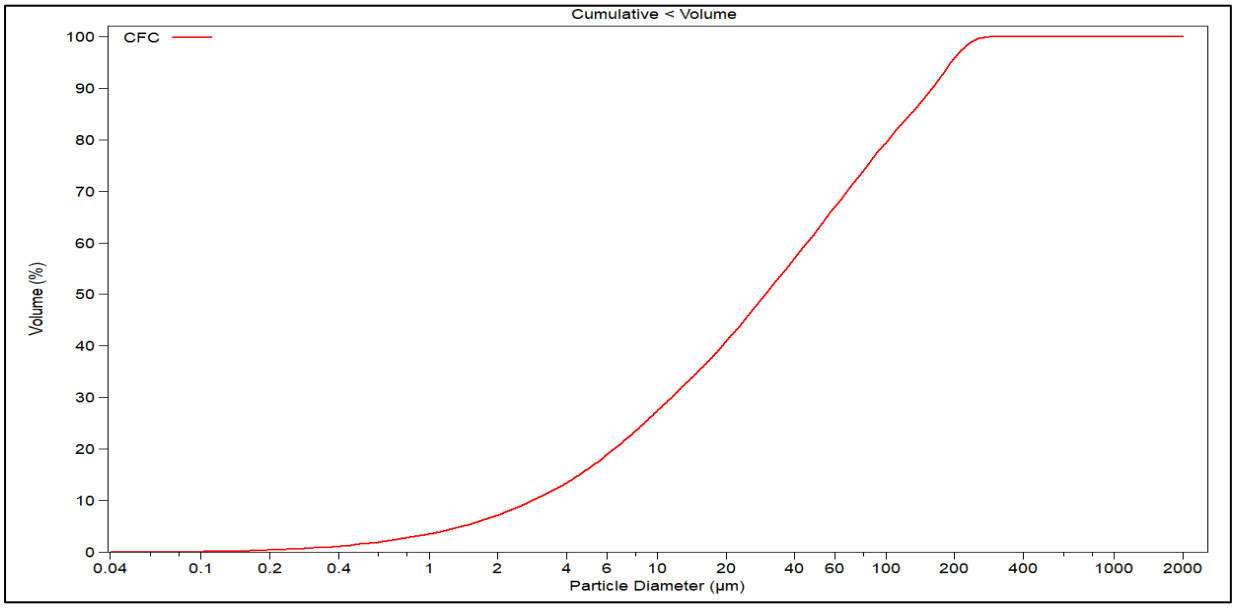


Figure 4-1. Particle size distribution of the CFC

Table 4-2. The Physical properties of the CFC.

| Item | CFC |
|---|---|
| **$d_{50}$ (µm)** | 29.72 |
| **Mean Diameter (µm)** | 55.82 |
| **Blaine SSA ($cm^2/g$)** | 3436 |
| **Specific gravity (Gs)** | 2.76 |

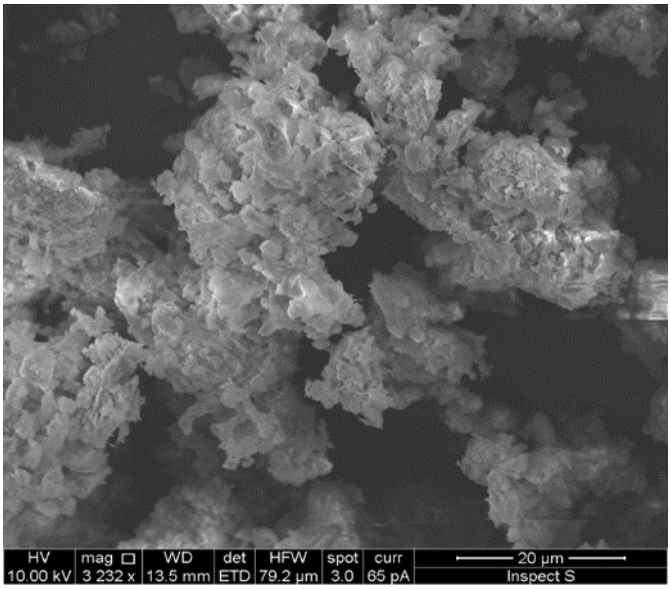


Figure 4-2. The SEM image of the CFC (dry powder)

### *4.2.3 Comparison between the chemical and physical properties of the candidate materials*

As stated in the methodology, four industrial by-product materials were investigated to evaluate their potential employment in the production of alkali activated unfired brick. This section presents a comparison between the chemical, physical and microstructural properties of all the candidate materials. The aim of the chemical and physical characterisation of the candidate materials is to evaluate the suitability of these materials to be used in combination with the CFC in the production of alkali activated unfired brick. It is well understood that the chemical compositions of the raw materials have significant influence upon the properties of the alkali activated unfired brick (Muñoz Velasco et al., 2014). Therefore, the chemical composition of the candidate materials was tested to elucidate the performance of these materials when they are combined with CFC and activated chemically by alkali activators to produce alkali activated brick. The chemical composition of all the candidate materials as collected from the EDXRF test are presented in Table 4-3.

Table 4-3. Comparative chemical properties of candidate materials.

| Item | GGBS | PFA | CFA | MK |
|---|---|---|---|---|
| **CaO %** | 43.83 | 4.81 | 28.46 | 0.02 |
| **$SiO_2$ %** | 38.13 | 58.83 | 43.47 | 45.25 |
| **$Al_2O_3$ %** | 5.98 | 18.83 | 4.74 | 44.63 |
| **$Fe_2O_3$ %** | 0.82 | 5.54 | 5.06 | 0.348 |
| **MgO %** | 4.99 | 3.86 | 4.91 | 0.41 |
| **$Na_2O$ %** | 2.93 | 1.17 | 1.41 | 0.90 |
| **$K_2O$ %** | 1.60 | 2.04 | 2.05 | 0.13 |
| **$TiO_2$ %** | 0.88 | 1.06 | 1.10 | 0.36 |
| **MnO %** | 0.83 | 0.19 | 0.18 | 0.12 |
| **LOI %** | 0.74 | 8.42 | 4.25 | 0.48 |
| **pH** | 10.92 | 10.68 | 12.36 | 6 |

As both GGBS and CFA have high content of calcium oxide alongside the content of silicates and aluminates, the blending of each of these materials with the CFC is chemically activated with alkali activators, and calcium silicate hydrates (C-S-H) gel is expected to be formed in conjunction with geopolymeric gel within the hydration products as reported previously (Yun-Ming et al., 2016, Yunsheng et al., 2007, Yip and Van Deventer, 2003). On the other hand, only geopolymeric products will be formed upon the blending of CFC with either PFA or MK due to the high content of silicates and aluminates of these two materials (Yun-Ming et al., 2016). Both SSA and PSD of the raw materials play such an important role in the strength and durability performance of the brick. Celik et al. (Celik et al., 2008) reported that better compressive strength could be achieved when the binder materials have finer particles and higher SSA.

Table 4-4. The Physical properties of the candidate materials.

| Item | GGBS | PFA | CFA | MK |
|---|---|---|---|---|
| **$d_{50}$ (µm)** | 7.52 | 7.916 | 14.84 | 7.935 |
| **Mean Diameter (µm)** | 5.40 | 12.58 | 20.24 | 7.161 |
| **Blaine SSA ($cm^2/g$)** | 6931 | 5236 | 4647 | 19600 |
| **Specific gravity (Gs)** | 3.05 | 2.49 | 2.71 | 2.70 |

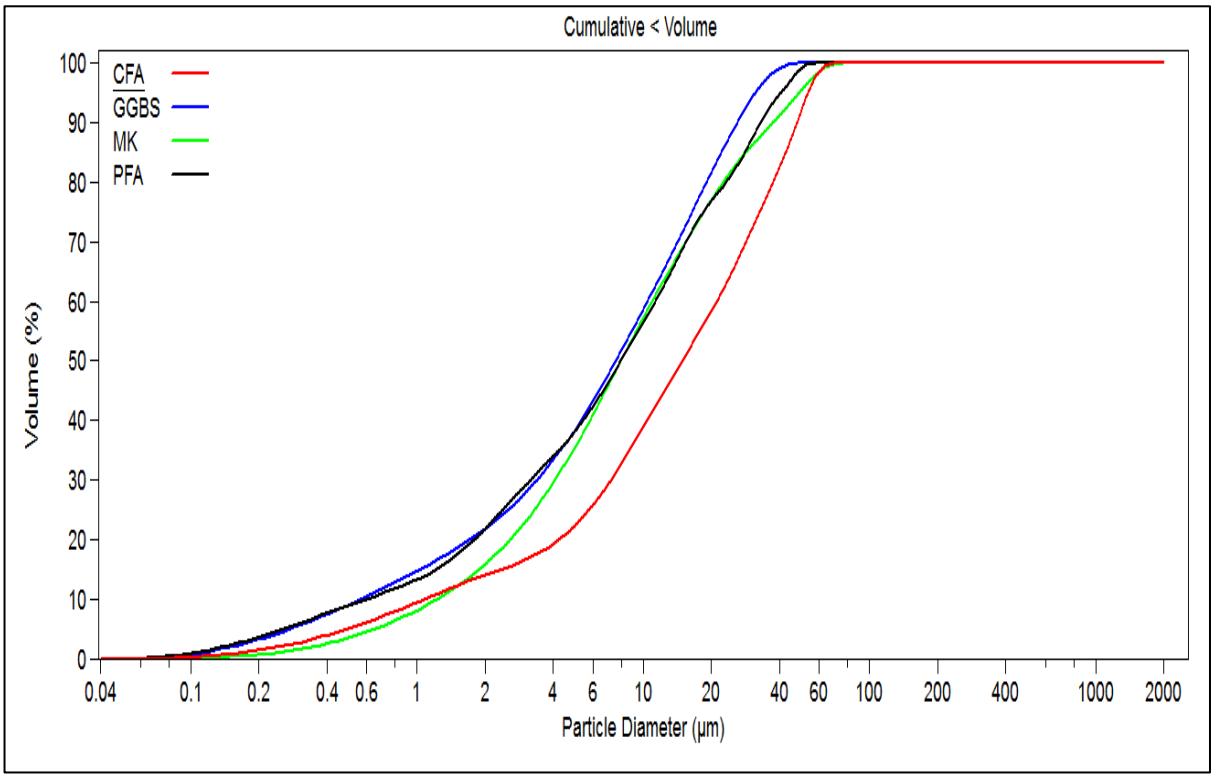


Figure 4-3. Comparative PSD of the candidate materials

From the overall PSD of all candidate materials (Figure 4-3) and their volume statistics (Table 4-4), it can be seen that GGBS is the finer material, while CFA is the coarser amongst the candidate materials. This means that the GGBS could improve the performance of the bricks during geopolymerisation reactivity (Gunasekara et al., 2016). Additionally, the very high SSA of the MK relative to other candidate materials means that MK has higher liquid demand than other candidate materials as reported by Mehdipour and Khayat (2017), Yun-Ming et al. (2016) and Hunger and Brouwers (2009)

The SEM tests were carried out on each of the candidate materials to identify the general shape of particles in their powder states. This helps to elucidate the behaviour of these materials when they were blended to produce alkali-activated binder (Wattimena et al., 2017). As shown in Figure 4-4, GGBS particles were either angular or irregular in shape. The angular shape of GGBS particles can significantly improve the compressive strength as angular particles can provide better adhesion or bond with the sand particles (Al-Negheimish et al., 1997). Figure 4-4 also shows that PFA particles were almost spherical in shape, while the CFA particles were almost spherical in shape with some irregular particles. The spherical particle shape of the PFA and CFA can reduce the yield stress and viscosity of the geopolymer materials. The SEM imaging of the MK as shown in Figure 4-4 revealed that MK particles have platy-like shape with different sizes. The platy-like shape particles of MK alongside its high SSA, are the main reasons for the high liquid demand of geopolymer materials with high MK content (Provis et al., 2010).

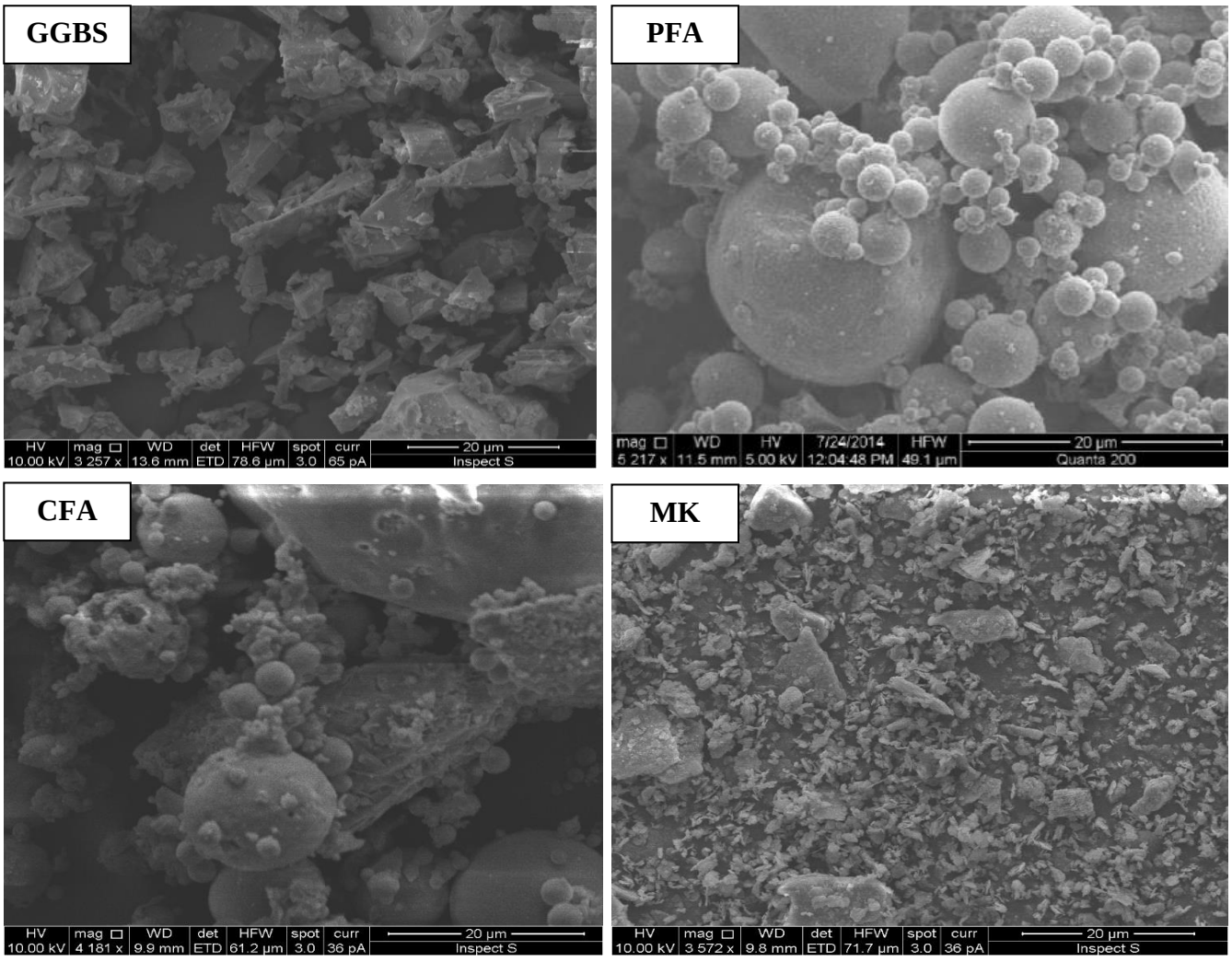


Figure 4-4. SEM imaging of the candidate materials (dry powder)

### *4.2.4 Summary of section (1)*

The main aim of this section was to identify the chemical, physical and microstructural properties of the CFC and the candidate materials. The output of this section can be summarised as follows:

- The chemical compositions of the CFC showed that it is rich with $SiO_2$ and has a high CaO content alongside moderate content of $Al_2O_3$.
- According to the comparative physicochemical properties of the candidate materials, GGBS and CFA are expected to form C-S-H gel in conjunction with geopolymeric gel upon blending with CFC due to the high CaO content of these materials.
- Based on the PSD and SSA comparison of the candidate materials, GGBS was found to have the finest particles relative to other candidate materials, while MK has the highest SSA.

## 4.3 Section 2: Candidate Mix Design

### *4.3.1 Introduction*

This section of Chapter 4 presents the results and dissection for all the investigation stages that were conducted in order to find the best combination of binder materials. In addition, this section also involved experiments to determine the best sand to binder (S/B) ratio, the best liquid to binder (L/B) ratio, the best $NaOH/Na_2SiO_3$ ratio and the best concentration of the NaOH. Compressive strength tests were conducted for evaluating the influence of each parameter on the performance of the alkali activated brick. The curing process of alkali activated materials is different from that of the conventional concrete. Unlike conventional concrete, water curing is not recommended for alkali activated materials as stated by the PAS 8820:2016 as this risks the leaching of alkali activators, leading to a friable surface with poor abrasion resistance (British Standards Institution, 2016). Therefore, air curing was considered in the production of alkali activated brick to activate the chemical reaction that takes place in the geopolymer matrix (Jindal, 2018). Additionally, although water curing is not recommend to be used for the curing of alkali activated materials according to PAS 8820:2016, however, it has been considered in this research for many reasons including that the CFC has high CaO and $SiO_2$ content, that in the presence of water, will form C-S-H gel simultaneously with geopolymer gel that in turn, could significantly enhance the mechanical and durability performance of the brick. The other reason for using water curing is that previous research (Lupo and Cheeseman, 2008) showed that in wet conditions, the properties of CFC aggregate were problematic due to deformation and crushing of the aggregate particles, therefore water curing was considered in order to be confident that the developed brick will be a viable alternative to fired clay brick in different conditions including contact with water. For evaluating the performance of the brick under different curing conditions, prism samples were cured either in air or immersed in water, with an average temperature of $20\pm2^{o}C$ during all the investigation stages. PAS 8820:2016 suggests a minimum of 10 bricks need to be tested to arrive at a quantitatively representative value of strength for an alkali activated material (British Standards Institution, 2016). However, in this project two specimens of dimensions 40 x 40 x 160 mm, were prepared for each mixing proportion, curing period and curing method. Each specimen was broken into two halves, using three-point loading of the prism samples and averages of four halves were taken to represent the final values for compressive strength. This as a deviation from PAS 8820:2016 specifications and it was implemented as this project is

mainly a 'proof of concept' as opposed to a commercial production commissioning document. The error bar was used to represent the minimum and maximum values obtained for each sample to demonstrate the reliability, repeatability and reproducibility of the results.

### *4.3.2 Selection of binder materials*

During this stage, the binder was prepared by blending the fine powder of CFC with GGBS, CFA, MK and PFA as shown in Table 4-5, to evaluate the performance of each of the candidate materials on the compressive strength of the alkali activated brick. The binder was a combination of 50% CFC and 50% of each of the candidate materials (GGBS, CFA, MK and PFA) and the compressive strength, after 7 days of air curing and water curing was measured. The synthesis of the binder materials in Table 4-5 were mixed with building sand to produce alkali activate brick. According to the available literature, the best Sand to Binder (S/B) ratio varies significantly for different studies. Therefore, during this study, the S/B ratio was initially started with 2 and in the next sections, the effect of different S/B ratios of the performance of the alkali activated materials will be investigated. The preparation of alkali activated brick also involved mixing the dry powder binder materials and the sand with the highly alkali activation solution. The activating solution was a combination of sodium silicate ($Na_2SiO_3$) and sodium hydroxide (NaOH). These two alkali activators were used together because NaOH is required for the dissolution of alumina-silicate precursor, while $Na_2SiO_3$ acts as binder or alkali reactant (Yun-Ming et al., 2016). During this stage, the NaOH was prepared with the concentration of 4M by dissolving the NaOH pellets in distilled water, then the NaOH solution was left to cool down at room temperature for 24 hours before use. The $Na_2SiO_3$/NaOH weight ratio was fixed as 2, while the ratio of alkali activator solution to binder (A/B) was kept as 0.4 for the GGBS, CFA and PFA and as 0.8 for the MK. The difference in the A/B ratio for the MK relative to the other binder materials was because the mixtures incorporated MK was very dry at the A/B ratio of 0.4 and it has been increased gradually to 0.8 in order to obtain a mixture that can be cast in the moulds. This behaviour of mixtures incorporated MK is attributed to the higher liquid demand of MK relative to other candidate materials as reported by Yun-Ming et al. (2016) and Kong et al. (2007a).

Additionally, during the development of alkali activated brick, water was added in addition to the alkali activations, because the water is essential to ensure the hydrolysis of dissolved $Al^{3+}$ and $Si^{4+}$ ions, along with the destruction of solid particles as reported by Zuhua et al. (2009). Therefore, in this investigation, the water was added with a water to binder (W/B) ratio of 0.1,

because if present in high quantity, it can hinder polycondensation of the alkali activated binder due to its dilution effect (Kim et al., 2015, Zuhua et al., 2009). During all stages of investigation, the term liquid to binder (L/B) ratio represent the A/B + W/B ratios.

Table 4-5. Mixing proportions of different candidate materials.

| Mix Id | CFC % | GGBS % | CFA % | MK % | PFA % | A/B | W/B | L/B | S/B | $Na_2SiO_3$/ NaOH | NaOH Concentration |
|---|---|---|---|---|---|---|---|---|---|---|---|
| **GGBS** | 50 | 50 | - | - | - | 0.4 | 0.1 | 0.5 | 2 | 2 | 4M |
| **CFA** | 50 | - | 50 | - | - | 0.4 | 0.1 | 0.5 | 2 | 2 | 4M |
| **MK** | 50 | - | - | 50 | - | 0.8 | 0.1 | 0.9 | 2 | 2 | 4M |
| **PFA** | 50 | - | - | - | 50 | 0.4 | 0.1 | 0.5 | 2 | 2 | 4M |

The 7 days compressive strengths of the alkali activated bricks made from different blends of CFC and the candidate materials, under both water curing and air curing, are presented in Figure 4-5. It can be seen from Figure 4-5 that all the mixtures under water curing have provided lower compressive strength than that under air curing. This was attributed to the differences in the conditions of samples under water curing and air curing subjected to compressive strength tests. At the designed age for testing the compressive strength, the samples cured under water curing were taken out from the water tanks and the water at the surface was removed using a damped cloth. After that, the samples were left in air at room temperature for 3 hours before conducting the compressive strength test. Therefore, the water in the voids inside the samples was not removed, to which the reduction in the compressive strength for samples under water curing is attributed relative to samples under air curing. This is because upon the compression of samples, the water in the voids induced internal stresses that accelerated the failure of samples relative to samples under air curing (Chen et al., 2012).

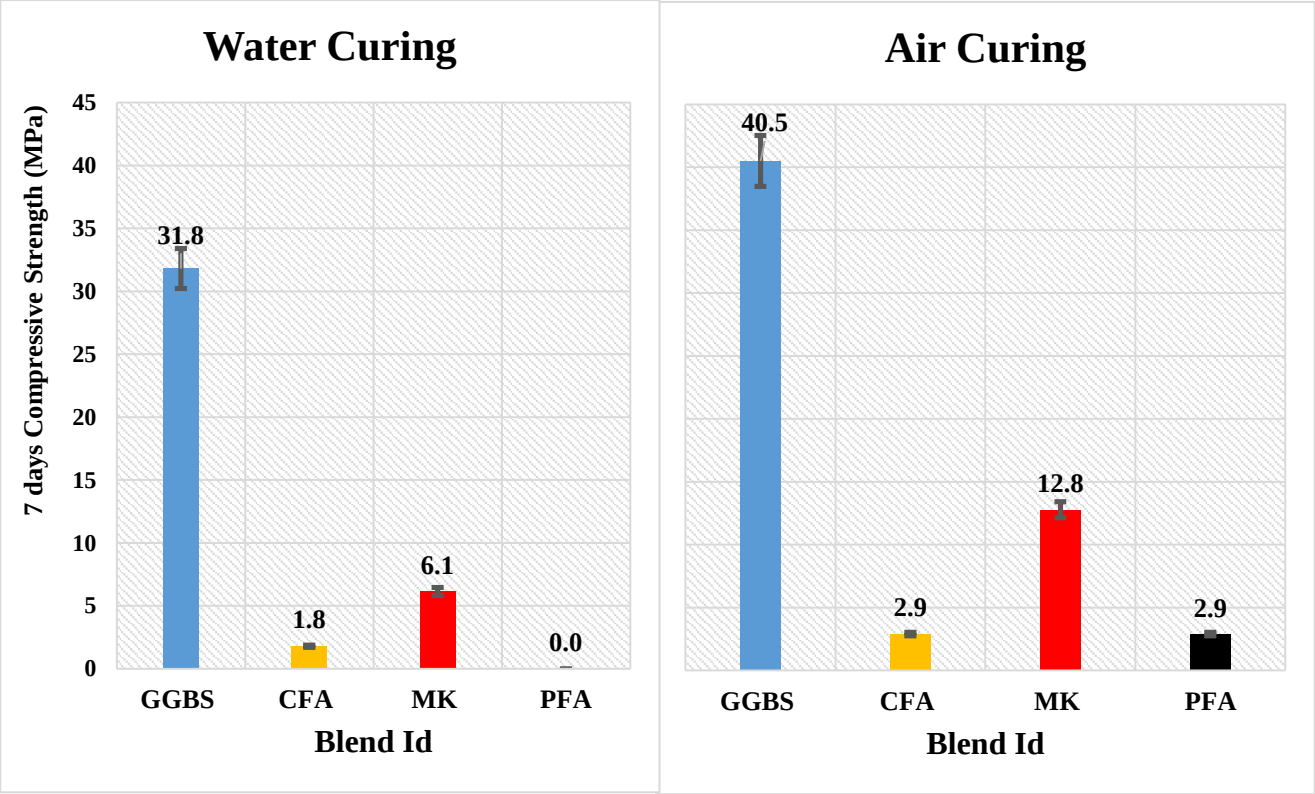


Figure 4-5. Development of compressive strength of different blends

Figure 4-5 clearly shows that the binary binder (CFC+GGBS) has provided the highest compressive strength relative to other candidate materials, for both curing methods. This performance was attributed to the chemical compositions of the candidate materials, (Table 4-3) the GGBS has a high $SiO_2/Al_2O_3$ ratio that leads to formation of Si-O-Si bonds, which were stronger than the Si-O-Al bonds thus, increased the compressive strength (Sasui et al., 2020). Additionally, according to the PSD curves (Figure 4-3), GGBS has the finest particles relative to other candidate materials. The fine particles of GGBS dissolve faster and more effectively in the alkali medium, thus fill the voids and produce a more densified structure, that leads to increased compressive strength relative to other candidate materials (Awang and Aljoumaily, 2017, Assi et al., 2018). Furthermore, the angular shape of GGBS particles enhanced the compressive strength as the angular particles of GGBS provided better adhesion or bond with the sand particles (Al-Negheimish et al., 1997).

Figure 4-5 also shows that the utilisation of CFA and PFA caused a significant reduction in the compressive strength of the alkali activated bricks for both methods of curing. This was due to the low SSA and coarse course particles of both CFC and PFA relative to GGBS, as stated in Figure 4-3 and Table 4-4. Therefore, the reactivity and dissolution of coarser particles of CFA

and PFA in the alkali activator and subsequent geopolymer gel formation was lower (Gunasekara1a et al., 2016). Additionally, the higher compressive strength of samples that incorporated CFA relative to PFA was due to both the high CaO content of CFA and subsequent formation of C-S-H gel along with geopolymer gel and also the lower content of unburnt carbon (measured by the LOI), that can weaken the bond with the aggregate if it presents in high quantity (Gunasekara1a et al., 2016, Liu et al., 2014).

Regarding the binary mixture (CFC+MK), it has showed about 19% and 32% of the compressive strength of the mixture made with GGBS under water curing and air curing, respectively. This low compressive strength was attributed to the high liquid to binder ratio that contributes to cause the reduction in compressive strength, as increasing the liquid will be associated with more porosity, due to the greater spacing between binder particles (Ng et al., 2018, Aïtcin, 2016). Additionally, this low compressive strength was due to the low $SiO_2/Al_2O_3$ ratio of the MK that leads to formation of fewer Si-O-Si bonds and reduces the compressive strength (Sasui et al., 2020, He et al., 2016).

The main reason of not combining CFC with more than one of GGBS, CFA, PFA and MK is that the results from Figure 4-5 clearly showed that blending CFC with GGBS is the only promising combination that can provide acceptable compressive strength and replacing part of the GGBS with any of the other candidate materials will negatively affect the compressive strength results. According to the obtained results, GGBS has been considered as the best candidate material to be used in the production of binary binder in combination with CFC in the production of alkali activated brick and the other candidate materials (CFA, PFA and MK) will not be further used in this research.

### *4.3.3 Selected Candidate Binder Material*

This stage of investigation was conducted to evaluate the effect of different combinations of CFC and GGBS on the compressive strength of the alkali activated bricks. Table 4-6 shows the mixing proportions of the binder materials.

Table 4-6. Mixing proportion of the binder materials.

| Mix Id | CFC % | GGBS % | S/B | A/B | W/B | L/B | $Na_2SiO_3$ /NaOH | NaOH Concentration |
|---|---|---|---|---|---|---|---|---|
| **FCW100** | 100 | 0 | 2 | 0.4 | 0.1 | 0.5 | 2 | 4M |
| **FCW90** | 90 | 10 | 2 | 0.4 | 0.1 | 0.5 | 2 | 4M |
| **FCW80** | 80 | 20 | 2 | 0.4 | 0.1 | 0.5 | 2 | 4M |
| **FCW70** | 70 | 30 | 2 | 0.4 | 0.1 | 0.5 | 2 | 4M |
| **FCW60** | 60 | 40 | 2 | 0.4 | 0.1 | 0.5 | 2 | 4M |
| **FCW50** | 50 | 50 | 2 | 0.4 | 0.1 | 0.5 | 2 | 4M |
| **FCW40** | 40 | 60 | 2 | 0.4 | 0.1 | 0.5 | 2 | 4M |
| **FCW30** | 30 | 70 | 2 | 0.4 | 0.1 | 0.5 | 2 | 4M |

The compressive strengths of different alkali activated bricks made from different blends of CFC and GGBS at different curing ages and under both water curing and air curing, are shown in Figure 4.6.

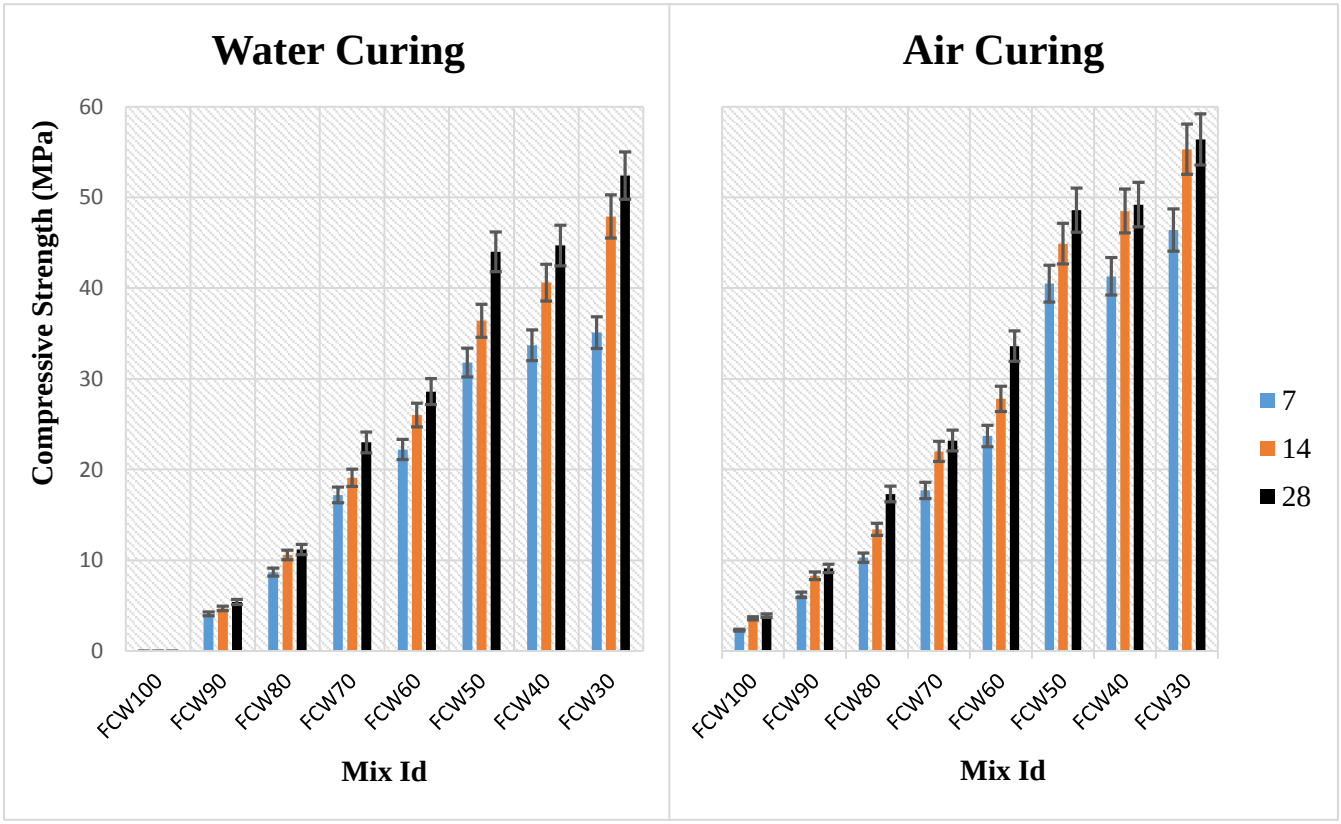


Figure 4-6. Compressive strength development of different alkali activated blends in different curing conditions

It can be seen from Figure 4-6, that the compressive strength of all the alkali activated bricks (except mixture FCW100 under water curing) has been increased with the increase in the period of curing for both curing regimes. Regarding the samples made from mixture FCW100, they were broken upon immersion in water. Figure 4-6 also shows that at all curing ages, the compressive strength for samples under water curing was lower than that of the same sample synthesis under air curing. This was attributed to the formation of internal stresses for samples under water curing that accelerated the failure of samples relative to samples under air curing (Chen et al., 2012).

The results in Figure 4-6 indicated that the utilisation of up to 50% CFC has provided a compressive strength of 44 MPa and 48.6 MPa after 28 days of water and air curing, respectively. At all curing ages, increasing the CFC content more than 50%, caused significant reduction in the compressive strength for both methods of curing. This was attributed to both (i) the formation of less C-S-H gel, as the CFC has lower calcium content relative to GGBS (Rakhimova and Rakhimov, 2015, Provis et al., 2012) and (ii) the coarse particles and the lower SSA of the CFC relative to GGBS particles that can retard the performance of the alkali activated bricks during the geopolymerisation process (Gunasekara et al., 2016). As the mixture FCW50 showed a compressive strength similar to that of mixture FCW40 and about 84% of the compressive strength of FCW30 and at the same time incorporated a higher amount of CFC relative to FCW30 and FCW40, this mixture was considered as the selected candidate combination of the binder materials that was used for further investigations.

### *4.3.4 Effect of sand to binder ratio on strength development of alkali activated brick*

After finding the selected candidate synthesis of the binder materials (FCW50), this blend was used with different S/B ratios to evaluate the effect of sand on the strength development of the alkali activated brick. In this stage, three different S/B ratios (1, 2 and 3) were evaluated for compressive strength after 7, 14 and 28 days of both air and water curing. Table 4-7 shows the mixing proportions of mixtures with various S/B ratios.

Table 4-7. Mixing proportions of various S/B ratios

| Mix Id | CFC % | GGBS % | S/B | A/B | W/B | L/B | $Na_2SiO_3$ /NaOH | NaOH Concentration |
|---|---|---|---|---|---|---|---|---|
| **S1** | 50 | 50 | 1 | 0.4 | 0.1 | 0.5 | 2 | 4M |
| **S2** | 50 | 50 | 2 | 0.4 | 0.1 | 0.5 | 2 | 4M |
| **S3** | 50 | 50 | 3 | 0.4 | 0.1 | 0.5 | 2 | 4M |

A comparison between the compressive strength of the alkali activated bricks for three different S/B ratios, cured in air and water at different curing ages is shown in Figure 4-7. The results in Figure 4-7 show that the compressive strength of the alkali activated bricks has been increased with the increase in the period of curing for all the investigated S/B ratios.

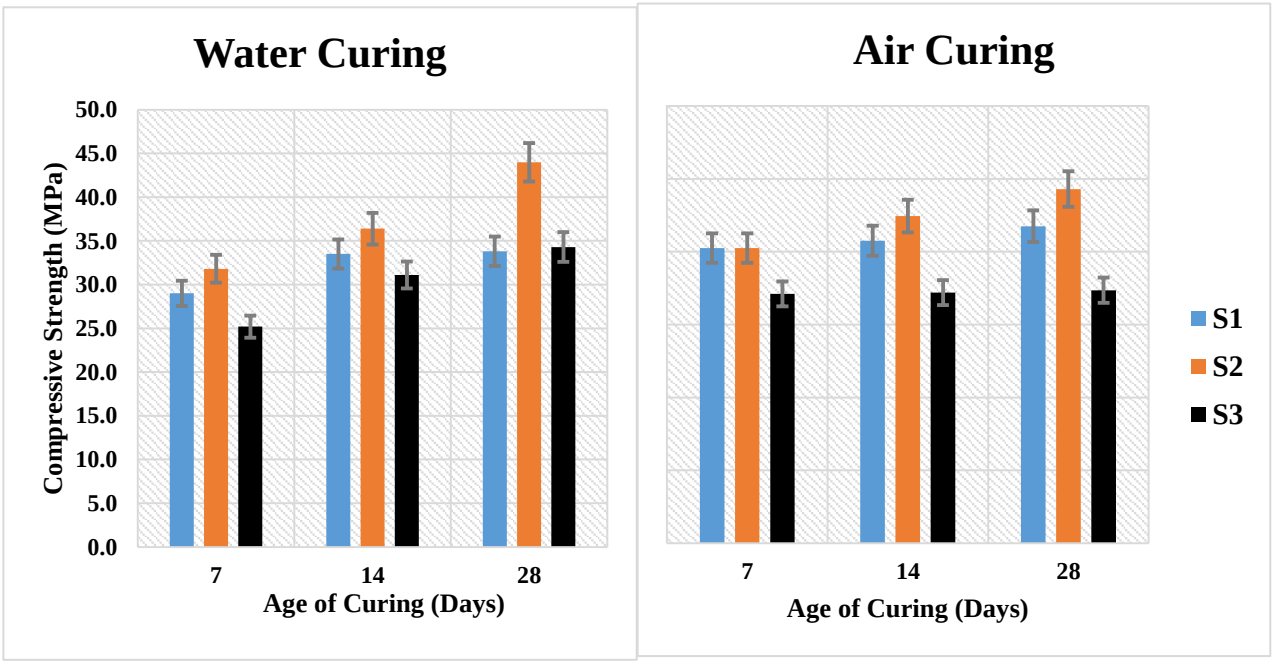


Figure 4-7. Compressive strength of FCW50 bricks with different S/B ratio in different curing conditions

For the water curing regime, the compressive strength of the brick with an S/B ratio of 1 was higher than that with an S/B ratio of 3 at 7 days. However, after 28 days of curing, the compressive strengths were very similar for both S/B ratios and were about 77% of the compressive strength for the alkali activated brick produced with a S/B ratio of 2.

Regarding the air curing technique, the compressive strengths of the bricks with S/B ratios of 1 and 2 were similar at 7 days and were higher than that of the brick with an S/B ratio of 3 by nearly 18%. The compressive strength for the bricks with S/B ratios of 1 and 2 after 28 days were improved by about 7% and 20% relative to the 7 days compressive strength, respectively. On the other hand, the compressive strength for the brick with an S/B ratio of 3 was almost the same for all curing ages.

The reduction in the compressive strength of bricks with an S/B ratio of 3 relative to that of 2 was attributed to the insufficient presence of the alkali solution and binder materials that caused a reduction in the formation of binding gels and poor bonding between the increased sand particles in the brick (Huseiena et al., 2018, Khan et al., 2018). However, the reduction in the compressive strength for the bricks with an S/B ratio of 1 relative to that with an S/B ratio of 2 was due to the increased alkali solution with the increase in the binder content. The reduced compressive strength with the increase in the alkali activation solution was due to the alkali activation solution not being consumed during geopolymerisation reaction resulting in increased porosity that leads to reduced compressive strength (Huseiena et al., 2018, Khan et al., 2018, Reig et al., 2013). Based on the obtained results, the selected candidate S/B ratio was 2, as it has provided the highest compressive strength at all ages. Therefore, this S/B ratio was used in the preparation of the alkali activated bricks for further investigations.

### *4.3.5 Effect of liquid to binder ratio on the compressive strength of alkali activated brick*

The alkali activators and water solution to binder ratio (L/B) play such an important role in the development of alkali activated brick, as they govern the workability & geopolymerisation reaction and significantly affect the performance of the final product (Yun-Ming et al., 2016). The effect of different L/B ratios on the performance of the alkali activated brick was investigated after finding the selected candidate synthesis of the binder materials and S/B ratio. During this stage, three different L/B ratios (0.4, 0.5 and 0.6) were investigated for compressive strength after 7, 14 and 28 days of both air and water curing. Table 4-8 shows the mixing proportions for mixtures with various L/B ratios.

Table 4-8. Mixing proportions of various L/B ratios

| Mix Id | CFC % | GGBS % | S/B | A/B | W/B | L/B | $Na_2SiO_3$ /NaOH | NaOH Concentration |
|---|---|---|---|---|---|---|---|---|
| **0.4** | 50 | 50 | 2 | 0.3 | 0.1 | 0.4 | 2 | 4M |
| **0.5** | 50 | 50 | 2 | 0.4 | 0.1 | 0.5 | 2 | 4M |
| **0.6** | 50 | 50 | 2 | 0.5 | 0.1 | 0.6 | 2 | 4M |

Figure 4-8 shows a comparison between the compressive strength of alkali activated bricks made with three different L/B ratios and cured either in air or in water at different curing ages. Figure 4-8 clearly shows that the compressive strength for the bricks with L/B ratio of 0.4 was almost the same at all curing ages for samples under water curing, while the compressive strength for samples under air curing increased slightly with an increase in the period of curing. This was attributed to the insufficient alkali activators to completely dissolve the $Si^{4+}$ and $Al^{3+}$ from the binder materials that results in hindering further geopolymerisation reaction (Yun-Ming et al., 2016, Rowlesa and O'Connor, 2003). Consequently, the compressive strength of the alkali activated brick was low.

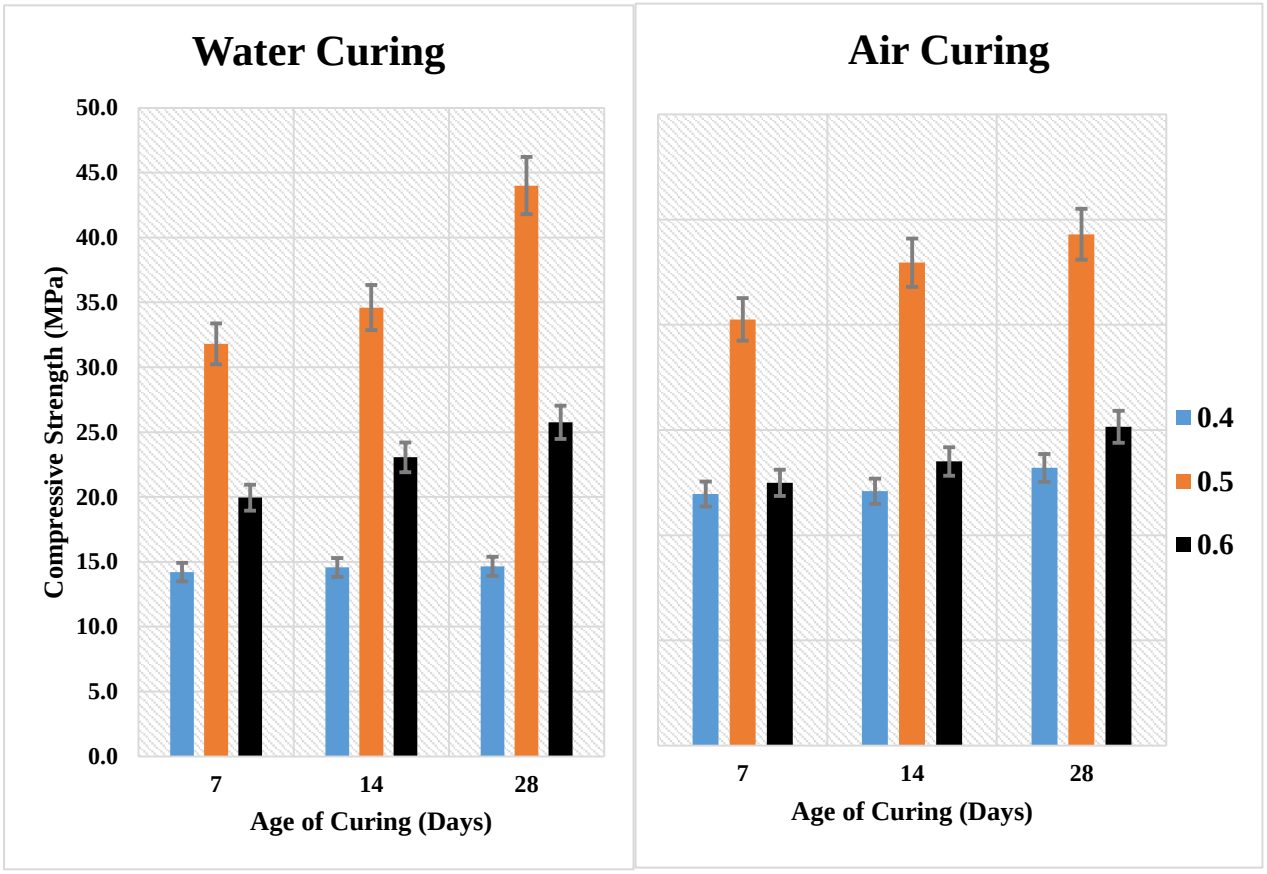


Figure 4-8. Compressive strength of alkali activated bricks with different L/B ratio in different curing conditions

The results of the compressive strength in Figure 4-8 indicated that for both methods of curing, the compressive strength of brick made with a L/B ratio of 0.6 were improved slightly with the increase in the period of curing and was lower than that with a L/B ratio of 0.5 at all curing ages. This was due to the fact that high alkali solution content hinders particle-to-particle interaction of binder materials due to the increased porosity and the large distance between particles, that in turn reduced the compressive strength (Yun-Ming et al., 2016, Heah et al., 2012). According to the obtained results, the selected candidate L/B ratio was 0.5, as it has provided the highest compressive strength at all ages. Therefore, this L/B ratio was utilised in the preparation of alkali activated bricks for further investigations.

### *4.3.6 Effect of $Na_2SiO_3$/NaOH ratio on the compressive strength of alkali activated brick*

The most commonly used alkali activator solutions are sodium silicate ($Na_2SiO_3$) and sodium hydroxide (NaOH) (Yun-Ming et al., 2016, Feng et al., 2012, Xu et al., 2002). NaOH or $Na_2SiO_3$ can be used alone as an activator (Yun-Ming et al., 2016). However, mixing NaOH and $Na_2SiO_3$ in the production of alkali activated brick is essential, as NaOH is required for the dissolution of alumina-silicate precursor, while $Na_2SiO_3$ acts as binder or alkali reactant (Yun-Ming et al., 2016).

During this stage, the effect of different $Na_2SiO_3$/NaOH ratios on the compressive strength of the alkali activated brick was examined after finding the selected candidate synthesis of the binder materials, S/B ratio and L/B ratio. During this stage, four different $Na_2SiO_3$/NaOH ratios (0.5, 1, 2 and 3) were tested for compressive strength after 7, 14 and 28 days of both air and water curing. Table 4-9 shows the mixing proportions of mixtures with various $Na_2SiO_3$/NaOH ratios.

Table 4-9. Mixing proportions of various $Na_2SiO_3$/NaOH ratios

| Mix Id | CFC % | GGBS % | S/B | A/B | W/B | L/B | $Na_2SiO_3$ /NaOH | NaOH Concentration |
|---|---|---|---|---|---|---|---|---|
| **0.5** | 50 | 50 | 2 | 0.4 | 0.1 | 0.5 | 0.5 | 4M |
| **1** | 50 | 50 | 2 | 0.4 | 0.1 | 0.5 | 1 | 4M |
| **2** | 50 | 50 | 2 | 0.4 | 0.1 | 0.5 | 2 | 4M |
| **3** | 50 | 50 | 2 | 0.4 | 0.1 | 0.5 | 3 | 4M |

The compressive strength performance of the alkali activated bricks prepared with different $Na_2SiO_3$/NaOH ratios at different curing ages and curing methods are shown in Figure 4-9 Additionally, Figure 4-9 shows that the compressive strengths of alkali activated bricks were improved with the increase in the $Na_2SiO_3$/NaOH ratio to reach the best value with a $Na_2SiO_3$/NaOH ratio of 2 for both methods of curing and at all curing ages. This was due to the increased (Si) content that aids in the production of more of Si-O-Si bonds, and significantly improved the compressive strength of the alkali activated bricks (Hameed et al., 2017a). However, the compressive strength started to decrease with a higher $Na_2SiO_3$/NaOH ratio. This was attributed to the excess Si content that hinders water evaporation and structure formation and negatively affects the geopolymerisation rate (Hameed et al., 2017a). Based on the

obtained results, the best $Na_2SiO_3$/NaOH ratio was 2. Therefore, this $Na_2SiO_3$/NaOH ratio was considered as the selected candidate $Na_2SiO_3$/NaOH ratio and it was used for further investigations.

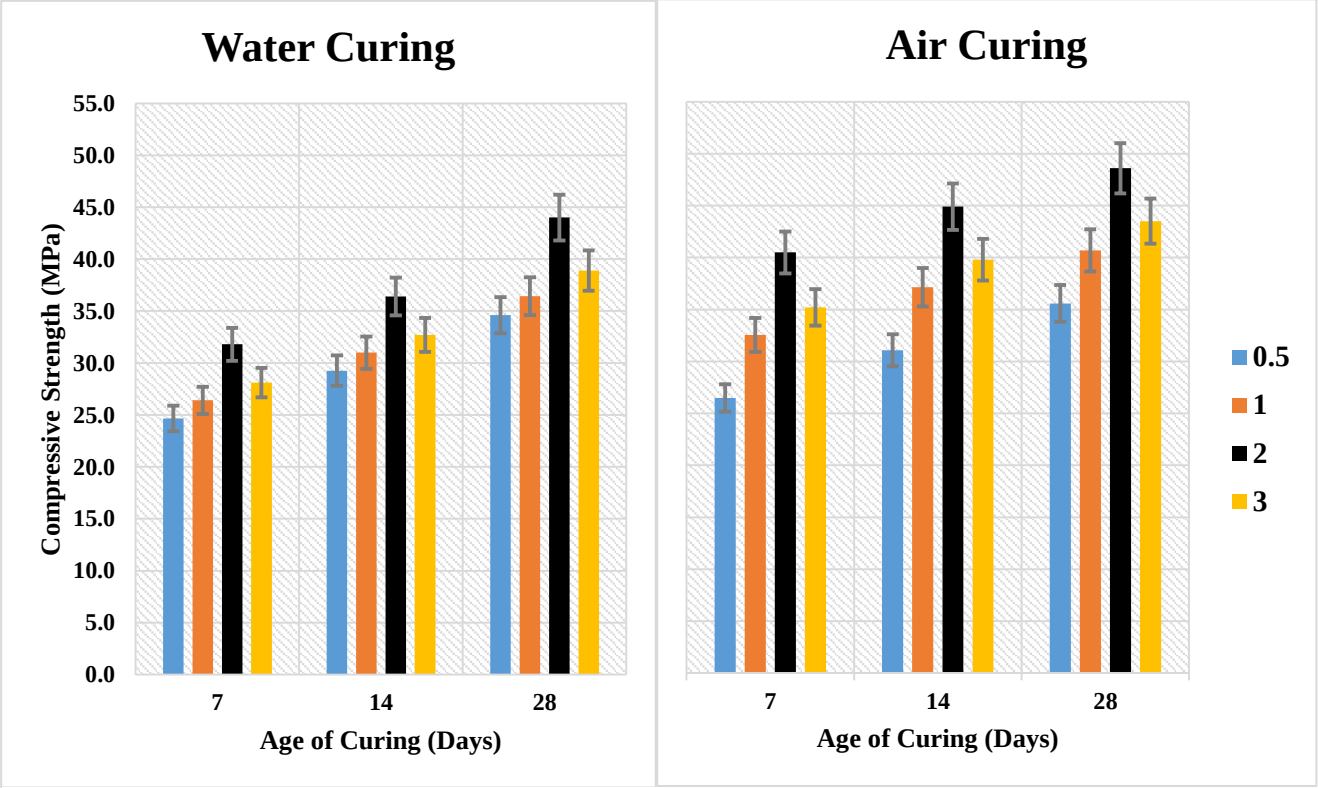


Figure 4-9. Compressive strength of alkali activated bricks with different $Na_2SiO_3$/NaOH ratio in different curing conditions

### *4.3.7 Effect of NaOH concentration on the compressive strength of alkali activated brick*

The concentration of the NaOH affects the compressive strength of alkali activated bricks (Yun-Ming et al., 2016). The influence of NaOH concentration upon the compressive strength of the alkali activated brick was examined after finding the selected candidate synthesis of the binder materials, S/B ratio, L/B ratio and $Na_2SiO_3$/NaOH ratio. During this stage, 3 different NaOH concentrations (2M, 4M and 6M) were tested for compressive strength after 7, 14 and 28 days of both air and water curing. Table 4-10 shows the mixing proportions of mixtures with various NaOH concentrations.

Table 4-10. Mixing proportions of various NaOH concentrations.

| Mix Id | CFC % | GGBS % | S/B | A/B | W/B | L/B | $Na_2SiO_3$ /NaOH | NaOH Concentration |
|---|---|---|---|---|---|---|---|---|
| **2M** | 50 | 50 | 2 | 0.4 | 0.1 | 0.5 | 2 | 2M |
| **4M** | 50 | 50 | 2 | 0.4 | 0.1 | 0.5 | 2 | 4M |
| **6M** | 50 | 50 | 2 | 0.4 | 0.1 | 0.5 | 2 | 6M |

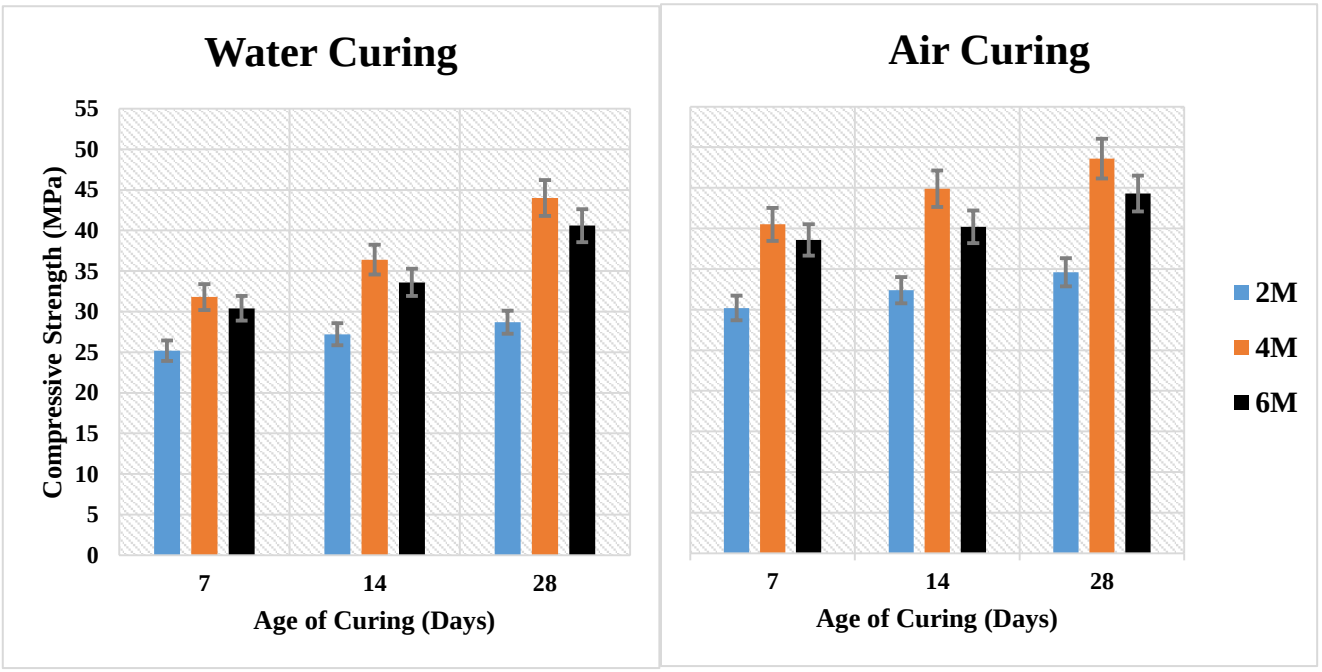


Figure 4-10. Effect of NaOH concentration upon the compressive strength of the alkali activated brick.

The results in Figure 4-10 indicated that the highest compressive strength was achieved when the concentration of the NaOH was 4M. Figure 4-10 also shows that increasing the concentration of NaOH to 6M resulted in lower compressive strength relative to 4M, at all curing ages and for both methods of curing. This was because the high concentration of NaOH is highly viscous and might disrupt the leaching of Si and Al ions from raw materials, premature precipitation of geopolymer gels and deterioration in compressive strength of the brick, as reported by Yun-Ming et al. (2016). Additionally, increasing the concentration of NaOH delays the polymerisation process as a large amount of dissolved ions in highly alkali solution causes saturation and limits the contact between the polymerised species and formation of coagulated structures, as reported by Khale and Chaudhary (2007) and Alonso and Palomo (2001). On

the other hand, using NaOH with concentration of 2M reduced the mechanical performance of the brick because there was insufficient $OH^-$ to completely dissolve $Si^{4+}$ and $Al^{3+}$ from the raw materials and insufficient $Na^+$ to allow for complete geopolymerisation as reported by Yun-Ming et al. (2016). Therefore, the NaOH with the concentration of 4M was considered as the selected candidate NaOH concentration in this research.

### *4.3.8 Summary of section (2)*

The selected candidate synthesis parameters of the novel alkali activated unfired brick (NAAUB) after all stages of investigations are presented in Table 4-11.

Table 4-11. Selected candidate synthesis parameters of the NAAUB.

| Design Parameter | Selected candidate value |
|---|---|
| **Binder materials composition** | 50% CFC + 50% GGBS |
| **Sand to binder ratio (S/B)** | 2 |
| **Liquid to binder ratio (L/B)** | 0.5 |
| **$Na_2SiO_3$/NaOH ratio** | 2 |
| **NaOH concentration** | 4M |

## 4.4. Section 3: Effect of different curing methods on the mechanical performance of the NAAUB

### *4.4.1 Introduction*

The term curing is a process that is normally associated with the production of different alkali activated construction and building materials such as concrete, mortar, bricks, etc. The curing process can significantly affect the performance of the produced material and it is usually aims at acquisition the full strength of developed product (Joel and Edeh, 2013). According to PAS 8820: 2016 (British Standards Institution, 2016), curing at elevated temperatures could be beneficial as it can reduce the required time for curing and at the same time provide similar performance, excessive heat applied in the pre-hardening period can result in a less dense matrix with reduced strength and durability. Both Kani and Allahverdi (2009) and Yun-Ming et al. (2016) reported that curing of alkali activated materials at temperatures in the range of 25-90$^{o}$C is essential for increasing the geopolymerisation reaction rate through faster dissolution of alumina and silica species from the raw materials. Several researchers (Lemougna et al., 2020, Hameed et al., 2017b, Kani et al., 2012, Heah et al., 2011, Kani and Allahverdi, 2009, Perera et al., 2007) have investigated the influence of different curing regimes on the performance of the alkali activated materials. However, the effect of different water curing temperatures on different properties of alkali activated brick produced using CFC has not been investigated in the available literature. Therefore, this section of Chapter 4 presents the results of experimental work conducted to investigate the effect of different water curing temperatures conditions on the mechanical performance of the NAAUB. Additionally, a comparison between the mechanical performances of the NAAUB under different curing methods was conducted during this section. It is worth mentioning that the effect of Relative Humidity (RH) on the performance of the NAAUB was not controlled and monitored during this section. It has been reported by Luukkonen et al. (2018) and Criado et al. (2012) that RH has an active role to play in the curing processes of alkali activated materials. Curing the alkali activated specimens at saturated conditions (i.e., RH of around 100%) is preferable to improve the compressive strength and reduce carbonation (Criado et al., 2012, Nematollahi et al., 2017)

Two specimens of dimensions 40 x 40 x 160 mm, were prepared for each curing period and curing method and each specimen was broken into two halves and averages of four halves were taken to represent the final values for compressive strength. Additionally, three specimens of

dimensions 40 x 40 x 160 mm, were prepared for each curing period and curing method and averages of three samples halves were taken to represent the final values for flexural strength. Similar to previous section, the error bar was used to represent the minimum and maximum values obtained for each sample to demonstrate the reliability, repeatability and reproducibility of the results.

### *4.4.2 Effect of different water curing temperatures*

The effect of different water curing temperatures on the performance of the NAAUB at different temperatures (30, 50, 70 and 90 $^{o}$C) for different curing periods (1, 3, 7, 14 and 28 days) is illustrated in Figure 4-11. It can be seen from Figure 4-11 that after 1 day of curing the compressive strength of the NAAUB increased with the increase in the temperature of curing. This was attributed to the fact that raising the curing temperature at an early stage is favourable for the alkali activation reaction, due to the formation of more geopolymeric gel from the raw materials, and it helps to eliminate the structural microcracks (Yun-Ming et al., 2016, Kani and Allahverdi, 2009).

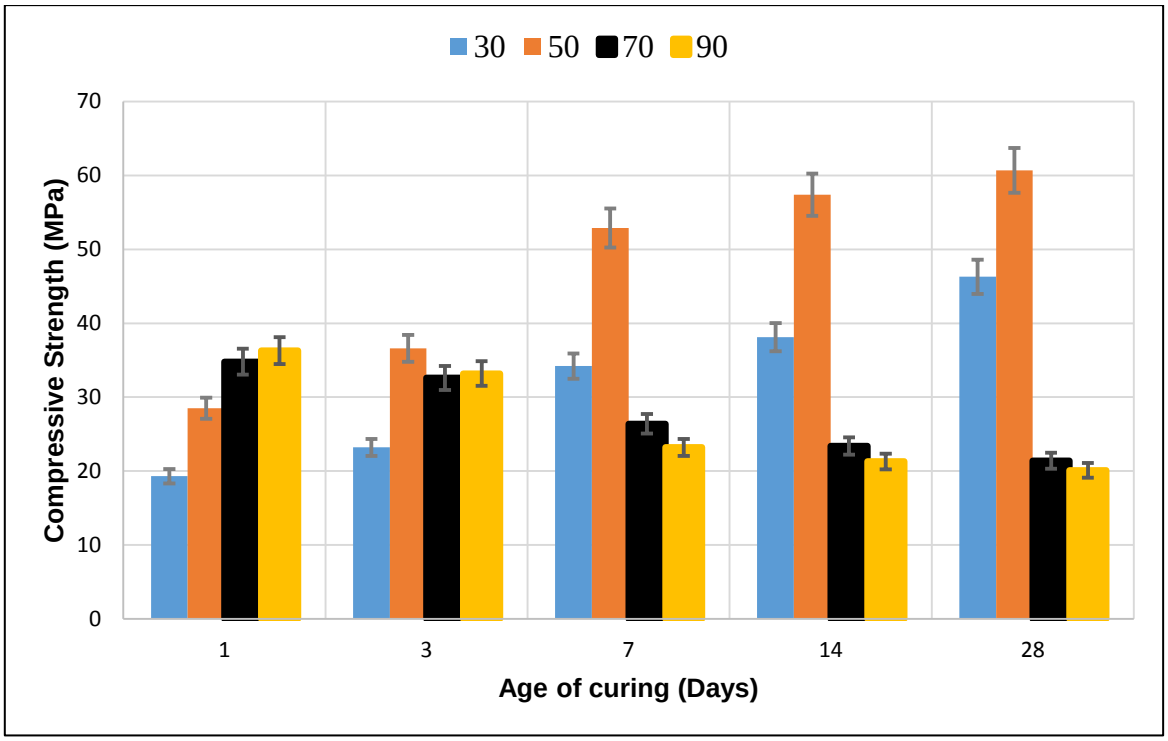


Figure 4-11. Effect different water curing temperatures on compressive strength development of the NAAUB.

Figure 4-11 also shows that the compressive strength of the NAAUB continued to improve with the increase in the period of curing at temperatures of 30$^{o}$C and 50$^{o}$C, however, curing of the NAAUB for more than 24 hours at temperatures of 70$^{o}$C and 90$^{o}$C resulted in deterioration of the compressive strength. The successful developments in the compressive strength with the increase in the period of curing at temperatures of 30$^{o}$C and 50$^{o}$C was due to the formation of additional geopolymeric gel and C-S-H gel (Robayo-Salazar et al., 2017b, Guo et al., 2009). The simultaneous co-existence of these two gels together tends to fill pores and grow into capillary spaces, resulting in a dense and higher-strength structure (Siddiqua and Barreto, 2018, Robayo-Salazar et al., 2017b, Yun-Ming et al., 2016). On the other hand, the reduction in compressive strength of the NAAUB samples at higher curing temperatures (70$^{o}$C and 90$^{o}$C) was attributed to dehydration of geopolymer gel and formation of microcracks (Lemougna et al., 2020, Singh et al., 2015). As the compressive strength of the NAAUB improved with the increase in the period of curing at 30$^{o}$C and 50$^{o}$C and the compressive strength at curing temperature of 50$^{o}$C was significantly higher than that of 30$^{o}$C at all curing ages, therefore, water curing at 50$^{o}$C is considered as the favourable temperature of curing that will be used for further investigations.

### *4.4.3 Effect of different methods of curing on long term strength of the NAAUB.*

In order to be confident to construct real structures with the NAAUB and the environmental benefits it can provide, in depth knowledge is required to ensure that the NAAUB will provide acceptable long term performance. Therefore, this section investigated the effect of long-term curing on the mechanical performance of the NAAUB. The results of the influence of different curing methods on the compressive strength and flexural strength development of the NAAUB from 1 day up to 180 days are presented in Figure 4-12 and Figure 4-13, respectively. It can be seen from Figure 4-12 that up to 28 days, the water curing temperature (NAAUB-H50) provided the highest compressive strength of the NAAUB followed by air curing (NAAUB-A) and then water curing (NAAUB-W). At 56 days, there was an improvement in the compressive strength of the NAAUB-H50 by about 3% relative to that at 28 days. For this period of curing, the NAAUB-W showed a slight improvement (0.1 MPa) in the compressive strength in comparison with that at 28 days. On the other hand, the NAAUB-A showed a reduction in the compressive strength with about 16% relative to that after 28 days of curing and it was lower than the compressive strength of the NAAUB-W by about 7%.

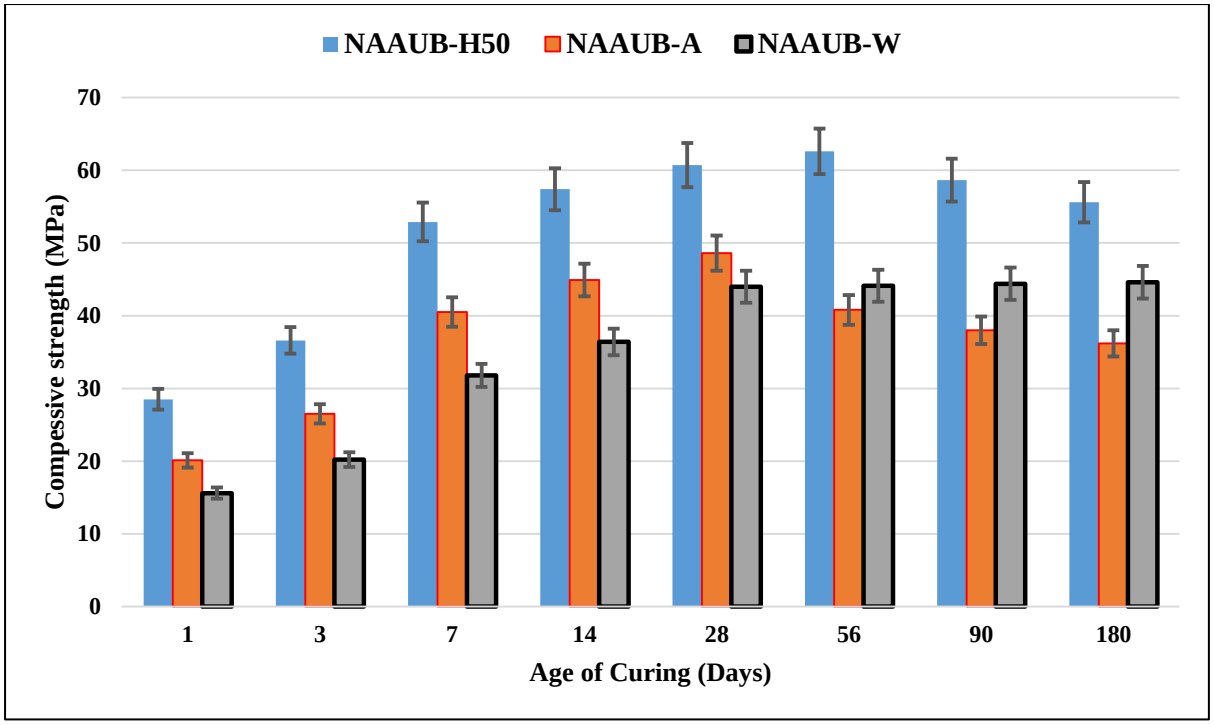


Figure 4-12. Effect of curing method on compressive strength development of the NAAUB.

The compressive strength of the NAAUB at 90 days was decreased for samples NAAUB-H50 and NAAUB-A by approximately 6% and 7% relative to that at 56 days, respectively. However, the NAAUB-W continued the improvement in the compressive strength with nearly 1% relative to that after 56 days. After 180 days of curing the compressive strength of the NAAUB-H50 and NAAUB-A decreased by about 5% relative to that at 90 days, while compressive strength of the NAAUB-W increased by 0.5%.

It can be seen from Figure 4-13 that at all curing ages the water curing temperature provided the highest flexural strength of the NAAUB. At the ages of 1 and 3 days, the flexural strength of the NAAUB-H50 was significantly higher than that of the NAAUB-A and NAAUB-W. Figure 4-13 also shows that the flexural strength of the NAAUB-H50 was increased slightly by only about 4% at 7 days relative to that at 3 days. On the other hand, the development in the flexural strength at 7 days for the NAAUB-A and NAAUB-W was increased nearly by 42% and 19%, respectively in comparison with that at 3 days.

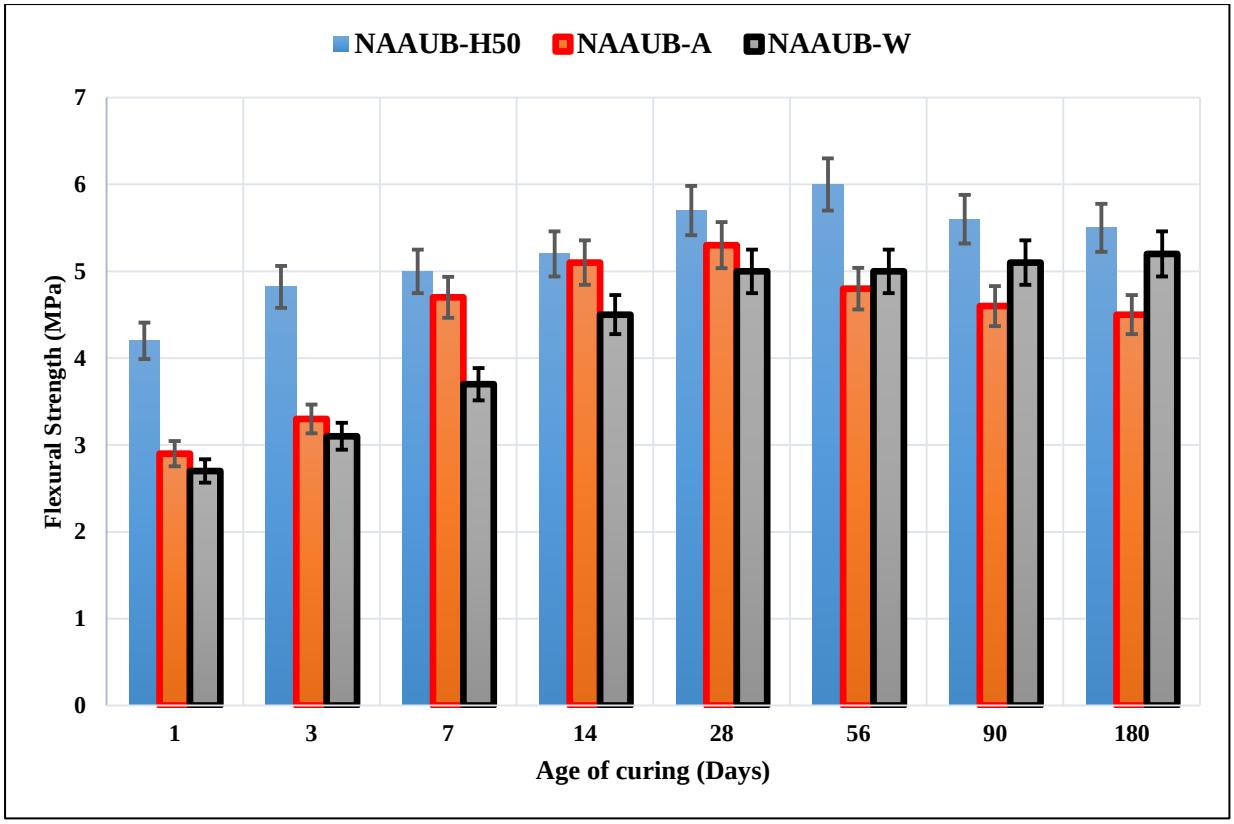


Figure 4-13. Effect of curing method on flexural strength development of the NAAUB

It can be seen from Figure 4-13 that up to 28 days, the NAAUB-A has showed higher flexural strength relative to the NAAUB-W. However, increasing the period of curing to more than 28 days, the NAAUB-A showed lower flexural strength relative to that of the NAAUB-W. The highest flexural strength of the NAAUB was 6 MPa obtained for the NAAUB-H50 at 56 days and then the flexural strength was decreased by about 7% at the ages of 90 days and 180 days. Generally, the flexural strength results were found to have similar trend to the compressive strength results presented in Figure 4-12. Similar findings were reported by Bakharev et al. (1999).

For the alkali activated materials, the dissolution of Si, Al, and Ca from the binder materials governs the initial stage of reactivity (Guo et al., 2009, van Deventer et al., 2007). The high compressive strength and flexural strength of the alkali activated bricks at 1 and 3 days is attributed to the availability of Si, Al, and Ca species in the alkaline medium that leads to the formation of geoplymerisation products (Robayo-Salazar et al., 2017b, Guo et al., 2009, Sasui et al., 2020). Additionally, the high compressive strength and flexural strength of the NAAUB-H50 relative to other curing methods is attributed to the increase in the polymerisation process

with an increase in the curing temperature that aids converting the 2D-polymer chains into 3D-polymer chain with strong bond as reported by Nagral et al. (2014).

The lower compressive strength of the NAAUB-W relative to NAAUB-A up to the age of 28 days is attributed to the samples' conditions at the time of testing, where the samples cured under water curing were taken out from the water tanks and the water at the surface was removed using a damped cloth. After that, the samples were left in air at room temperature for 3 hours before conducting the compressive strength test. Therefore, the water in the voids inside the samples was not removed, to which the reduction in the compressive strength for samples under water curing is attributed relative to samples under air curing. This is because upon the compression of samples, the water in the voids induced internal stresses that accelerated the failure of samples relative to samples under air curing (Chen et al., 2012).

On the other hand, the reduction in the compressive strength and flexural strength of the NAAUB-A after 28 days was due to the continuous moisture loss (fast dehydration) from the specimens that cause the formation of voids and low chance of C-S-H gel formation, that resulted in strength degradation as reported by Nagral et al. (2014) and Ahmari and Zhang (2013). Additionally, the reduction in the strength of the NAAUB-H50 at later ages is due to the formation of a large amount of hydration products at early ages that form a barrier for ion diffusion, thus causing an inhomogeneity in the microstructure as reported by Chi et al. (2012), Bakharev et al. (1999) and Fernández-Jiménez et al. (1999).

In addition to the aforementioned methods of curing, there are other methods of curing that have not been investigated and that would influence the performance of the NAAUB such as oven curing and cure-and-seal. The use of oven curing is not recommended as it will accelerate the evaporation of internal water that could hinder the hydration process (Lemougna et al., 2020). Considering the high CaO content of the NAAUB, curing the NAAUB by sealing the surface is effective, providing that there is no loss of moisture leading to premature drying and that would significantly help in improving the hydration process (British Standards Institution, 2016).

### *4.4.4 Summary of section (3)*

Further to the results and conclusions of the stages from section 4.3, the effects of different water curing temperatures and different curing regimes on the mechanical performance of the NAAUB were investigated at different periods of curing. According to the obtained results, the following points can be drawn:

- Increasing the temperature of water curing at the first 24 hours of curing resulted in higher compressive strength.
- The compressive strength of the NAAUB tends to decrease with the increase in the period of curing for samples subjected to water curing temperature at temperatures of 70$^{o}$C and 90$^{o}$C.
- Increasing the period of curing for samples subjected to water curing temperature at temperatures of 30$^{o}$C and 50$^{o}$C resulted in improved compressive strength.
- The selected candidate temperature of water curing temperature was found to be 50$^{o}$C.
- The compressive strength and flexural strength of the NAAUB-H50 increased with extending the period of curing with the highest compressive strength and flexural strength of 62.6 MPa and 6 MPa achieved after 56 days of curing then tended to decrease slightly with the increase in the period of curing.
- The compressive strength and flexural strength of the NAAUB-A enhanced significantly with the increase in the period of curing up to 28 days after that the compressive strength and flexural strength decreased with increasing the period of curing.
- The NAAUB-W showed an improvement in the compressive strength and flexural strength with the increase in the period of curing from 1 to 180 days.

## 4.5 Section 4: Physical, Chemical and Microstructural properties of the NAAUB

### *4.5.1 Introduction*

This section of Chapter 4 presents the results of the physical, chemical and microstructural properties of the NAAUB. The physical properties include PSD and SSA, while the chemical properties include the pH value and EDXRF analysis of the NAAUB'S binder (dry powder). All the physical and chemical properties of the NAAUB investigated in this section were repeated three times and the average value was considered. The microstructural properties, including evaluating the morphology of each of the binder raw materials (CFC and GGBS) using the SEM and then evaluating the SEM/EDS micrographs of the NAAUB paste after 3, 7, 28 and 180 days using different methods of curing.

### *4.5.2 Physical and chemical Properties*

The Physical properties such as the Blain Specific Surface Area (SSA), specific gravity (Gs), mean PSD, and the median ($d_{50}$) PSD of the NAAUB's binder powder are presented in Table 4-12, while the PSD of the NAAUB's binder powder is presented in Figure 4-14.

Table 4-12. The Physical properties of the NAAUB.

| Item | NAAUB |
|---|---|
| **$d_{50}$ (µm)** | 15.63 |
| **Mean Diameter (µm)** | 28.10 |
| **Blaine SSA ($cm^2/g$)** | 5429 |
| **Gs** | 2.71 |

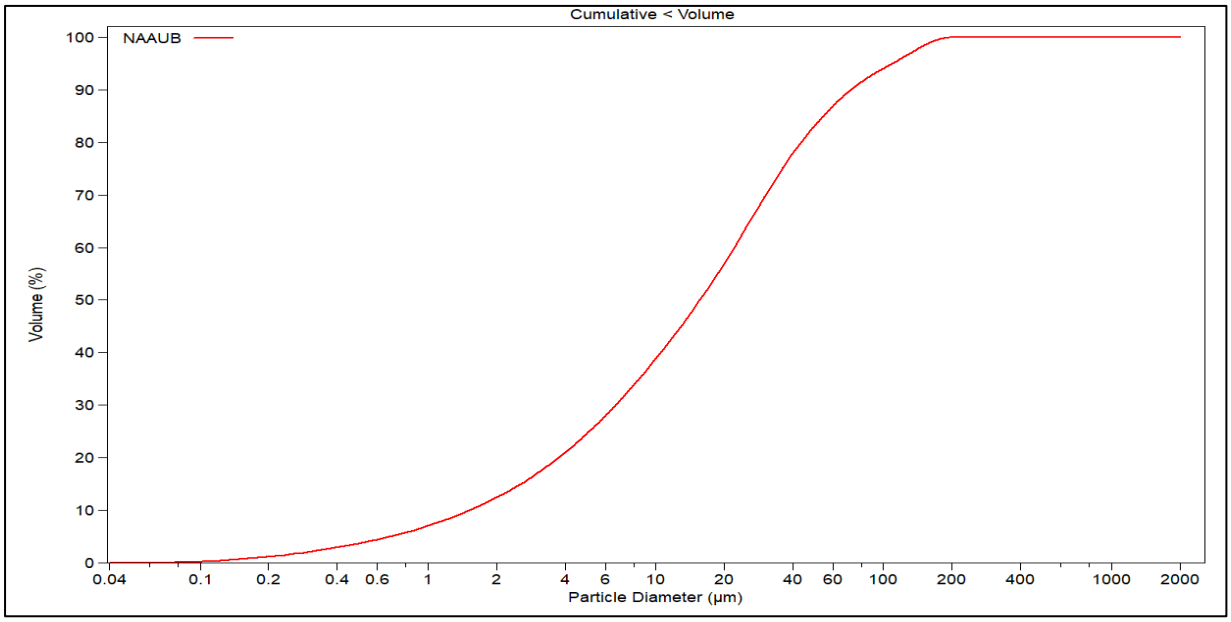


Figure 4-14. Particle size distribution of the NAAUB

The chemical properties of the NAAUB are presented in Table 4-13. The dissolution, coagulation and the formation of geopolymer gel relies on the reactivity of the binder materials (Gunasekara et al., 2016). Both, the high SSA and fine particles of the NAAUB binder along with the high amount of $SiO_2$ and CaO and the moderate amount of $Al_2O_3$, leads to the quick reaction with the alkali solution and produces large amounts of geopolymer gel and C-S-H gel (Gunasekara et al., 2016). The results of the compressive strength and flexural strength obtained in Figure 4-12 and Figure 4-13 are well in agreement with this claim.

Table 4-13. The chemical properties and EDXRF analysis of the NAAUB.

| Item | NAAUB |
|---|---|
| **CaO %** | 38.40 |
| **$SiO_2$ %** | 45.46 |
| **$Al_2O_3$ %** | 4.56 |
| **$Fe_2O_3$ %** | 1.49 |
| **MgO %** | 3.82 |
| **$Na_2O$ %** | 2.63 |
| **$K_2O$ %** | 1.02 |
| **$TiO_2$ %** | 0.80 |
| **MnO %** | 0.19 |
| **LOI %** | 4.21 |
| **pH** | 9.95 |

### *4.5.3 Microstructural properties*

SEM imaging testing has been increasingly employed in cement, concrete and brick research, especially for the purpose of microstructural investigation. Such images help to distinguish the changes in the microstructure over curing time (Robayo-Salazar et al., 2017b, Scrivener et al., 2016, Dodds, 2012). In addition, the combination of SEM and EDS analysis can provide information about the morphology and elemental composition of the hydrated phases of binders (Rossen and Scrivener, 2017).

#### *4.5.3.1 SEM analysis of the NAAUB paste under different curing methods*

Figures 4.15 to 4.20 present the SEM micrographs of the NAAUB paste after 3, 7, 28 and 180 days of air curing (NAAUB-A), water curing (NAAUB-W) and water curing temperature (NAAUB-H50). For all methods of curing and at all curing ages, no intact powder particles of binder materials were detected; the particles of the CFC and GGBS, were transformed into hydration products due to a successful geopolymerisation reaction. At the age of 3 days, the SEM images in Figure 4-15 and Figure 4.17 evidenced the formation of geopolymer gel correlated with an inhomogeneity of microstructure and associated with some microcracks. The NAAUB-H50 (Figure 4-18) showed a compact matrix with small microcracks upon closer observation. These observations of the microstructure explained the high mechanical

performance of the NAAUB-H50 relative to the NAAUB-A and NAAUB-W at this period of curing. At 7 days, the SEM images in Figure 4-15, Figure 4-17 and Figure 4-18 showed denser microstructure with finer microcracks relative to that at 3 days. These findings are in agreement with the improved compressive strength and flexural strength for all the methods of curing.

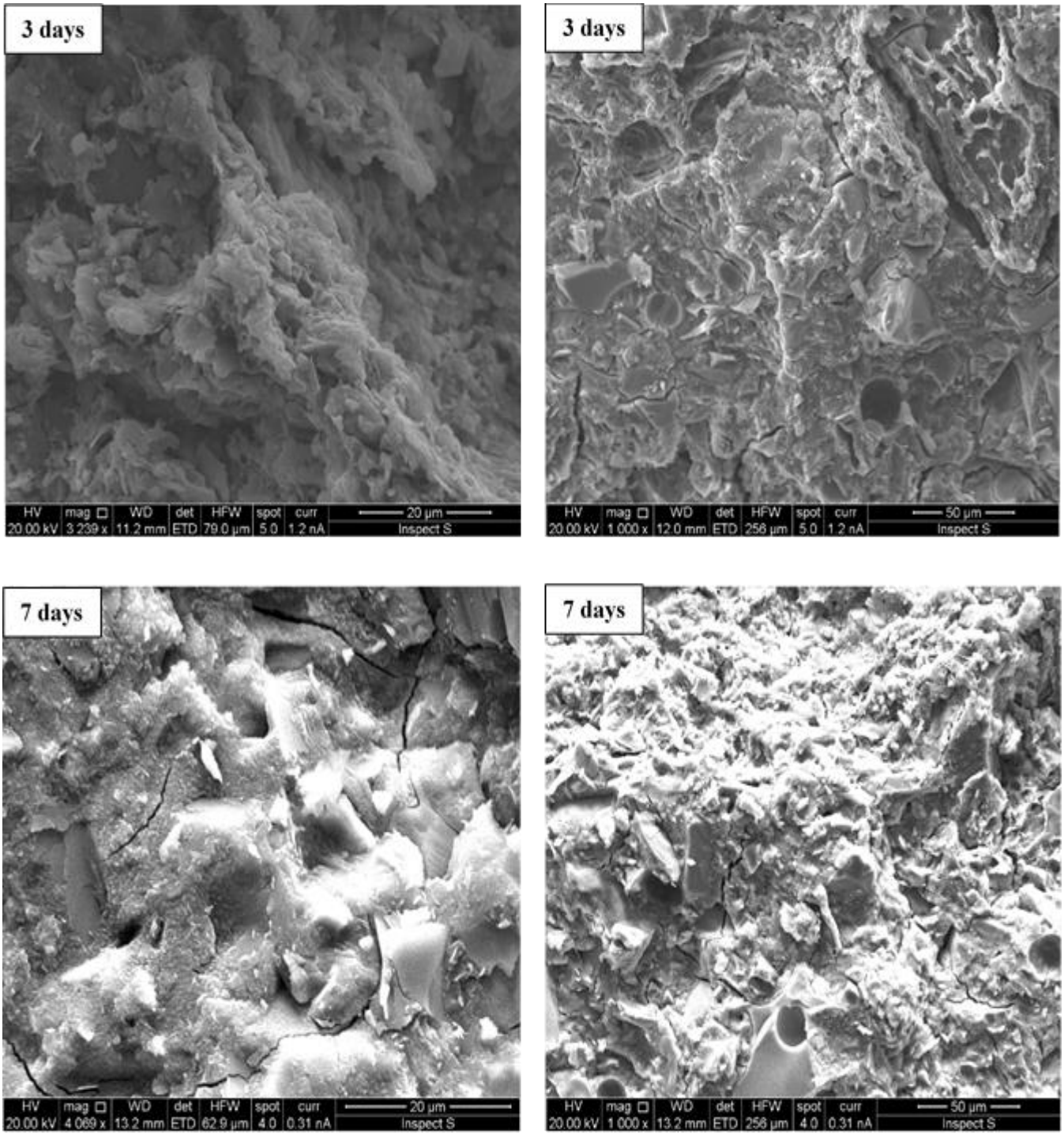


Figure 4-15. SEM micrographs of the NAAUB paste from 3 days to 7 days of air curing

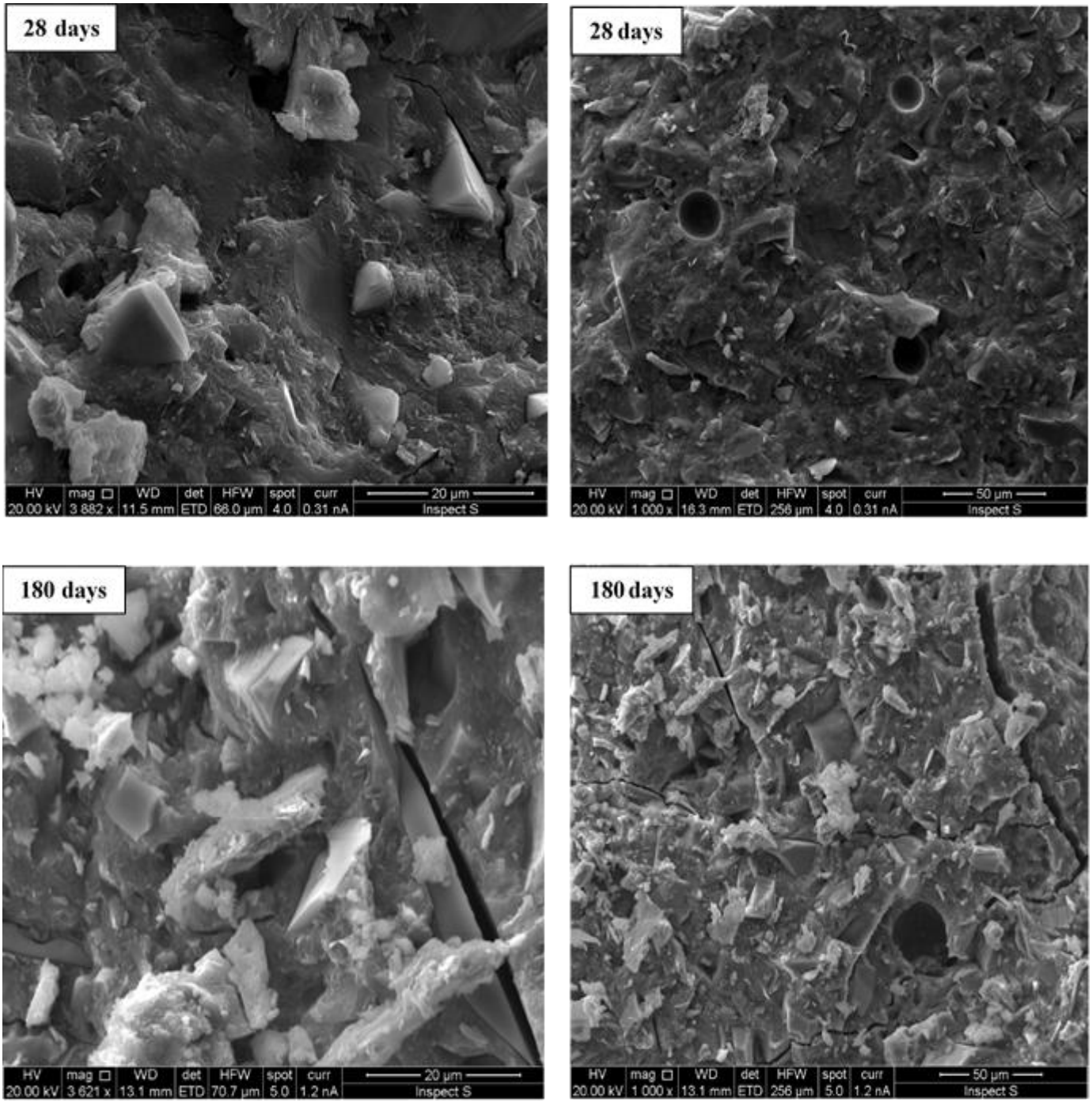


Figure 4-16. SEM micrographs of the NAAUB paste from 28 days to 180 days of air curing

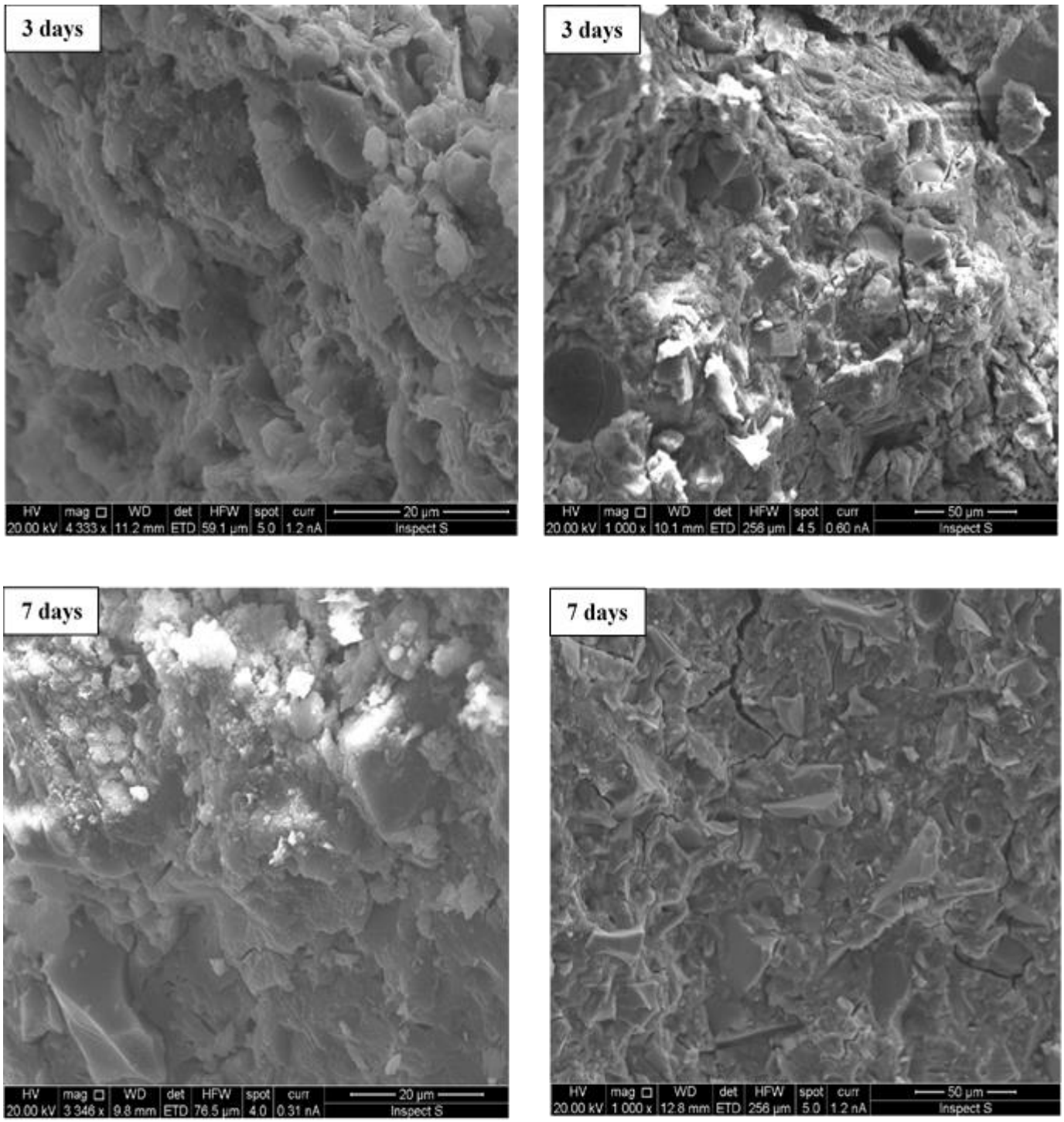


Figure 4-17. SEM micrographs of the NAAUB paste from 3 days to 7 days of water curing

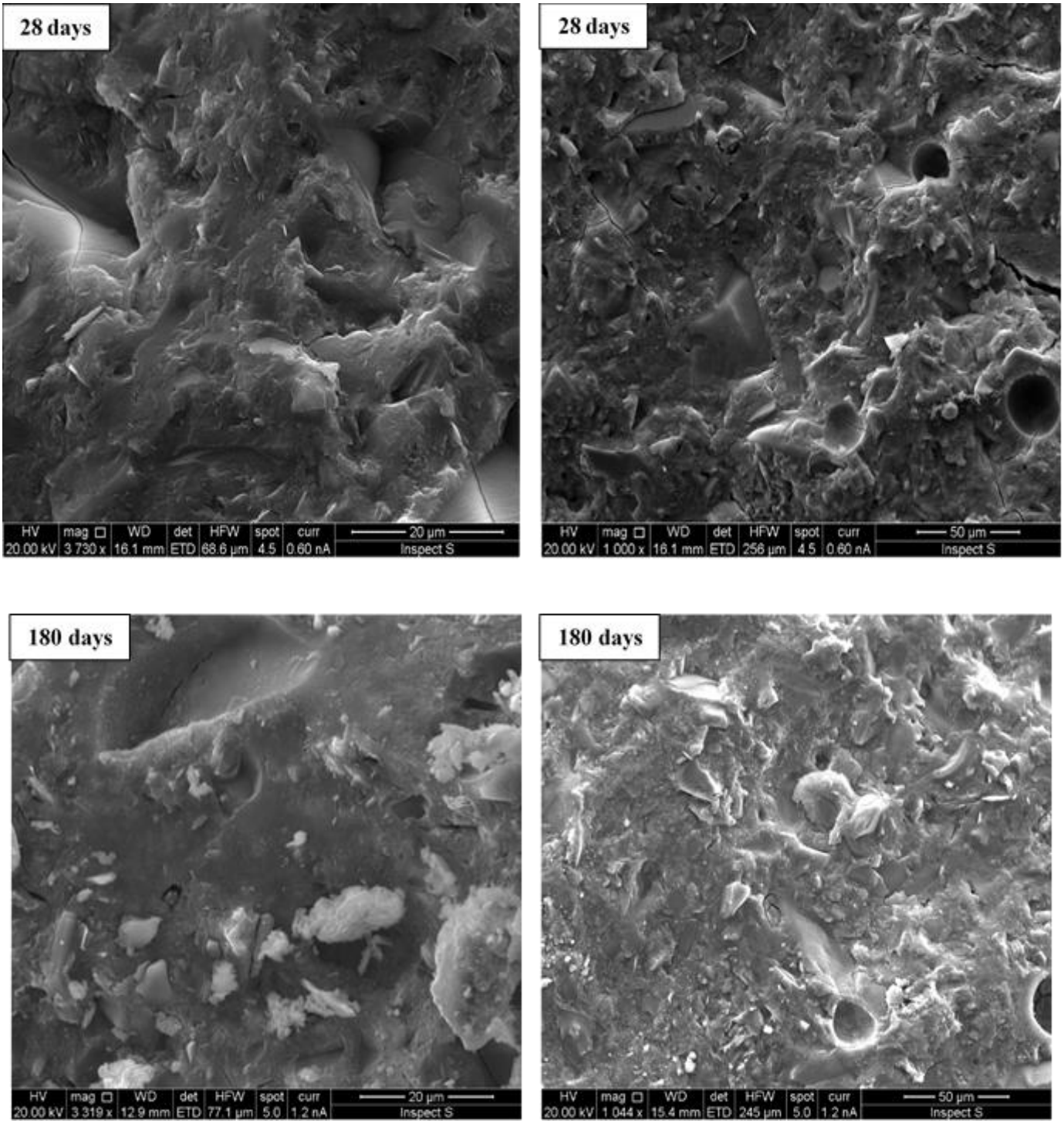


Figure 4-17. SEM micrographs of the NAAUB paste from 28 days to 180 days of water curing

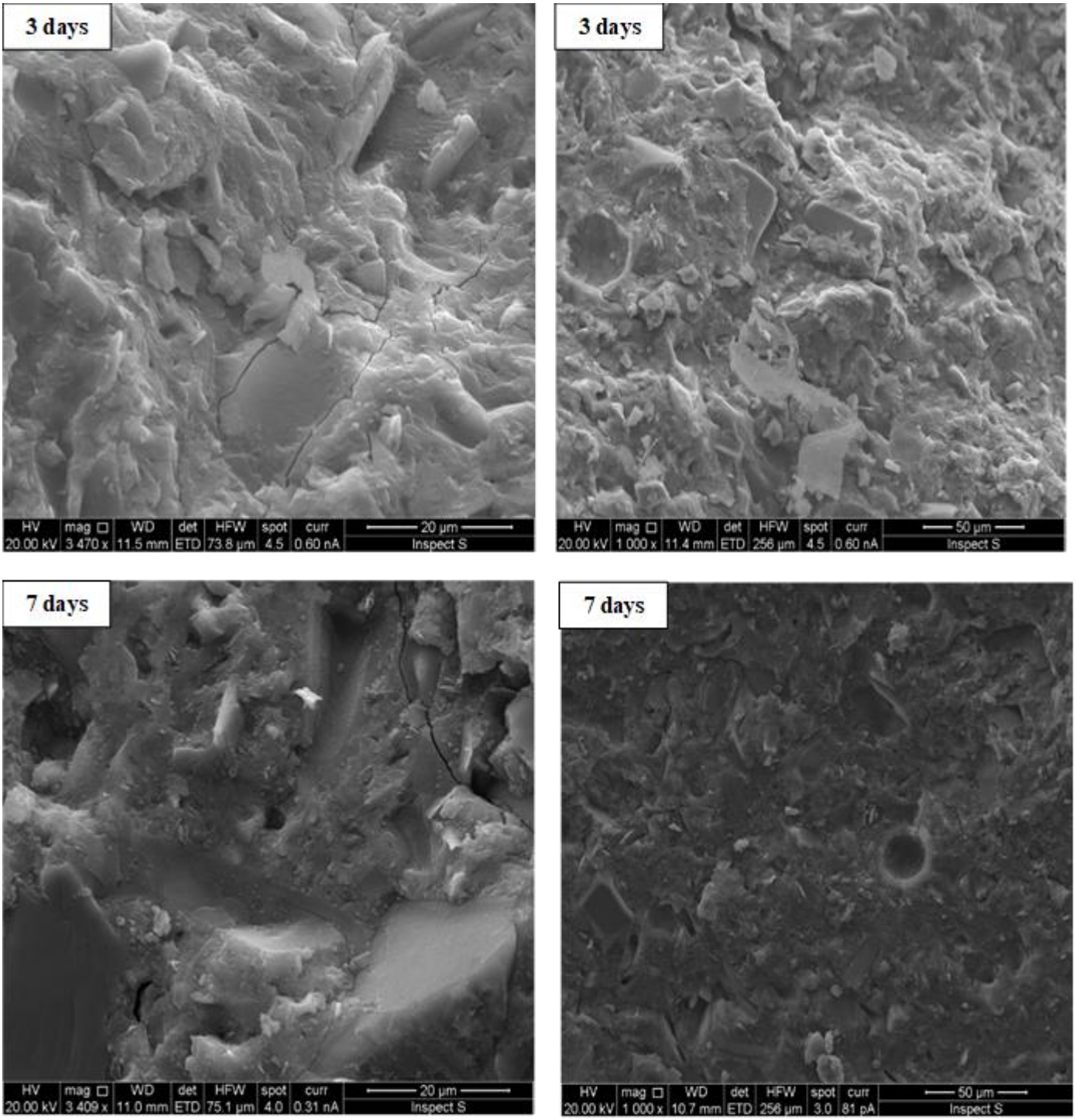


Figure 4-18. SEM micrographs of the NAAUB paste from 3 days to 7 days of water curing temperature

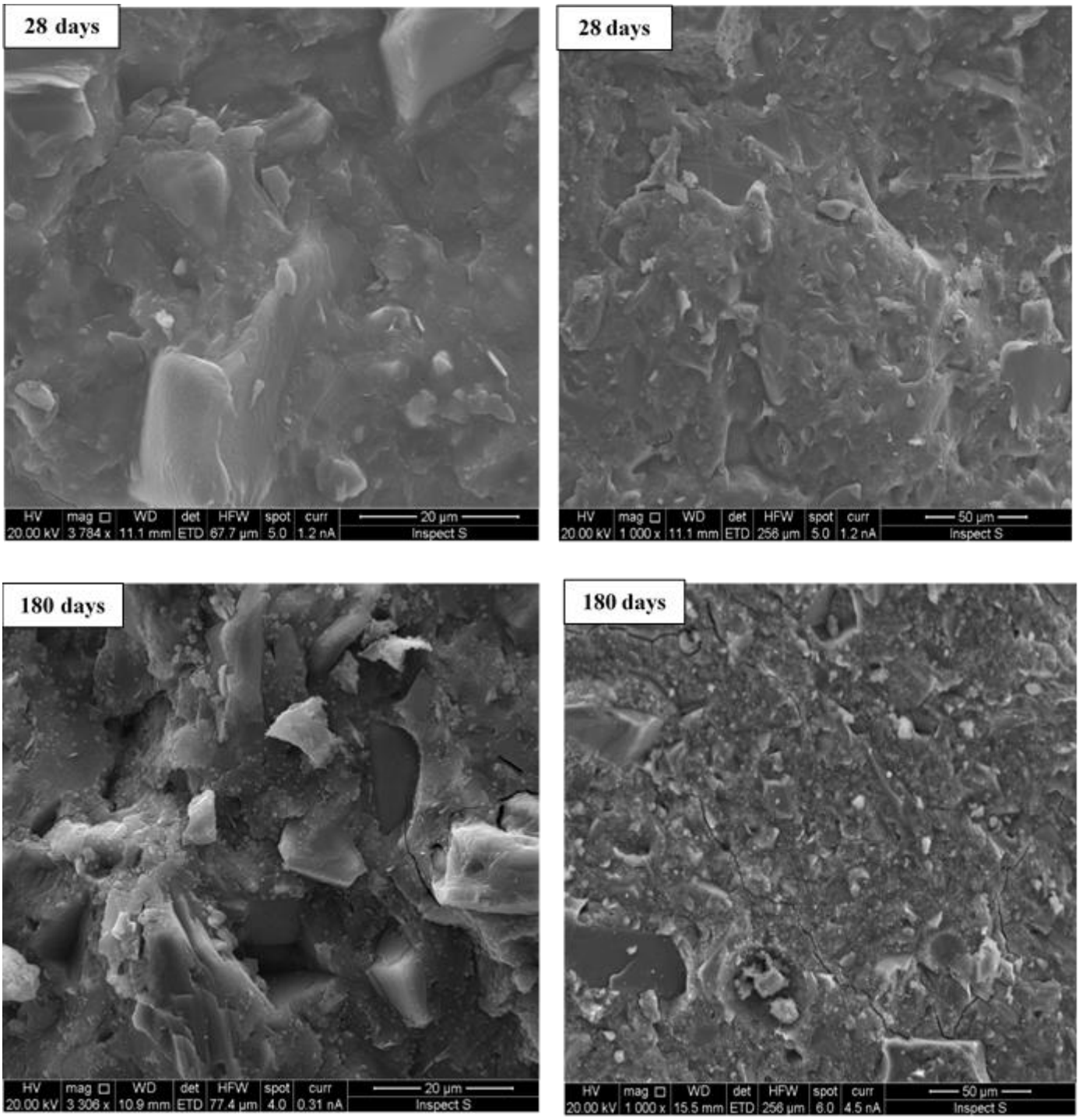


Figure 4-19. SEM micrographs of the NAAUB paste from 28 days to 180 days of water curing temperature

At 28 days, the gel appears evenly distributed, covering most of the NAAUB paste surface with a very dense microstructure. As the curing period increased from 3 to 28 days, it was found that the gel continues to fill up the interior spaces and forms a strongly compacted and very dense microstructure, thus resulting in a reduced number of microcracks. These observations were consistent with the improvement in the compressive strength and flexural strength of the NAAUB for all methods of curing.

Many researchers (Lemougna et al., 2020, Robayo-Salazar et al., 2017b, Guo et al., 2009, Yip and Van Deventer, 2003, Sasui et al., 2020) have reported the simultaneous formation of geopolymer gel and C-S-H gel in alkali activated systems with high CaO content. Therefore, due to the high CaO content in the NAAUB powder, C-S-H gel was also formed simultaneously with the geopolymer gel within the same system. However, the SEM images of the NAAUB paste at different curing conditions do not show a clear difference between the geopolymer gel and the C-S-H gel. Although, the C-S-H gel could not be recognised from the SEM images, however, the formation of a homogeneous and dense microstructure with the extension of the period of curing was attributed to the slow formation of the C-S-H gel relative to geopolymer gel (Ahmari and Zhang, 2013). It has been reported by Robayo-Salazar et al. (2017b) and Rakhimova and Rakhimov (2015) that the stable coexistence of geopolymer gel and C-S-H gel means that these binders are expected to show good mechanical performance. This is in agreement with the improved mechanical performance of the developed brick with the increase in the period of curing.

At 180 days, the SEM micrographs of the NAAUB-A (Figure 4-16) showed the formation of large cracks with some voids, these microcracks would limit the binding capacity that negatively affects the strength of the NAAUB as reported by Liu et al. (2016). The reason behind the formation of these voids and microcracks was due to the continuous moisture loss from the specimens with the increase in the period of curing that resulted in the reduction in the compressive strength as obtained in Figure 4-12. Similar observations were reported by Nagral et al. (2014). On the other hand, the SEM micrographs of the NAAUB-W (Figure 4-17) and the NAAUB-H50 (Figure 4-) showed the continuous formation of a dense and compact geopolymer matrix associated with finer cracks (which are barely visible) to which the slight reduction in the compressive strength and flexural strength of the NAAUB-H50 was attributed.

### *4.5.3.2 SEM/EDS analysis of the NAAUB paste under different curing methods*

The elemental compositions of the surface of the NAAUB paste at different curing ages and for air curing, water curing and water curing temperature were analysed by SEM/EDS testing as shown in Table 4-14, Table 4-015 and Table 4-16, respectively. The main elements detected for the NAAUB paste for all curing methods are O, Si, Ca and Al along with some Na, Mg, K, Fe and Ti. However, the Ti has not been detected at 28 days for the NAAUB-A and at 180 days for the NAAUB-W.

Table 4-14. Element analysis of NAAUB paste by EDS under air curing (NAAUB-A)

| Element | 3 days | | 7 days | | 28 days | | 180 days | |
|---|---|---|---|---|---|---|---|---|
| | Weight% | Atomic % | Weight % | Atomic % | Weight % | Atomic % | Weight % | Atomic % |
| **O** | 54.69 | 70.17 | 51.05 | 65.6 | 60.02 | 73.34 | 53.31 | 68.64 |
| **Na** | 2.99 | 2.67 | 10.28 | 9.19 | 6.03 | 5.13 | 2.2 | 1.97 |
| **Mg** | 1.53 | 1.29 | 2.33 | 1.97 | 2.56 | 2.06 | 3.69 | 3.13 |
| **Al** | 6.09 | 4.64 | 4.61 | 3.51 | 4.64 | 3.36 | 6.34 | 4.84 |
| **Si** | 19.33 | 14.13 | 16.55 | 12.12 | 15.28 | 10.64 | 17.67 | 12.96 |
| **K** | 2.38 | 1.25 | 0.62 | 0.32 | 0.69 | 0.35 | 0.68 | 0.36 |
| **Ca** | 7.16 | 3.67 | 13.11 | 6.73 | 9.79 | 4.78 | 14.71 | 7.56 |
| **Ti** | 0.7 | 0.3 | 0.44 | 0.19 | - | - | 0.27 | 0.12 |
| **Fe** | 5.12 | 1.88 | 1.01 | 0.37 | 0.97 | 0.34 | 1.12 | 0.41 |
| **Si/Al** | | **3.05** | | **3.45** | | **3.17** | | **2.68** |

In the SEM/EDS testing, the most important ratio is the Si/Al (atomic) ratio because it determines the main gel structure formed and it has a linear relationship with the compressive strength of the geopolymer products, as reported previously by Gunasekara et al. (2016), Yun-Ming et al. (2016) and Liu et al. (2016). It can be seen from Table 4-14, Table 4-015 and Table 4-16 that up to the age of 28 days, the highest Si/Al ratio was reported for the NAAUB-H50 followed by the NAAUB-A and then the NAAUB-W. This explains why the NAAUB-H50

samples exhibit higher mechanical strength relative to NAAUB-A and the NAAUB-W samples although, they show similar microstructure (Ahmari and Zhang, 2013).

Table 4-015. Element analysis of NAAUB paste by EDS under water curing (NAAUB-W)

| Element | 3 days | | 7 days | | 28 days | | 180 days | |
|---|---|---|---|---|---|---|---|---|
| | Weight% | Atomic % | Weight % | Atomic % | Weight % | Atomic % | Weight % | Atomic % |
| **O** | 57.66 | 71.95 | 52.57 | 68.16 | 48.33 | 64.02 | 57.47 | 71.98 |
| **Na** | 5.71 | 4.95 | 2.28 | 2.06 | 5.25 | 4.84 | 3.41 | 2.97 |
| **Mg** | 2.61 | 2.15 | 2.8 | 2.39 | 3.14 | 2.73 | 2.8 | 2.31 |
| **Al** | 4.68 | 3.47 | 5.87 | 4.51 | 6.12 | 4.81 | 5.41 | 4.02 |
| **Si** | 14.32 | 10.18 | 19.42 | 14.34 | 18.81 | 14.2 | 16.07 | 11.46 |
| **K** | 0.71 | 0.36 | 1.15 | 0.61 | 0.97 | 0.52 | 0.77 | 0.39 |
| **Ca** | 12.75 | 6.35 | 13.68 | 7.08 | 15.08 | 7.98 | 12.88 | 6.44 |
| **Ti** | 0.5 | 0.21 | 0.35 | 0.15 | 0.42 | 0.19 | - | - |
| **Fe** | 1.06 | 0.38 | 1.9 | 0.71 | 1.89 | 0.72 | 1.19 | 0.43 |
| **Si/Al** | | **2.93** | | **3.18** | | **2.95** | | **2.85** |

Sadique et al. (2013) and Guo et al. (2009) reported that the high Si/Al ratio from the EDS test confirms the simultaneous formation of geopolymer gel and C–S–H gel within the hydration product. Therefore, the increased Si/Al ratio indicates the formation of a more rigid and homogenous geopolymer gel and C-S-H gel, thus enhancing the mechanical performance of the developed brick for all methods of curing (Lemougna et al., 2020, 2017b, Yun-Ming et al., 2016, Lloyd et al., 2008, Rowles and O'connor, 2003). However, the decreased Si/Al ratio at the ages of 28 and 180 days, was attributed to the ongoing geopolymerisation and the consumption of more silica in the production of more C-S-H gel along with the contribution of

more dissolved Al species in the system (Gunasekara et al., 2016, Yun-Ming et al., 2016). Similar findings were reported by Gunasekara et al. (2016) and Zhang et al. (2005).

Table 4-16. Element analysis of NAAUB paste by EDS under water curing temperature (NAAUB-H50)

| Element | 3 days | | 7 days | | 28 days | | 180 days | |
|---|---|---|---|---|---|---|---|---|
| | Weight % | Atomic % | Weight % | Atomic % | Weight % | Atomic % | Weight % | Atomic % |
| **O** | 49.06 | 64.77 | 48.74 | 64.41 | 49.92 | 65.9 | 51.34 | 66.87 |
| **Na** | 4.57 | 4.2 | 5.75 | 5.29 | 2.1 | 1.93 | 2.56 | 2.32 |
| **Mg** | 2.97 | 2.58 | 2.29 | 1.99 | 3.07 | 2.66 | 3.63 | 3.11 |
| **Al** | 5.73 | 4.48 | 5.24 | 4.11 | 5.91 | 4.62 | 6.04 | 4.67 |
| **Si** | 19.36 | 14.56 | 19.49 | 14.67 | 20.56 | 15.47 | 19.51 | 14.48 |
| **K** | 0.95 | 0.51 | 1.01 | 0.55 | 1.23 | 0.66 | 0.74 | 0.39 |
| **Ca** | 15.52 | 8.18 | 15.78 | 8.32 | 14.85 | 7.83 | 14.35 | 7.46 |
| **Ti** | 0.35 | 0.15 | 0.38 | 0.17 | 0.44 | 0.19 | 0.3 | 0.13 |
| **Fe** | 1.48 | 0.56 | 1.32 | 0.5 | 1.93 | 0.73 | 1.53 | 0.57 |
| **Si/Al** | | **3.25** | | **3.57** | | **3.35** | | **3.10** |

### *4.5.4 Summary of section (4)*

The EDXRF analyses of the NAAUB powder showed a high amount of $SiO_2$ and CaO along with a moderate amount of $Al_2O_3$, while the physical properties of the NAAUB powder showed that it has a high SSA with fine particles, that all lead to the quick reaction with the alkali solution and produces a large amount of geopolymer gel and C-S-H gel as evident from the SEM and SEM/EDS analyses.

Following the successful production of a novel unfired brick using the technique of alkali activation, with excellent mechanical performance, under different methods of curing, as presented in previous sections, the reasons for achieving such improvements were elucidated in this section by employing the SEM imaging and SEM/EDX analyses. Pastes of the NAAUB were subjected to SEM testing and SEM/EDS analyses at different ages of curing and for different methods of curing for microstructural and morphological investigation.

SEM imaging revealed the formation of geopolymer gel at early ages, which is correlated with an inhomogeneity of microstructure and associated with some microcracks, except for the NAAUB-H50, that revealed a compact microstructure with the formation of finer microcracks. Increasing the period of curing to 28 days resulted in the formation of very dense microstructure with gel appearing evenly distributed, covering most of the NAAUB paste surface. Beyond this age, the NAAUB-A paste surface showed the formation of large cracks with some voids while the SEM micrographs of the NAAUB-W and the NAAUB-H50 showed the continuous formation of a dense and compact geopolymer matrix.

SEM/EDS analyses were found to be well in agreement with the results obtained from the SEM testing for each corresponding period of testing. Increases in the Si/Al (atomic) ratio obtained with the increase in the period of curing from 3 to 7 days are evidence of the formation of a more rigid and homogenous geopolymer gel and C-S-H gel. However, increasing the period of curing to 28 days and 180 days resulted in the decrease of the Si/Al ratio, that indicates the ongoing geopolymerisation and the consumption of more silica in the production of more C-S-H gel, along with the contribution of more dissolved Al species in the system.

The techniques employed in this section clearly aided to understand the performance of the NAAUB under different curing conditions and for different periods of curing. In addition, the results obtained in this section were found to be consistent with those obtained from the results of the mechanical performance (Compressive strength and Flexural strength).

According to the obtained results obtained in previous sections, it was found that the compressive strength of the NAAUB-A and NAAUB-H50 decreased at later ages of curing and only the NAAUB-W continued to develop strength with the increase in the period of curing. Therefore, water curing at the temperature of 20$^{o}$C has been chosen as the selected candidate method of curing in this study to be considered in the production of NAAUB with the same dimensions (215mm x 102.5mm x 65mm) of building bricks.

## 4.6 Section 5: Comparative Performance of the NAAUB against standards specifications

### *4.6.1 Introduction*

In order to make a direct comparison with conventional fired bricks, this section presents the production of NAAUB with the same dimensions (215mm x 102.5mm x 65mm) as building bricks and evaluates its performance against standard specifications. The evaluation programme including compressive strength, durability (water absorption and freezing and thawing) and thermal properties (thermal conductivity, specific heat capacity and volume heat capacity) of the NAAUB. Figure 4-20 shows the NAAUB with dimensions 215mm x 102.5mm x 65mm. The same aforementioned tests were conducted on a randomly chosen sample of brick that is commonly available in the UK market in order to make a direct comparisons with the NAAUB to evaluate the suitability of the NAAUB to be used in the UK construction industry. The sample of brick was collected from Travis Perkins Trading Company Limited (Travis Perkins, 2019).

Figure 4-20. The NAAUB with dimensions 215mm x 102.5mm x 65mm.

### *4.6.2 Compressive strength*

The compressive strength test was performed for the NAAUB with dimensions of (215 x 102.5 x 65 mm) after 7, 14 and 28 days of water curing in order to make a direct comparison with commercially available fired bricks according to BS 3921 (British Standard, 1998). The results of the compressive strength of the standard size NAAUB (215mm x 102.5mm x 65mm) after 7, 14 and 28 days of water curing (NAAUB-W) are presented in Figure 4-21. PAS 8820:2016 suggests a minimum of 10 bricks need to be tested to arrive at a quantitatively representative value of strength for an alkali activated material (British Standards Institution, 2016).

However, in this project five samples of each of the NAAUB and conventional fired brick were tested for compressive strength and the averages of five values were considered to represent the final values presented in Figure 4-21 and Figure 4-22. This as a deviation from PAS 8820:2016 specifications and it was implemented as this project is mainly a 'proof of concept' as opposed to a commercial production commissioning document. The error bar was used to represent the minimum and maximum values obtained for each sample to demonstrate the reliability, repeatability and reproducibility of the results.

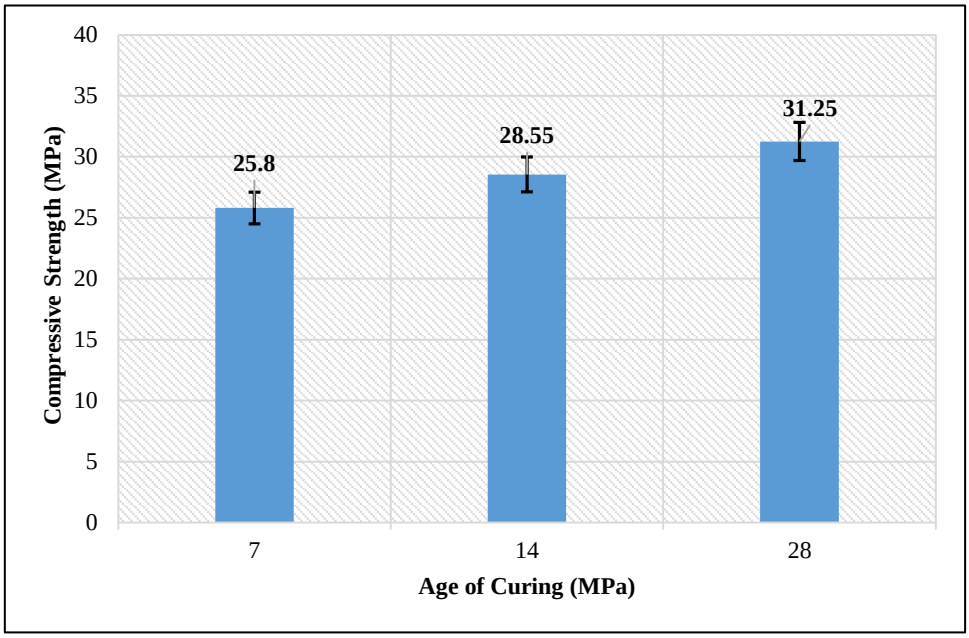


Figure 4-21. Compressive strength of the standard size NAAUB

Generally, the compressive strength of the NAAUB with standard size (Figure 4-21) was lower than the corresponding 7, 14 and 28 days compressive strength for the NAAUB with the dimensions of 160mm x 40mm x 40mm (Figure 4-12). This was attributed to the phenomenon of "size effect", where the compressive strength decreases as specimen size increases as reported by Graytee et al. (2018). This size effect is quite apparent in the compressive failure of quasi-brittle materials such as brick and block that fail due to the formation of cracks (Graytee et al., 2018, Bažant, 1996, Bazant et al., 1991, Bažant, 1984). Similar observation were obtained by Robayo-Salazar et al. (2017b).

It can be seen from Figure 4-21 that after only 7 days of water curing, the compressive strength of NAAUB-W satisfied the requirements for clay bricks given in the standard BS 3921 (British Standard, 1998) with a minimum compressive strength of 7 MPa. The satisfaction of the

minimum compressive strength requirements for clay bricks after only 7 days of curing can significantly help in improving the sustainability and reducing the cost of the NAAUB, as a shorter curing period is required. Additionally, a direct comparison between the results of the compressive strength of the NAAUB after 7 days of curing and commercially available fired brick was conducted and the results presented in Figure 4-22. It can be seen from Figure 4-22 that 7 days of water curing was sufficient to produce unfired brick with comparable compressive strength to conventional fired brick.

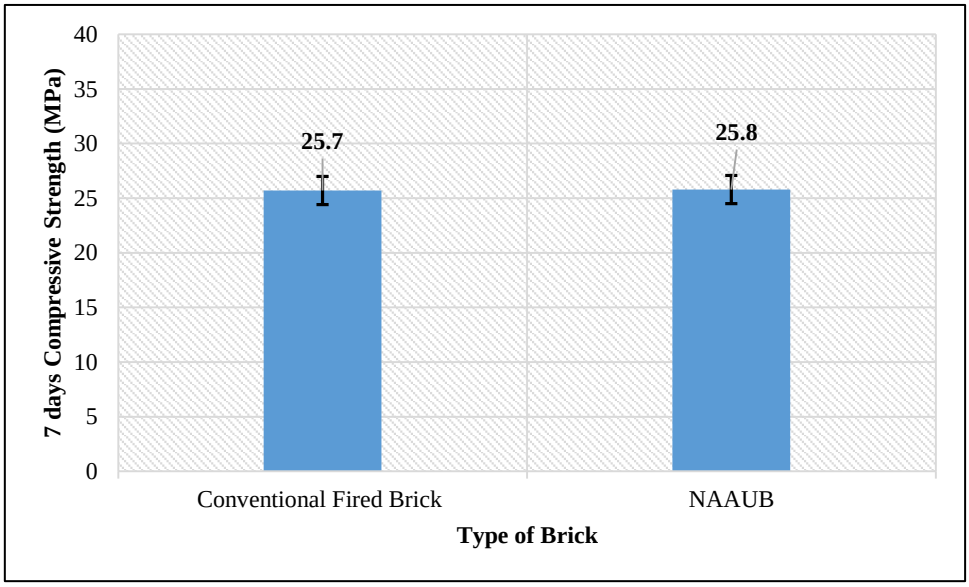


Figure 4-22. Compressive strength of conventional fired brick and NAAUB

### *4.6.3 Dry Density*

The dry density of the NAAUB and conventional fired brick was calculated according to BS EN772-13 (British Standard, 2000). Table 4.17 presents the results of the dry density of the NAAUB and conventional fired brick.

Table 4-17. Dry density of the NAAUB and conventional fired brick

| Property | Test Reference | NAAUB | Conventional fired brick |
|---|---|---|---|
| **Dry Density (kg/m$^3$)** | BS EN772-13 | 2300 | 1507 |

### *4.6.4 Durability*

Saturation by water is the commonest potential enemy of brickwork (Brick Development Association, 2011). Bricks, (especially bricks for external use) in the UK, are usually subjected to saturation with water (ground water and rain) combined with frequent freeze/thaw-cycling, due to climatic conditions, especially during winters, as night frosts are common, even in mild winters (Brick Development Association, 2011, British Standard, 2005b). The destructive effect of frost is attributed to the increase in volume that occurs when water inside the bricks at $0^{o}$C is converted into ice that causes expansion within the pore spaces and lead to stresses that result in the formation of cracks and spall of bricks (Brick Development Association, 2011). Therefore, for evaluating the durability of the NAAUB, two tests were conducted; water absorption test and freezing and thawing tests.

#### *4.6.4.1 Water absorption*

The water absorption test is a very important test that is usually conducted to evaluate the durability performance of bricks. The water absorption test is considered as a measurement to the compactness of bricks and it can provide direct measurement for the resistance of bricks to damage by freezing. The water absorption test was conducted for the NAAUB specimens according to BS EN 771-1:2003+A1:2005 (British Standard, 2005b). As stated in section 4.6.2 above, there was a need for 7 days water curing for the NAAUB to provide the required compressive strength, therefore, the production of NAAUB will be always associated with water curing for 7 days before it can be tested or used for any application. In this section all the tested NAAUB samples were cured in water for 7 days before the water absorption test was conducted. Additionally, the conventional fired bricks were submerged in water for 7 days in order to perform direct comparison with the NAAUB. After the 7 days, ten bricks (both NAAUB and fired clay bricks) were dried in an oven at 105 ± 5 °C for 24 hours and then the dry mass ($m_d$) of samples was recorded. Then each sample was submerged in a water tank at room temperature for 24 hours. After that, the samples were taken out from tank and any surplus water from their surfaces was removed using a damp cloth. The wet mass ($m_w$) of each sample was recorded. Then the mean water absorption (W***m***) was determined using Equation 2.

Similar to the compressive strength test, a direct comparison between the results of the water absorption of the NAAUB and commercially available fired brick was conducted and the results presented in Figure 4-23. The error bar was used to represent the minimum and

maximum values obtained for each sample to demonstrate the reliability, repeatability and reproducibility of the results. It can be seen from Figure 4-23 that the NAAUB has only about 3.7% of the water absorption relative to conventional fired brick. Generally, the water absorption rate of the NAAUB was very low and satisfied the requirements for engineering bricks class A given in the standard BS EN 771-1:2003+A1:2005 (British Standard, 2005b) with a maximum water absorption rate of 4.5 %. The very low water absorption rate of the NAAUB was attributed to the formation of the very dense microstructure of the NAAUB, as can be seen from the SEM images (Figure 4.15 and Figure 4-17). Therefore, the durability performance of the NAAUB is significantly higher than that of the conventional fired brick.

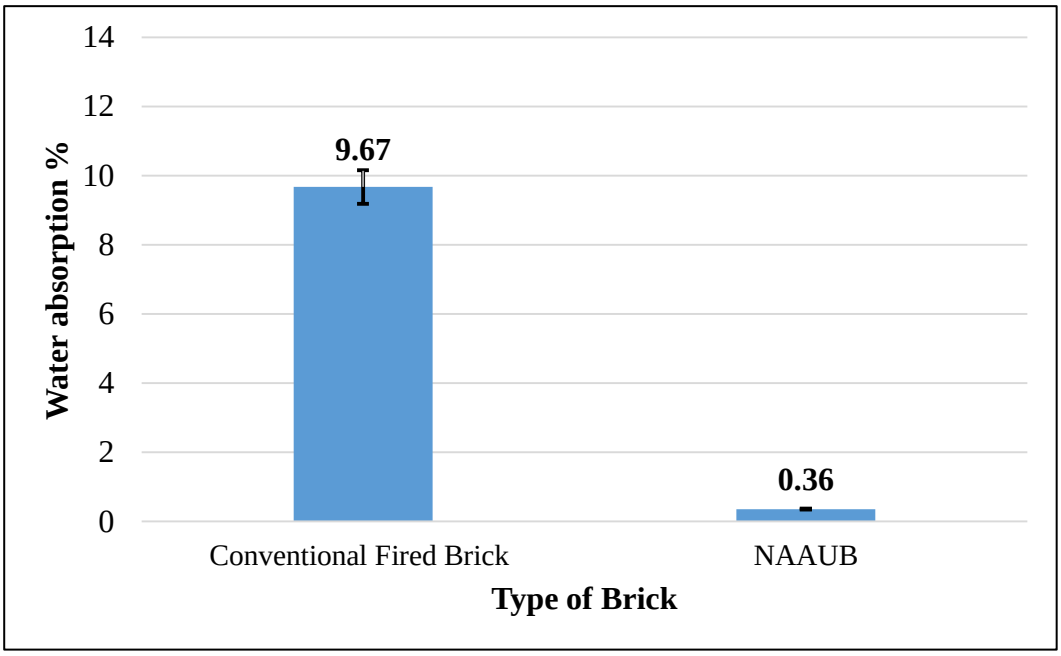


Figure 4-23. Water absorption rate of conventional fired brick and NAAUB.

### *4.6.4.2 Freezing and thawing*

The NAAUB samples were immersed in de-ionized water and subjected to freeze–thaw attack. The freeze–thaw resistance is evaluated by the measurement of mass loss of the NAAUB after 7, 14, 21, 28, 42, 56, 90 and 180 freeze–thaw cycles according to DD CEN/TS 12390-9:2006 (British Standard, 2006). The freeze-thaw cycles were at the temperature of +20$^{o}$C to -20$^{o}$C and the period for each cycle was 24 h. Additionally, as part of the test, visual examination of the physical conditions of the NAAUB was conducted after 180 freeze–thaw cycles to determine whether cracks or other substantial changes have occurred. In this section all the tested NAAUB were cured in water for 7 days before the water absorption test was conducted. Additionally, the conventional fired bricks were submerged in water for 7 days in order to

perform direct comparison with the NAAUB. PAS 8820:2016 suggests a minimum of 5 bricks need to be tested to arrive at a quantitatively representative value of freeze and thaw for an alkali activated material (British Standards Institution, 2016). However, in this project three samples with the dimensions of (215 x 102.5 x 65 mm) were subjected to the freeze and thaw cycles, and the average weight loss after 7, 14, 21, 28, 42, 56, 90 and 180 cycles of freeze and thaw was recorded and compared with that of the conventional fired brick. This as a deviation from PAS 8820:2016 specifications and it was implemented as this project is mainly a 'proof of concept' as opposed to a commercial production commissioning document. The error bar was used to represent the minimum and maximum values obtained for each sample to demonstrate the reliability, repeatability and reproducibility of the results.

The results of the weight loss due to wet freezing and thawing cycles of the NAAUB and conventional fired brick samples after 7, 14, 21, 28, 42, 56, 90 and 180 cycles are displayed in Figure 4-24. It can be seen from Figure 4-24 that the weight loss of both types of brick increased as the freezing-thawing cycles increased.

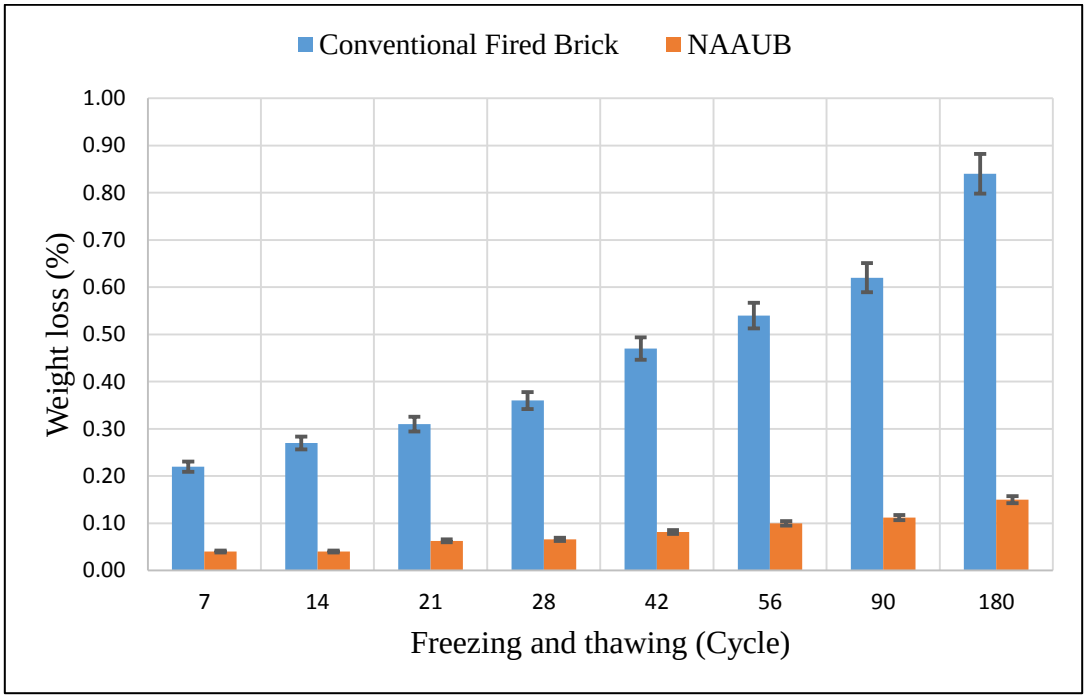


Figure 4-24. Percentage weight loss for the conventional fired brick and NAAUB.

It can be seen from Figure 4-24 that the weight loss of the NAAUB was significantly lower than that of the conventional fired brick at all the freezing and thawing cycles. This was mainly attributed to the high water absorption rate of fired brick relative to the NAAUB, that resulted in higher internal stresses and higher weight loss (Brick Development Association, 2011). The

obtained results indicated that the performance of the NAAUB is acceptable as it has showed lower weight loss relative to the conventional fired brick as stated by the PAS 8820:2016 (British Standards Institution, 2016). The highest weight loss for the NAAUB was 0.15% reported after 180 cycles of freezing and thawing that was only about 18% of weight loss of the conventional fired brick. The weight loss of the NAAUB was in the range of 0.04% to 0.15%, thus it indicated that the NAAUB with only 7 days of water curing was able to withstand 180 cycles of freezing and thawing and according to the obtained results it can be concluded that the NAAUB can be classified as Frost resistant (F) brick according to BS 3921(British Standard, 1998).

Detailed assessment of the NAAUB and conventional fired brick after the end of 180$^{th}$ freezing-thawing cycle is presented in Table 4-18. The analysis of the physical assessment of the NAAUB specimens indicated no damage of any type, while the conventional fired brick has showed some chipping after the end of the 180$^{th}$ freezing-thawing cycle.

Table 4-18 Assessment of physical damage of the NAAUB and conventional fired brick at the end of the 180th freezing and thawing cycle

| Description of damage | Remarks | |
|---|---|---|
| | Conventional Fired Brick | NAAUB |
| **Minor cracks** | No | No |
| **Surface cracks** | No | No |
| **Peeling** | No | No |
| **Chipping** | Yes | No |
| **Breaking** | No | No |
| **Fracture** | No | No |

### *4.6.5 Thermal Properties*

The thermal properties of the NAAUB were investigated under a range of temperatures (-5$^{o}$C to 40$^{o}$C). The main reason behind measuring the thermal properties of the NAAUB in the range of (-5$^{o}$C to 40$^{o}$C) was to evaluate the suitability of the newly developed brick to be used in the UK, taking into considerations expected temperatures during all seasons. Figure 4-25, Figure 4-27 and Figure 4-28 show the results of thermal conductivity, volume heat capacity and

specific heat capacity of the NAAUB, respectively. These tests were conducted for the NAAUB in dry conditions according to BS EN 1745 (British Standard, 2002b). For evaluating the thermal properties, three samples of the NAAUB and conventional fired brick were tested and the error bar was used to represent the minimum and maximum values obtained for each sample to demonstrate the reliability, repeatability and reproducibility of the results.

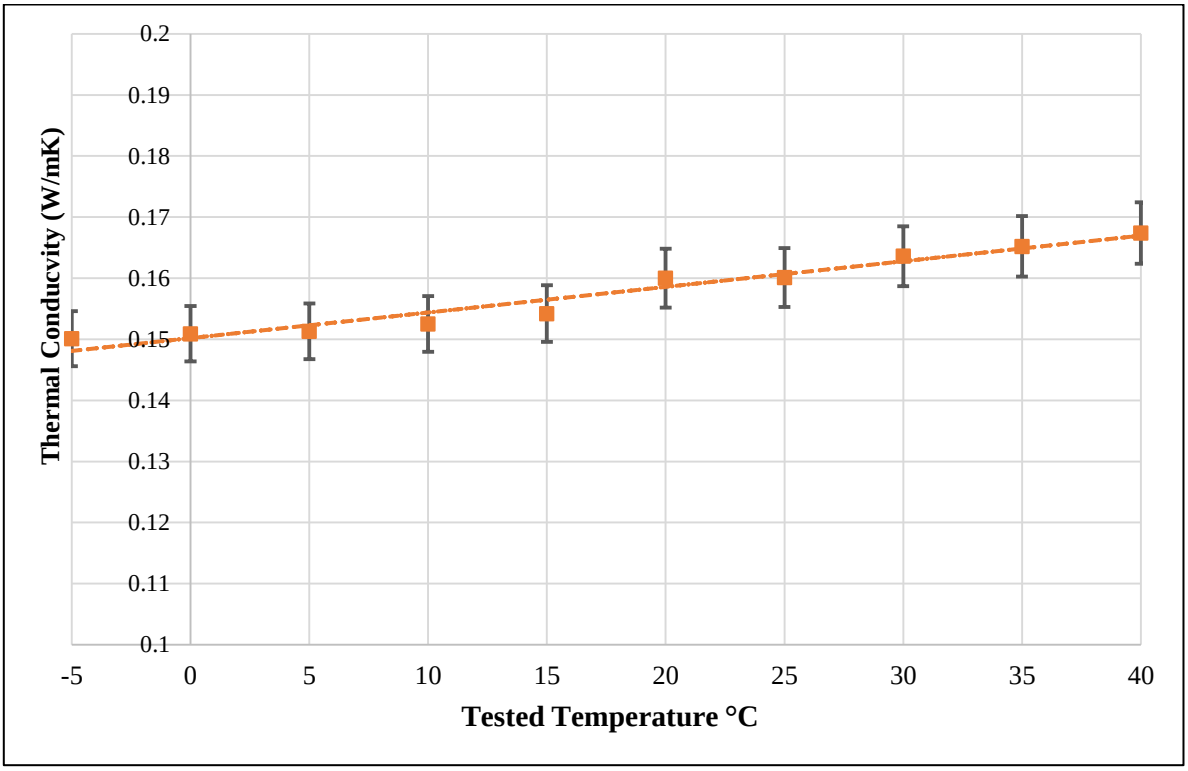


Figure 4-25. Thermal conductivity against temperature of the NAAUB

It can be seen from Figure 4-25 that the thermal conductivity of the NAAUB increased slightly with the increase in the temperature and the highest thermal conductivity value was 0.1674 W/mK obtained at 40$^{o}$C, while the lowest thermal conductivity value was 0.1501 W/mK obtained at -5$^{o}$C. The increase in thermal conductivity of the NAAUB with increase temperature was attributed to the formation of denser microstructure with reduced pores for alkali activated materials at elevated temperatures due to the formation of more geopolymeric gel (Hassan et al., 2019, Leitão et al., 2017). Additionally, there was no significant difference in thermal conductivity values for the NAAUB at all tested temperatures. Therefore, this can help in increasing the indoor comfort and decreasing the energy needed for heating or cooling for buildings made with the developed brick (Sore et al., 2018, Leitão et al., 2017). Additionally, the thermal conductivity test was conducted at room temperature (20$^{o}$C) for both conventional fired brick and the NAAUB (Figure 4-26). In comparison with conventional fired

clay brick, the NAAUB have shown only about 21% of the thermal conductivity of the tested conventional fired clay brick (0.75 W/mK) and about 22% of thermal conductivity specified in BS EN 1745 (British Standard, 2002a) taking into consideration that the mean value for dry density of the NAAUB is 2300 kg/m$^3$. On the other hand, the thermal conductivity of the NAAUB according to CIBSE Guide section A3 (CIBSE, 2006), should be about 1.9 W/mK taking into consideration the dry density is 2300 kg/m$^3$. This deviation from the CIBSE Guide section A3 is mainly attributed to the method of testing that where followed in this research, which was a transient method not steady state method.

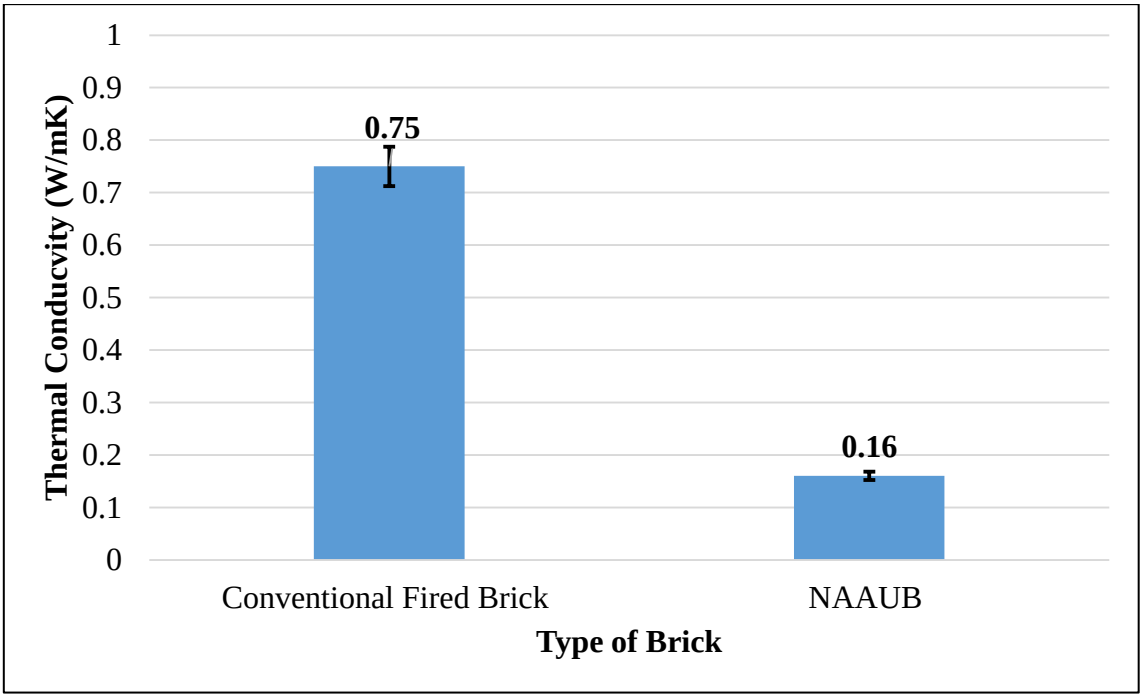


Figure 4-26. Thermal conductivity of the conventional fired brick and NAAUB

Figure 4-27 presents the results of the volume heat capacity of the NAAUB. The results of the volume heat capacity of the NAAUB was in the range of 1.5884x10$^6$ J/m$^3$.K to 1.6094 x10$^6$ J/m$^3$.K. The ISOMET 2104 measures only the volumetric heat capacity (cp), however, in civil engineering practice, the most common and most used, is the specific heat capacity (c) (Koňáková et al., 2013). Therefore, in order to obtain the specific heat capacity of the NAAUB, the Equation 3 was applied:

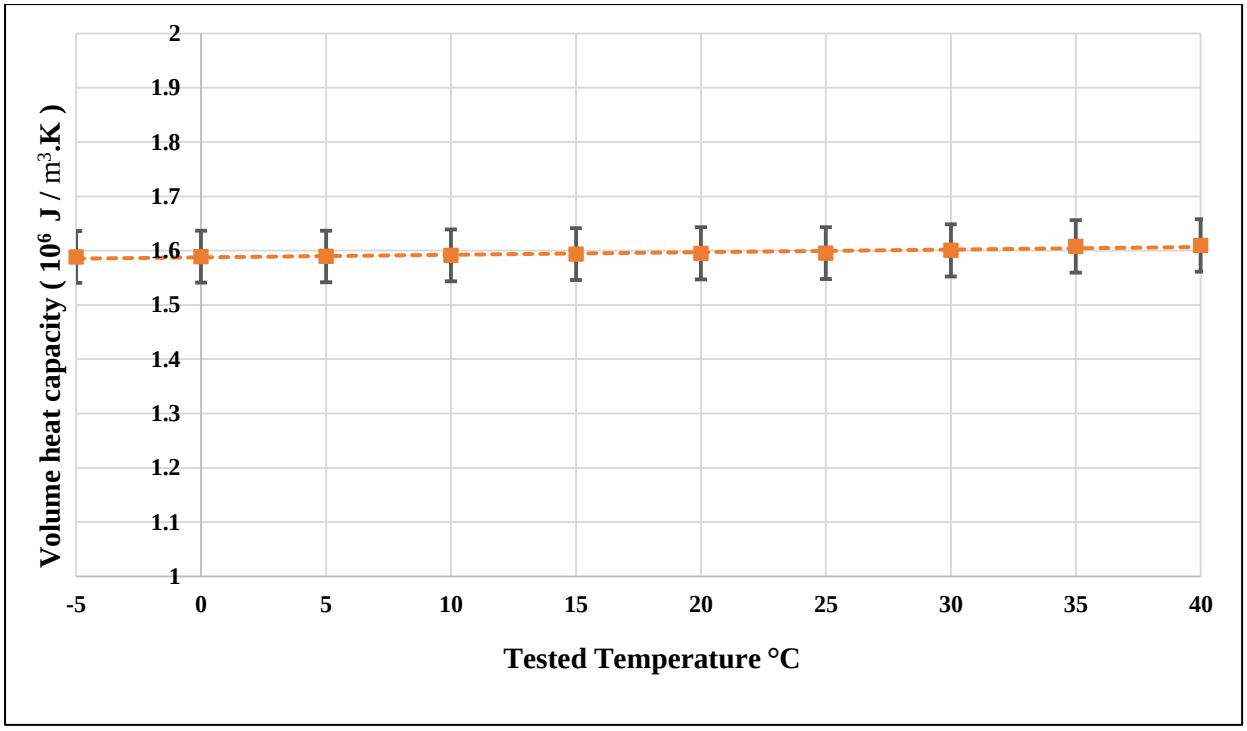


Figure 4-27. Volume heat capacity against temperature of the NAAUB.

$c = \frac{Cp}{p}$ (Koňáková et al., 2013)……(3)

Where:

c: the specific heat capacity

Cp: the volumetric heat capacity

p: the bulk density

Figure 4-28 presents the results of the specific heat capacity of the NAAUB. The values of the specific heat capacity were determined using Equation 3 and taking into consideration that the mean value for the dry density of the NAAUB is 2300 kg/m$^3$. It can be seen from Figure 4-28, that the specific heat capacity of the NAAUB was in the range of 696.67 J/kg.°C to 705.88 J/kg.°C) that was only about 70% of the specific heat capacity of fired clay brick (1000 J/kg.°C) specified in the BS EN 1745 (British Standard, 2002a). The slight increase in the specific heat capacity with the increase in temperature was due to the fact that as the NAAUB heats up with the increase in temperature, the average kinetic energy of the molecules increases, they collide and they are more likely to impart enough energy to allow rotation that in turn contributes to the internal energy and raises the specific heat capacity (Dwayne, 2014)

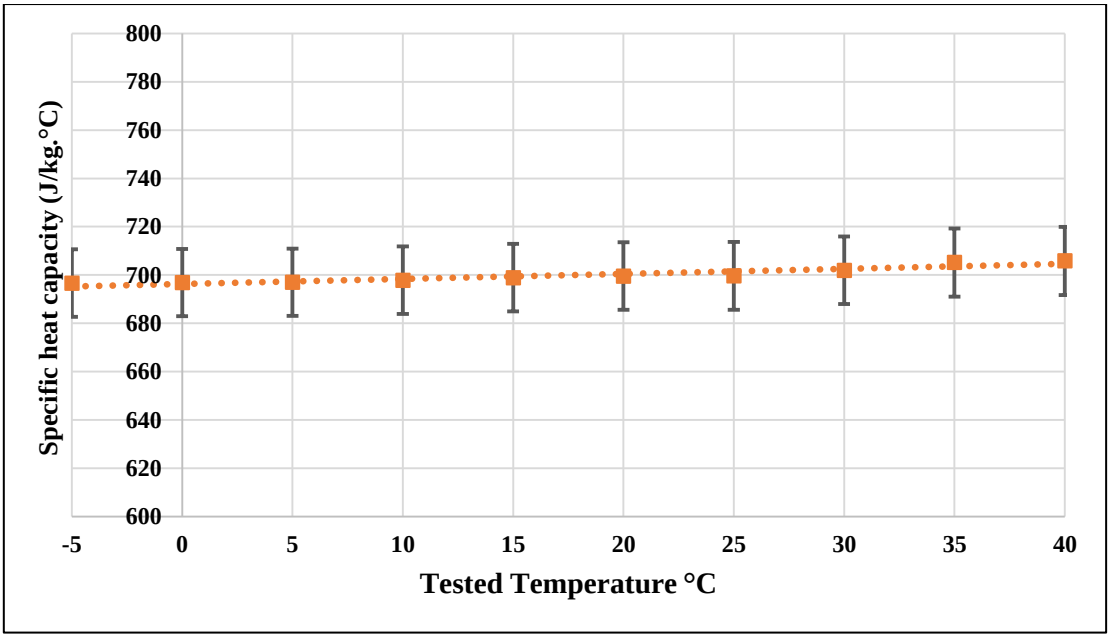


Figure 4-28. Specific heat capacity against temperature of the NAAUB

The different mechanical, durability and thermal properties of the NAAUB were determined following the procedures specified in the relevant standards. The measured properties are summarised in Table 4-19.

Table 4-19. Mechanical, durability and thermal properties of the NAAUB against conventional fired brick

| Property | Test Reference | NAAUB | Conventional fired brick | Requirement |
|---|---|---|---|---|
| **Compressive Strength (MPa)** | BS 3921 | 25.8 | 25.7 | 7-100 |
| **Water absorption (%)** | BS 3921 | 0.36 | 9.67 | <4.5 |
| **Thermal conductivity (W/mK)** | BS EN 1745 | 0.16 | 0.75 | 0.72 |
| **Specific heat capacity (J/kg.°C)** | BS EN 1745 | 700 | 846 | 1000 |

### *4.6.7 Summary of section (5)*

In this section, the mechanical, durability and thermal properties of the NAAUB were evaluated. The results of the compressive strength indicated that 7 days of water curing was sufficient to satisfy the requirements for clay bricks given in the standard BS 3921 (British Standard, 1998). Regarding the durability performance of the NAAUB, the results indicated the water absorption rate of the NAAUB was very low and satisfied the requirements for engineering bricks class A according to BS EN 771-1:2003+A1:2005 (British Standard, 2005b). Additionally, the results of the freezing and thawing showed that the NAAUB has no physical damage after 180 cycles of freezing and thawing and it can be classified as a frost resistant brick according to BS 3921(British Standard, 1998). The overall results of thermal properties of the NAAUB indicated good thermal behaviour of the NAAUB, which will help in increasing indoor comfort and reducing the overall consumption of energy required for heating/cooling of any structure that is built using this brick relative to conventional fired bricks.

## 4.7 Section 6: A comparison between $CO_2$ emission of the NAAUB and conventional fired brick.

### *4.7.1 Introduction*

In the UK, the construction and operation of buildings contribute to about 50% of the $CO_2$ emissions with an annual increase of approximately 1.5% (Azzouz et al., 2017). Therefore, in the context of sustainable development, buildings should be constructed in such a way that they cause low environmental impact in order to maintain adequate occupant comfort level during their service life. In this section, a comparison between the $CO_2$ emission of the NAAUB and conventional fired brick during the manufacturing and operational processes was conducted.

### *4.7.2 $CO_2$ emission during the manufacturing process*

The comparison used in this section includes quantification of the $CO_2$ emissions for each of the raw materials used in the production of the NAAUB, along with the electricity needed for the preparation of the brick (crushing, grinding and mixing of the raw materials). The methodology that has been followed to quantify the $CO_2$ emissions of each of the raw materials was by multiplying the mass of each of the raw materials that is needed to produce one brick (calculated during the lab work to get the required shape of the bricks) by the amount of $CO_2$ kg/t associated with the production of these materials. Additionally, the $CO_2$ of the electricity needed for the preparation of the brick (crushing, grinding and mixing of the raw materials) was taken as 19% of the $CO_2$ associated with the production of conventional fired brick as reported by Carbon Trust (2010). The report published by the Department for Business; Energy & Industrial Strategy (2018) was used to quantify the $CO_2$ emissions of the conventional fired brick, CFC, sand and water, as this information is available within that report, while the missing information was collected from the available literature. The source of date considered in the calculation of the $CO_2$ emissions of all the raw materials is presented in Table 4-20.The $CO_2$ quantification presented in Table 4-20 is considered only for the production process of the NAAUB. Detailed calculation of quantification for $CO_2$ emissions for the NAAUB and conventional fired brick is presented in Table 4.20.

**Example of $CO_2$ calculation**

An example of the calculation of $CO_2$ emissions of the sand can be seen below:

The production of 1 NAAUB required 1.89 kg of sand

The total weight of the materials required in the production of 1 NAAUB is 3.306 kg

The $CO_2$ emissions associated with sand production is 7.8123 ($CO_2$ kg/t) according to Department for Business; Energy & Industrial Strategy (2018).

Therefore, the $CO_2$ emissions of sand in the production of 1 NAAUB can be calculated as

$((1.89\ x\ 7.8123)/1000 = 0.0148$ ($CO_2$ kg/brick))

Additionally, in order to calculate the $CO_2$ emissions of sand in the production of 1 tonne of the NAAUB, the obtained number (0. 0148) was then multiplied by the number of bricks required to produce 1 tonne of NAAUB as seen below:

The total mass of the NAAUB (according to Table 4-20) is 3.306 kg

Thus, the total number of bricks in one tonne is $(1000\ )/3.306$ =302.4803 bricks)

Therefore, the total $CO_2$ emissions of sand in the production of 1 tonne of NAAUB can be calculated as 0.0148 x 302.4803= 4.4662 ($CO_2$ kg/t)

Similar procedure in the calculations were followed to calculate the CO2 emissions of the CFC and the GGBS. On the other hand, the calculation of the $CO_2$ emissions of the solutions (NaOH, $Na_2SiO_3$ and water) different as the quantifications of $CO_2$ emissions of solution is provided in volumetric quantity. Example of the method of calculating the $CO_2$ emissions of the water used in the NAAUB can be seen as below:

The number of bricks in 1 $m^3$ = (1/ (0.215 x 0.1025 x 0.065)) = 698.1107 bricks.

The $CO_2$ emissions associated with water production is 0.344 ($CO_2$ kg/t) according to Department for Business; Energy & Industrial Strategy (2018).

Therefore, the $CO_2$ emissions of water in the production of 1 NAAUB can be calculated as

$((0.344/698.1107) = 0.0005$ ($CO_2$ kg/brick))

The obtained number (0.0005) was multiplied by the number of bricks required to produce 1 tonne of NAAUB. (0.0005 x 302.4803= 0.1490 ($CO_2$ kg/t).

Table 4-20. Quantification for $CO_2$ emission for the NAAUB and conventional fired brick.

| **Material** | **Mass in kg - per brick** | **Embedded $CO_2$ - per brick** | **Embedded kg $CO_2$ - per tonne of bricks** | **Notes** | **Source of data** | **Compressive strength/embodied $CO_2$ (MPa/kg)** |
|---|---|---|---|---|---|---|
| **Conventional fired brick** | | | | | | **(25.7/0.665)= 38.647** |
| | 2.75 | **0.6650** | **241.8123** | - | (Department for Business; Energy & Industrial Strategy, 2018) | |
| **NAAUB** | | | | | | **(25.8/0.3629)= 71.094** |
| **CFC** | 0.472 | 0.0005 | 0.1455 | 1.0192 ($CO_2$ kg/t) | (Department for Business; Energy & Industrial Strategy, 2018) | |
| **GGBS** | 0.472 | 0.0245 | 7.4241 | 52.0 ($CO_2$ kg/t) | (Rahmat et al., 2016) | |
| **Sand** | 1.89 | 0.0148 | 4.4662 | 7.8123 ($CO_2$ kg/t) | (Department for Business; Energy & Industrial Strategy, 2018) | |
| NaOH | 0.126 | 0.0487 | 14.7317 | 34.0 ($CO_2$kg/m3) | (Turner and Collins, 2013) | |
| $Na_2SiO_3$ | 0.252 | 0.1475 | 44.6283 | 103.0 ($CO_2$ kg/m3) | (Turner and Collins, 2013) | |
| Water | 0.094 | 0.0005 | 0.1490 | 0.344 ($CO_2$ kg/$m^3$) | (Department for Business; Energy & Industrial Strategy, 2018) | |
| Electricity | | 0.1263 | 45.9443 | 19% of the total process for conventional fired brick | (Carbon Trust, 2010) | |
| Total Mass | 3.306 | **0.3629** | **117.4891** | | | |
| **Class A Brick** | | | | | | **(50/0.665)= 75.188** |

It can be seen from Table 4-20 and Figure 4-30 that the $CO_2$ emissions for conventional fired brick are 241.8123 $CO_2$kg/t while the $CO_2$ emissions for the NAAUB are 117.4891 $CO_2$kg/t. Thus, the utilisation of the NAAUB in the construction industry could reduce the $CO_2$ emissions by about 51.4% relative to conventional fired brick. The outcome product (NAAUB) of this study is certainly acceptable in terms of the environmental point of view and it is compatible with the sustainability concept that had been set by most of the environmental analysis methods.

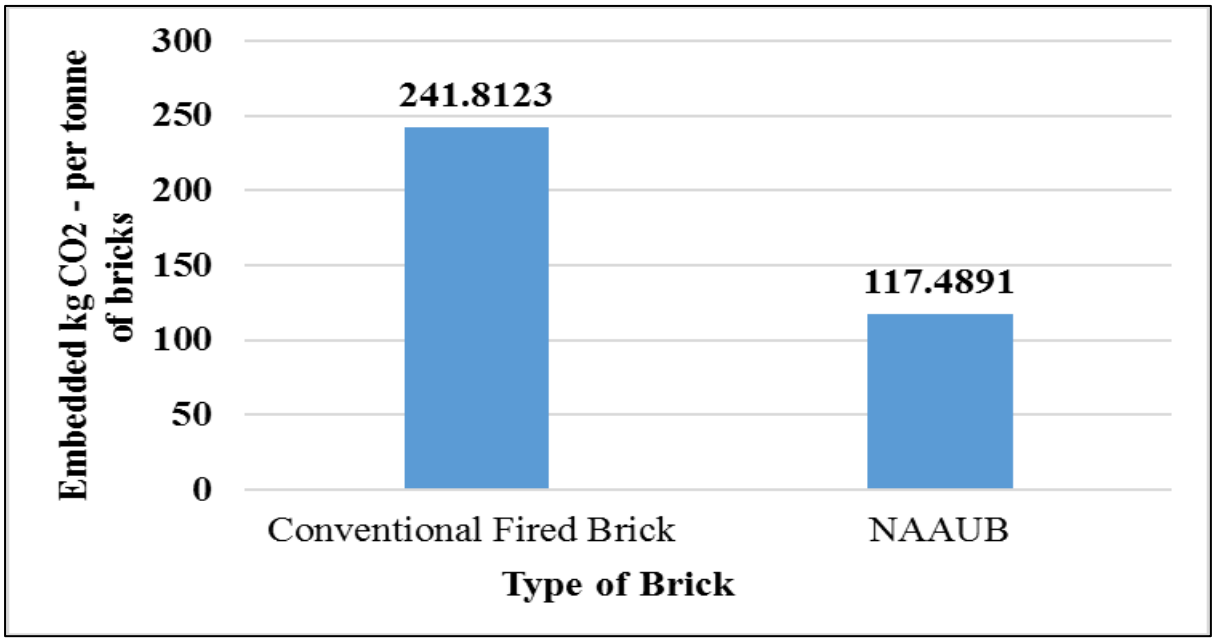


Figure 4-29. Embedded kg $CO_2$ - per tonne of conventional fired brick and NAAUB.

### *4.7.3 $CO_2$ emissions during the operational process*

For buildings constructed in temperate or cold regions such as the UK, the majority of the $CO_2$ emissions are due to the energy required for space heating, cooling, lighting, ventilation and to run domestic appliances. The higher heat gain or loss for the materials used in the construction of building, the more $CO_2$ emissions due to the higher energy (electricity, oil, gas) consumption required to maintain comfort conditions inside the building during the operational phase (Ramesh et al., 2012). In this section, energy simulation software "Design Builder" was used to model an office building in Liverpool, UK to evaluate the $CO_2$ emissions of conventional fired brick against the NAAUB during the operational phase. Design Builder is one of the most comprehensive user interfaces for EnergyPlus dynamic thermal simulation engine (Ramesh et al., 2012). Design Builder generates detailed $CO_2$ emissions data for 1 year by simulation using

real weather data (Ramesh et al., 2012). Hourly weather files of Liverpool from the Design Builder database were used for the simulation.

**The case study**

The building examined in this study was an office building located in the city of Liverpool, UK. The total gross floor area is 20 $m^2$ and the net internal area is 15.32 $m^2$ (Figure 4-30). The main geometric features and design parameters of the office building are reported in Table 4-21 while characteristics of the conventional fired brick and the NAAUB used in the simulation are presented in Table 4-22. The characteristics of the conventional fired brick used in the simulation were the default characteristics provided by the Design Builder.

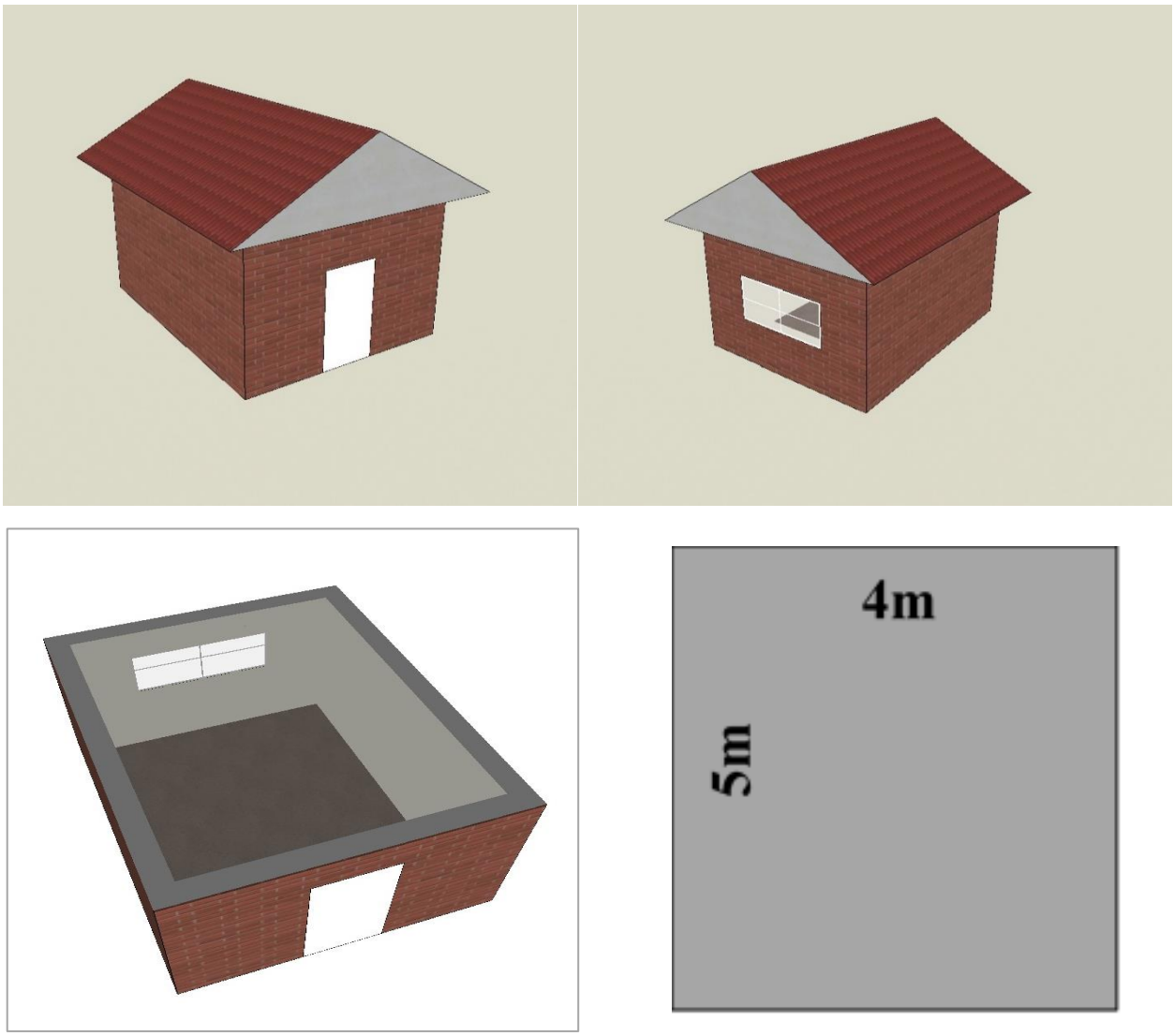


Figure 4-30. The studied office building

Table 4-21. The geometric features and design parameters of the office building

| Items | Descriptions |
|---|---|
| **Weather file** | Liverpool |
| **Building type** | Office |
| **Wall** | |
| **Height** | 3 m |
| **Length** | 5 m |
| **Width** | 4 m |
| **Wall materials (external to internal)** | |
| **Brick** | 215 mm |
| **Rockwool insulation** | 50 mm |
| **Gypsum plaster** | 12 mm |
| **False ceiling (1 layer)** | |
| **Plaster board** | 10 mm |
| **New ground floor (bottom to top)** | |
| **Sand and gravel** | 100 mm |
| **Cast concrete** | 100 mm |
| **Timber flooring** | 10 mm |
| **Door** | |
| **Width** | 1 m |
| **Height** | 2 m |
| **Type** | Default |
| **Window** | |
| **Type** | Clear double glazing |
| **Glass thickness** | 6 mm |
| **Air gap** | 13 mm |
| **Normal Pitch Roof (external to internal)** | |
| **Clay tile roofing** | 25 mm |
| **Air gap** | 20 mm |
| **Roofing felt** | 5 mm |
| **Sides wood wall (external to internal)** | |
| **Type** | Wood frame |
| **Stucco** | 5 mm |
| **Air gap** | 50 mm |
| **Plaster board** | 10 mm |
| **Normal Pitch Roof Flooring (bottom to top)** | |
| **Flooring wood sub floor** | 19 mm |
| **Rockwool insulation** | 50 mm |
| **Activity** | |
| **Occupancy** | 2 people |
| **Lighting** | Default |
| **HVAC** | Radiator electric with natural ventilation |

Table 4-22. Characteristics of the conventional fired brick and the NAAUB used for the simulation

| Materials Characterisation | Conventional Fired Brick | NAAUB |
|---|---|---|
| **Thermal Conductivity (W/mK)** | 0.72 | 0.16 |
| **Specific Heat Capacity (J/kg.°C)** | 840 | 700 |
| **Density (kg/m$^3$)** | 1920 | 2300 |

### The $CO_2$ emissions of the office building

During this investigation, the office building was modelled firstly using conventional fired brick for the external wall and then by replacing the conventional fired brick by the NAAUB and the simulation was conducted for one year's duration. The results of the $CO_2$ emissions during the operational phase of the office building (Figure 4-31) indicated that replacing the conventional fired brick by the NAAUB could reduce the $CO_2$ emissions by about 5.65%. This reduction in the $CO_2$ emissions is attributed to the low thermal conductivity and low heat capacity of the NAAUB relative to conventional fired brick (Ramesh et al., 2012).

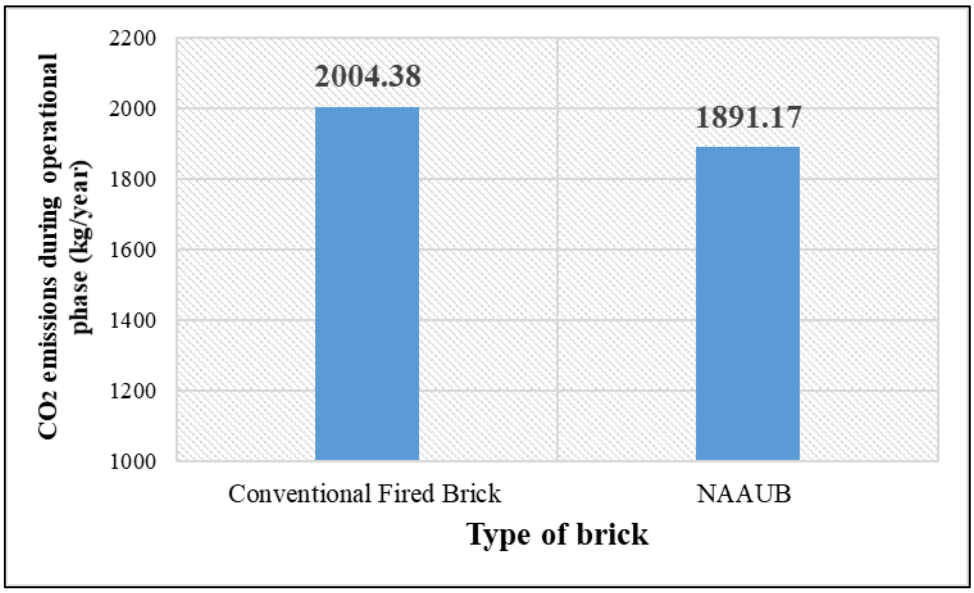


Figure 4-31. $CO_2$ emissions for conventional fired brick and NAAUB during the operational phase.

### *4.7.4 Summary of section (6)*

In this section, a comparison between the $CO_2$ emissions of the NAAUB and conventional fired brick during the manufacturing and operational processes was conducted. The results obtained from the investigated case study indicated that replacing the conventional fired brick with the NAAUB could reduce the $CO_2$ emissions by about 51.5% and 5.65% during the manufacturing process and operational process, respectively. This means that using the NAAUB in the construction industry can significantly reduce the $CO_2$ production, as well as reduce the energy demand for heating and cooling of buildings.

## 4.8 Section 7: A comparison between the cost of NAAUB and conventional fired brick.

### *4.8.1 Introduction*

The financial costs analysis of the production the final product (NAAUB) is essential to conduct a direct comparison with commercially available fired clay bricks prior to the introduction of this brick to the construction industry. Therefore, this section is devoted to present a breakdown for the cost associated with the production of the NAAUB and conduct a direct comparison with commercially available fired clay bricks.

### *4.8.2 Breakdown of the costs associated with production of NAAUB.*

The comparison used in this section includes cost for each of the raw materials used in the production of the NAAUB, the electricity needed for the preparation of the brick (crushing, grinding and mixing of the raw materials), labour cost, operating costs and the interest. The methodology that has been followed to calculate the cost of each of the raw materials was by multiplying the mass of each of the raw materials that is needed to produce one brick (calculated during the lab work to get the required shape of the bricks) by the cost (£/tonne or £/Litre) of these materials. Additionally, the cost of the electricity needed for the preparation of the brick (crushing, grinding and mixing of the raw materials) labour cost, operating costs and the interest was taken as 32.3% of the total cost of conventional fired brick as reported by Mathews (2020). The prices of the raw materials are based on a direct phone calls with sales managers from different suppliers, while the missing information was collected from the available literature. Table 4-23 present full details about the sources where the prices were collected from. Detailed calculation of cost of the NAAUB and conventional fired brick is presented in Table 4.23.

**Example of cost calculation of the NAAUB.**

An example of the cost calculation of the sand can be seen below:

The production of 1 NAAUB required 1.89 kg of sand

The cost of sand is 19.200 (£/t) according to PPC Aggregate (2020).

Therefore, the cost of sand in the production of 1 NAAUB can be calculated as

$((1.89\ x\ 19.200)/1000 = 0.03629$(£/brick))

Similar procedure in the calculations were followed to calculate the cost of the CFC and the GGBS. On the other hand, the calculation of the cost of the solutions (NaOH, $Na_2SiO_3$ and water) different as the prices of the solution were provided in volumetric quantity. Example of the method of calculating the cost of the water used in the NAAUB can be seen as below:

The cost of water supply is 0.0017 (£/Litre) according to United Utilities (2020).

Therefore, the cost of water in the production of 1 NAAUB can be calculated as

$(( 0.094\ x\ 0.0017/1000) = 0.0016$ (£/brick))

Table 4-23. Breakdown of production costs of NAAUB and conventional fired bricks.

| Material | Mass in kg - per brick | Price per brick (£) | Notes | Source of data |
|---|---|---|---|---|
| **Conventional fired brick** | | | | |
| | | **0.600** | - | (Travis Perkins, 2019) |
| **NAAUB** | | | | |
| **CFC** | 0.472 | 0.0000 | 0.00000 (£/tonne) | (Cronin, 2020) |
| **GGBS** | 0.472 | 0.03304 | 70.00000 (£/tonne) | (Savjani, 2020) |
| **Sand** | 1.89 | 0.03629 | 19.20000 (£/tonne) | (PPC Aggregate, 2020) |
| **NaOH** | 0.126 | 0.04619 | 0.36656 (£/Litre) | (Kelly, 2020) |
| **$Na_2SiO_3$** | 0.252 | 0.26057 | 1.03400 (£/Litre) | (Kelly, 2020) |
| **Water** | 0.094 | 0.00016 | 0.00170 (£/Litre) | (United Utilities, 2020) |
| **Energy and labour costs** | | 0.18000 | 30% of the total cost for conventional fired brick | (Mathews, 2020) |
| **Interest** | | 0.01380 | 2.3% of the total cost for conventional fired brick | (Mathews, 2020) |
| **Total Price** | | **0.570** | | |

It can be seen from Table 4-23 that the estimated total cost of the NAAUB is about £0.57 that is cheaper than the price of the conventional fired brick by about 5%. It is worth mentioning that the price of the conventional fired bricks varies according to different suppliers and the comparison was made with the same samples that were tested for compressive strength, durability and thermal properties, which were collected from Travis Perkins Trading Company Limited (Travis Perkins, 2019).

### 4.9 Summary of the chapter

The current chapter presents the results obtained from the experimental work of this project. As stated before, this chapter was divided into six sections in order to clearly present the results of the experimental work. The outcomes of each section are presented in Table 4-24 below:

Table 4-24. Summary of Chapter 4

| Section | Descriptions |
|---|---|
| **Section 1** | The chemical compositions of the CFC showed that it is rich in $SiO_2$ and has a high CaO content alongside moderate content of $Al_2O_3$, $Fe_2O_3$and MgO. Additionally, the PSD and SSA tests of the candidate materials showed that GGBS has the finest particles relative to other candidate materials while MK has the highest SSA. |
| **Section 2** | The selected candidate synthesis parameters of the NAAUB are: binder materials composition (50% CFC + 50% GGBS), S/B ratio= 2, L/B ratio= 0.5, W/B ratio= 0.1, $Na_2SiO_3$/NaOH ratio=2 and NaOH concentration=4M |
| **Section 3** | Increasing the period of curing for samples subjected to water curing temperature at temperatures of 30$^o$C and 50$^o$C resulted in improved compressive strength however, the compressive strength tended to decrease for samples subjected to water curing temperature at temperatures of 70$^o$C and 90$^o$C. Additionally, the selected candidate temperature of water curing temperature was found to be 50$^o$C. The compressive strength and flexural strength of the NAAUB samples tended to decrease at 28 days and 56 days for samples subjected to air curing and water curing temperature, respectively while the samples under water curing showed continuous improvement in the compressive strength and flexural strength with the increase in the period of curing from 1 to 180 days. |
| **Section 4** | SEM imaging revealed the formation of geopolymer gel at early ages (1 and 3 days) that is correlated with an inhomogeneity of microstructure and associated with some microcracks except for the NAAUB-H50. Increasing the period of curing to 28 days resulted in the formation of very dense microstructure with gel appearing evenly distributed covering most of the NAAUB paste surface. However, curing for more than 28 days resulted in the formation of large cracks with some voids for the NAAUB-A paste |

| Section | Descriptions |
|---|---|
| | surface while the SEM micrographs of the NAAUB-W and the NAAUB-H50 showed the continuous formation of dense and compact geopolymer matrix. Additionally, SEM/EDS analyses were found to be well in agreement with the results obtained from the SEM testing for each corresponding period of testing. Finally, the techniques employed in this section (SEM/EDS) clearly helped in understanding the performance of the NAAUB under different curing conditions and for different periods of curing. |
| **Section 5** | The NAAUB with the dimensions (215mm x 102.5mm x 65mm) indicated that 7 days of water curing was sufficient to satisfy the mechanical, durability and thermal properties required for conventional fired bricks |
| **Section 6** | The comparison between the $CO_2$ emissions during the manufacturing and operational processes of the NAAUB and conventional fired brick indicated that replacing the conventional fired brick with the NAAUB could reduce the $CO_2$ emissions by about 51.5% during the manufacturing process and 5.65% during the operational process. |
| **Section 7** | The comparison between the cost of the NAAUB and conventional fired brick indicated that the NAAUB is cheaper than the conventional fired brick by about 5%. |

# CHAPTER 5: CONCLUSIONS AND RECOMMENDATIONS

## 5.1 Conclusions

The aim of this research project was to develop unfired brick through alkali activation of waste from aggregate recycling facilities as an alternative to conventional fired clay brick. Initially, chemical and physical analyses of the CFC were conducted to characterise the properties of CFC. Then, the performance of four candidate materials (GGBS, PFA, CFA and MK) used to activate the CFC were investigated by conducting compressive strength tests to identify the best candidate material that can be utilised in the formation of binder material for the unfired brick. After finding the best candidate materials, a comprehensive investigation of the mix design was conducted. Mechanical and microstructural performance of the developed brick (produced by activating the CFC with selected candidate material) under different methods of curing and for different curing periods were investigated to find out the best method of curing. Then, a standard size brick was produced using the selected candidate synthesis parameters from all the investigation stages. The developed brick was assessed and compared with the performance of fired clay bricks in terms of compressive strength, durability (water absorption and freeze and thaw cycles), thermal performance (thermal conductivity and specific heat capacity), $CO_2$ emissions (during the manufacturing and operational processes) and cost. According to the results presented in this research, the following conclusions can be drawn:

- Mixing the CFC with various candidate materials in order to harmonize their existing characteristics through utilising them in a controllable system was found to play a fundamental role in activating the CFC and developing binary binder for the unfired brick.
- GGBS was found to be the best candidate material to be used in combination with the CFC in the production of binary binder for the new unfired brick and the selected candidate synthesis parameters of the NAAUB are: binder materials composition (50% CFC + 50% GGBS), S/B ratio= 2, L/B ratio= 0.5, W/B ratio= 0.1, $Na_2SiO_3$/NaOH ratio=2 and NaOH concentration=4M.
- Water curing temperature was found to be effective to improve the mechanical properties (compressive strength and flexural strength) at all ages of curing relative to other methods of curing (air curing and water curing) with a selected candidate curing temperature of 50$^{o}$C.

- The compressive strength and flexural strength of the NAAUB-H50 increased with the extension of the period of curing with the highest compressive strength and flexural strength of 62.6 MPa and 6 MPa achieved after 56 days of curing, then they tend to decrease slightly with an increase in the period of curing. Additionally, the compressive strength and flexural strength of the NAAUB-A were enhanced significantly with the increase in the period of curing up to 28 days, after that they decreased with the increase in the period of curing. On the other hand, water curing of the NAAUB (NAAUB-W) was found to enhance the compressive strength and flexural strength with the increase in the period of curing from 1 to 180 days.
- The chemical compositions of the NAAUB powder indicated a high amount of $SiO_2$ (45.46%) and CaO (38.40%) along with a moderate amount of $Al_2O_3$ (4.56%), while the physical properties of the NAAUB powder indicated that it has a high SSA (Blaine SSA= 5429 $cm^2/g$) with fine particles ($d_{50}$= 15.63 μm).
- Compacted and well condensed microstructure with few microcracks was identified by the SEM/EDS testing with the extension of the period of curing for all curing methods, due to the stable coexistence of geopolymer gel and C-S-H gel. This confirmed the obtained results from the compressive strength and flexural strength tests.
- The mechanical performance (compressive strength and flexural strength) of the NAAUB under water curing temperature ( NAAUB-H50 ) and air curing (NAAUB-A) was found to decrease after the ages of 28 days and 56 days for the NAAUB-A and NAAUB-H50, respectively and only the NAAUB-W continued to develop strength with the increase in the period of curing. Therefore, water curing at temperature of 20$^oC$ has been chosen as the selected candidate method of curing in this study to be considered in the production of standard size (215mm x 102.5mm x 65mm) building bricks.
- The compressive strength results of the NAAUB with standard brick size was 25.8 MPa after 7 days of curing which was sufficient to satisfy the requirements for clay bricks given in the standard BS 3921. Additionally, a direct comparison between the results of the compressive strength of the NAAUB after 7 days of curing and commercially available fired brick indicated that 7 days of water curing was sufficient to produce unfired brick with comparable compressive strength to commercially available fired brick.

- The durability performance of the NAAUB indicated the water absorption rate was very low (0.36%) and was about 3.7% of the water absorption rate of the tested commercially available fired brick (9.67%). Additionally, the weight loss of the NAAUB due to the freezing and thawing cycles was in the range of 0.04% to 0.15% and the NAAUB was able to withstand 180 cycles of freezing and thawing without any physical damage. According to the obtained results the NAAUB can be classified as Frost resistant (F) brick according to BS 3921.
- The results of the thermal properties indicated that the thermal conductivity of the NAAUB was about 21% of the thermal conductivity of the tested commercially available fired brick (0.75 W/mK).
- The $CO_2$ emissions calculation of the NAAUB and conventional fired brick during the manufacturing and operational processes indicated that replacing the conventional fired brick with the NAAUB could reduce the $CO_2$ emissions by about 51.4% and 5.65% during the manufacturing process and operational process, respectively. This means that using the NAAUB in the construction industry can significantly reduce the $CO_2$ production, as well as reducing the energy demand for heating and cooling of buildings.
- The comparison between the cost of the NAAUB and conventional fired brick indicated that the NAAUB is cheaper than the conventional fired brick by about 5%.

This project will meet the unmet needs of recovering valuable materials from the recycling process of different C&D wastes along with developing a business-oriented disposal route of these wastes by providing a fully characterised unfired brick for use at commercial scale. This is very timely with respect to the ongoing debate about moving to a low carbon economy and the current discussions regarding the future of the $CO_2$ allowances currently allocated to the construction sector. Producers of conventional bricks are under increasing pressure to reduce the embodied carbon in their products due to increasingly strict environmental legislation. Consequently, the developed low carbon brick, with validated characteristics, will be highly attractive to construction companies, as this cannot currently be provided with existing bricks. Additionally, the other key benefit arising from this project is the production of a low carbon building material, which would reduce the environmental impact and energy intensity of brick production by reducing the use of natural clay, saving fossil fuel, and reclaiming landfill sites.

## 5.2 Research Limitations

The findings of this research are restricted to the investigated parameters and there were some limitations that have been faced during this study. For example, exploiting the developed unfired brick through a pilot study that involves building a small room and monitoring the real performance of the developed brick subjected to weather conditions of the UK for at least one year long. This can significantly help in validating the fundamental characteristics of the new brick and hence generate wider acceptable performance for the market sectors and can significantly aid in rapid industrialisation of this brick. This pilot study was planned to be conducted over the final year of this project, however, due to the lockdown of the university due to Covid-19 pandemic, this pilot study was not conducted. Additionally, due to the extensive experiments of investigation that were carried out in this study, not all the durability properties of the developed unfired brick were investigated in this study.

## 5.3 Recommendations for future work

Despite the comprehensive research investigation that was conducted to develop alkali activated unfired brick using waste from aggregate recycling facilities, several possible future studies can be recommended as stated below:

1) Building a small room and monitoring the real performance of the developed brick subjected to weather conditions of the UK for at least one year long.
2) Using a minimum of 10 samples for testing the compressive strength and 5 samples for testing the freezing and thawing to arrive at a quantitatively representative value of strength and durability for an alkali activated material and comply with the recommendations of the PAS 8820:2016.
3) Perform more durability tests on the produced unfired brick such as active soluble salts content and water vapour permeability. Additionally, carbonation test is an important aspect for alkali activated materials, therefore carbonation test is highly recommended to be investigated for the NAAUB.
4) Investigate the possibility of replacing the used virgin building sand with recycled sand.
5) According to the obtained results from $CO_2$ calculations and cost analysis of the NAAUB, the alkaline activators and especially $Na_2SiO_3$ were the highest contributors of the $CO_2$ emissions and cost. Therefore, investigating the possibility of using different molar strengths of $Na_2SiO_3$ and NaOH in different combination is highly recommended

along with exploring the possibility of replacing the alkali solutions with alkali powder materials to improve the sustainability performance of the NAAUB.

6) Investigating the effect of cure-and-seal as a method of curing in the production of the NAAUB and compare it with the obtained results from the adapted methods of curing that were investigated in this study.
7) Perform X-Ray Diffraction (XRD) analysis for tracking the hydration analysis of the binder materials over time.
8) Leaching Test is suggested to be carried out for the developed unfired brick to ensure that the new product has no potential contamination to the local environment system and watercourses.

# REFERENCES


ABDULLAH, A. H., NAGAPAN, S., ANTONYOVA, A., RASIAH, K., YUNUS, R. & SOHU, S. 2017. Comparison of Strength Between Laterite Soil and Clay Compressed Stabilized Earth Bricks (CSEBs). *MATEC Web of Conferences,* 103.

ADESANYA, E., OHENOJA, K., DI MARIA, A., KINNUNEN, P. & ILLIKAINEN, M. 2020. Alternative alkali-activator from steel-making waste for one-part alkali-activated slag. *Journal of Cleaner Production,* 274**,** 123020.

ADESANYA, E., OHENOJA, K., LUUKKONEN, T., KINNUNEN, P. & ILLIKAINEN, M. 2018. One-part geopolymer cement from slag and pretreated paper sludge. *Journal of Cleaner Production,* 185**,** 168-175.

AHMARI, S. & ZHANG, L. 2012. Production of eco-friendly bricks from copper mine tailings through geopolymerization. *Construction and building materials,* 29**,** 323-331.

AHMARI, S. & ZHANG, L. 2013. Utilization of cement kiln dust (CKD) to enhance mine tailings-based geopolymer bricks. *Construction and Building Materials,* 40**,** 1002-1011.

AÏTCIN, P. C. 2016. The importance of the water–cement and water–binder ratios. *Science and Technology of Concrete Admixtures.*

AKINSHIPE, O. & KORNELIUS, G. 2017. Chemical and thermodynamic processes in clay brick firing technologies and associated atmospheric emissions metrics-a review. *J Pollut Eff Cont,* 5**,** 190.

AL-NEGHEIMISH, A. I., AL-SUGAIR, F. H. & AL-ZAID, R. Z. 1997. Utilization of local steelmaking slag in concrete. *Journal of King Saud University-Engineering Sciences,* 9**,** 39-54.

ALONSO, S. & PALOMO, A. 2001. Alkaline activation of metakaolin and calcium hydroxide mixtures: influence of temperature, activator concentration and solids ratio. *Materials Letters,* 47**,** 55-62.

AMIN, S. K., EL–SHERBINY, S. A., EL–MAGD, A. A. M. A., BELAL, A. & ABADIR, M. F. 2017. Fabrication of geopolymer bricks using ceramic dust waste. *Construction and Building Materials,* 157**,** 610-620.

APRIANTI, E., SHAFIGH, P., BAHRI, S. & FARAHANI, J. N. 2015. Supplementary cementitious materials origin from agricultural wastes – A review. *Construction and Building Materials,* 74**,** 176-187.

ARıÖZ, Ö., KILINÇ, K., TUNCAN, M., TUNCAN, A. & KAVAS, T. Physical, mechanical and micro-structural properties of F type fly-ash based geopolymeric bricks produced by pressure forming process. Advances in Science and Technology, 2010. Trans Tech Publ, 69-74.

ASSI, L. N., DEAVER, E. E. & ZIEHL, P. 2018. Effect of source and particle size distribution on the mechanical and microstructural properties of fly Ash-Based geopolymer concrete. *Construction and Building Materials,* 167**,** 372-380.

ATLAS OBSCURA. 2017. *Shibam* [Online]. Available: https://www.atlasobscura.com/places/shibam-hadhramaut [Accessed 22/07 2018].

AUBERT, J. E., FABBRI, A., MOREL, J. C. & MAILLARD, P. 2013. An earth block with a compressive strength higher than 45MPa! *Construction and Building Materials,* 47**,** 366-369.

AWANG, H. & ALJOUMAILY, Z. S. 2017. Influence of granulated blast furnace slag on mechanical properties of foam concrete. *Cogent Engineering,* 4**,** 1409853.

AZZOUZ, A., BORCHERS, M., MOREIRA, J. & MAVROGIANNI, A. 2017. Life cycle assessment of energy conservation measures during early stage office building design: A case study in London, UK. *Energy and Buildings,* 139**,** 547-568.

BAKHAREV, T., SANJAYAN, J. & CHENG, Y.-B. 1999. Effect of elevated temperature curing on properties of alkali-activated slag concrete. *Cement and concrete research,* 29**,** 1619-1625.

BAŽANT, Z. P. 1984. Size effect in blunt fracture: concrete, rock, metal. *Journal of engineering mechanics,* 110**,** 518-535.

BAŽANT, Z. P. 1996. Size effect aspects of measurement of fracture characteristics of quasibrittle material. *Advanced Cement Based Materials,* 4**,** 128-137.

BAZANT, Z. P., XI, Y. & REID, S. G. 1991. Statistical size effect in quasi-brittle structures: I. Is Weibull theory applicable? *Journal of engineering Mechanics,* 117**,** 2609-2622.

BECKMAN COULTER 2009. Meeting and exceeding the standard for laser diffraction particle size analysis: Ls 13 320 particle size analyzer. USA.

BRICK DEVELOPMENT ASSOCIATION 2011. Brickwork durability. London.

BRICK DEVELOPMENT ASSOCIATION 2017. The UK Clay Brickmaking Process London

BRITISH STANDARD 1998. BS 3921:1985, Specification for Clay bricks. London: British Standard Institute

BRITISH STANDARD 1999. BS EN 450:1995 - fly ash for concrete - definitions, requirments and quality control. London: British Standard Institution.

BRITISH STANDARD 2000. BS EN 772-13, Methods of test for masonry units, Part 13: Determination of net and gross dry density of masonry units (except for natural stone). London British Standard Insititute

BRITISH STANDARD 2002a. BS EN1745, Masonry and masonry products — Methods for determining design thermal values. London British Standard Institute.

BRITISH STANDARD 2002b. BS EN 1745:2002, Masonry and masonry products — Methods for determining design thermal values. London British Standard Insitute

BRITISH STANDARD 2005a. BS EN 196-2, Methods of testing cement — Part 2: Chemical analysis of cement. British Standard.

BRITISH STANDARD 2005b. BS EN 771-1:2003+A1:2005, Specification for masonry units, Part 1: Clay masonry units. London: British Standard Institute

BRITISH STANDARD 2006. DD CEN/TS 12390-9:2006, Testing hardened concrete. Freeze-thaw resistance scaling. . London: British Standard Institute. .

BRITISH STANDARD 2015. BS EN 772-1:2011+A1:2015, Methods of test for masonryunitsPart 1: Determination of compressivestrength. London, UK: British Standard Institute. .

BRITISH STANDARD 2018. BS EN 196-6:2018, Methods of testing cement Determination of fineness. British Standard insitute, .

BRITISH STANDARDS INSTITUTION 2016. PAS 8820: 2016 Construction materials – Alkali-activated cementitious material and concrete – Specification. London British Standards Institution.

BSI 2005. Methods of testing cement–Part 1: Determination of strength. London: British Standard Inistitute.

CARBON TRUST. 2010. *Industrial Energy Efficiency Accelerator; Guide to the Brick Sector* [Online]. Available: http://www.carbontrust.com/media/206484/ctg043-brick-industrial-energy-efficiency.pdf. [Accessed June 2018].

CARBON TRUST 2012. Industrial Energy Efficiency Accelerator (Guide to the brick sector).

CELIK, O., DAMCI, E. & PASKIN, S. 2008. Characterisation of fly ash and its effect on the compressive strength properties of portland cement. *Indian Journal of Engineering & Materials Science* 15**,** 433-440.

CHEN, X., HUANG, W. & ZHOU, J. 2012. Effect of moisture content on compressive and split tensile strength of concrete.

CHENG, T.-W. & CHIU, J. 2003. Fire-resistant geopolymer produced by granulated blast furnace slag. *Minerals engineering,* 16**,** 205-210.

CHI, M.-C., CHANG, J.-J. & HUANG, R. 2012. Strength and drying shrinkage of alkali-activated slag paste and mortar. *Advances in Civil Engineering,* 2012.

CHONG, W. K., KUMAR, S., HAAS, C. T., BEHEIRY, S. M., COPLEN, L. & OEY, M. 2009. Understanding and Interpreting Baseline Perceptions of Sustainability in Construction among Civil Engineers in the United States. *Journal of Management in Engineering,* 25**,** 143-154.

CIBSE 2006. Environmental design: CIBSE Guide A. London: The Chartered Institution ofBuilding Services Engineers

CLIMATE AND CLEAN AIR COALITION. 2016. *Mitigating black carbon and other pollutants from brick production* [Online]. Available: https://www.ccacoalition.org/en/initiatives/bricks [Accessed].

CRIADO, M., JIMÉNEZ, A. F., SOBRADOS, I., PALOMO, A. & SANZ, J. 2012. Effect of relative humidity on the reaction products of alkali activated fly ash. *Journal of the European Ceramic Society,* 32**,** 2799-2807.

CRISTELO, N., FERNÁNDEZ-JIMÉNEZ, A., CASTRO, F., FERNANDES, L. & TAVARES, P. 2019. Sustainable alkaline activation of fly ash, aluminium anodising sludge and glass powder blends with a recycled alkaline cleaning solution. *Construction and Building Materials,* 204**,** 609-620.

CRONIN, P. 2020. *RE: Price of Clay Filter Cake* Type to SHUBBAR, A.

DASSEKPO, J.-B. M., NING, J. & ZHA, X. 2018. Potential solidification/stabilization of clay-waste using green geopolymer remediation technologies. *Process Safety and Environmental Protection,* 117**,** 684-693.

DAVIDOVITS, J. Properties of geopolymer cements. First international conference on alkaline cements and concretes, 1994. Kiev State Technical University, Ukraine: Scientific Research Institute on …, 131-149.

DAVIDOVITS, J. G. 1991. Inorganic polymer new materials. *Journal of Thermal Analysis,* 37**,** 663-1.

DEPARTMENT FOR BUSINESS; ENERGY & INDUSTRIAL STRATEGY. 2018. *Greenhouse gas reporting: conversion factors 2018* [Online]. GOV.UK. Available: https://www.gov.uk/government/publications/greenhouse-gas-reporting-conversion-factors-2018 [Accessed 01 December 2019].

DEPARTMENT OF ENERGY & CLIMATE CHANGE 2015. 2013 UK Greenhouse Gas Emissions, Final Figures. *Statistical release.* National Statistics.

DIMAS, D., GIANNOPOULOU, I. & PANIAS, D. 2009. Polymerization in sodium silicate solutions: a fundamental process in geopolymerization technology. *Journal of materials science,* 44**,** 3719-3730.

DODDS, L. 2012. *Microstructure Characterisation of Ordinary Portland Cement Composites for the Immobilisation of Nuclear Waste.* Master of Philosophy, University of Manchester.

DWAYNE, E. Z. 2014. *How does specific heat change with temperature* [Online]. Socratic Q&A. Available: https://api-project-1022638073839.appspot.com/questions/how-does-specific-heat-change-with-temperature#101877 [Accessed 20 April 2020].

EL-MAHLLAWY, M. S. & KANDEEL, A. M. 2014. Engineering and mineralogical characteristics of stabilized unfired montmorillonitic clay bricks. *HBRC Journal,* 10**,** 82-91.

EL-MAHLLAWY, M. S., KANDEEL, A. M., LATIF, M. L. & EL NAGAR, A. M. 2018. The Feasibility of Using Marble Cutting Waste in a Sustainable Building Clay Industry. *Preprints,* 1-14.

ESPUELAS, S., OMER, J., MARCELINO, S., ECHEVERRÍA, A. M. & SECO, A. 2017. Magnesium oxide as alternative binder for unfired clay bricks manufacturing. *Applied Clay Science,* 146**,** 23-26.

EUROPEAN COMMITTEE FOR STANDARDIZATION 2014. BS EN iso 17892-1. Geotechnical investigation and testing - laboratory testing of soil, part 1: Determination of water content. London, uk British Standard Institution.

FAQIR, N. M., SHAWABKEH, R., AL-HARTHI, M. & WAHHAB, H. A. 2019. Fabrication of Geopolymers from Untreated Kaolin Clay for Construction Purposes. *Geotechnical and Geological Engineering,* 37**,** 129-137.

FENG, D., PROVIS, J. L., DEVENTER, J. S. J. & SCHERER, G. 2012. Thermal Activation of Albite for the Synthesis of One-Part Mix Geopolymers. *Journal of the American Ceramic Society,* 95**,** 565-572.

FERNÁNDEZ-JIMÉNEZ, A., PALOMO, J. & PUERTAS, F. 1999. Alkali-activated slag mortars: mechanical strength behaviour. *Cement and Concrete Research,* 29**,** 1313-1321.

FERONE, C., LIGUORI, B., CAPASSO, I., COLANGELO, F., CIOFFI, R., CAPPELLETTO, E. & DI MAGGIO, R. 2015. Thermally treated clay sediments as geopolymer source material. *Applied Clay Science,* 107**,** 195-204.

GHOSH, A. & SUBBARAO, C. 2007. Strength Characteristics of Class F Fly Ash Modified with Lime and Gypsum. *Journal Of Geotechnical And Geoenvironmental Engineering,* 133**,** 757-766.

GILLOTT, J. E. 2000. CLAY MINERALOGY IN BUILDING RESEARCH. Division of Building Research, National Research Council, Ottawa, Canada.

GOVERNMENT STATISTICAL SERVICE 2016. UK Statistics on Waste. York.

GOVERNMENT STATISTICAL SERVICE 2019. UK Statistics on Waste. York Department for Environment Food & Rural Affairs.

GRAYTEE, A., SANJAYAN, J. G. & NAZARI, A. 2018. Development of a high strength fly ash-based geopolymer in short time by using microwave curing. *Ceramics International,* 44**,** 8216-8222.

GUNASEKARA1A, C., LAW1B, D. W. & SETUNGE1C, S. 2016. Long Term Engineering Properties of Fly Ash Geopolymer Concrete.

GUNASEKARA, C., LAW, D. W. & SETUNGE, S. 2016. Long Term Engineering Properties of Fly Ash Geopolymer Concrete. *Fourth International Conference on Sustainable Construction Materials and Technologies.* Las Vegas, USA.

GUO, X., SHI, H., CHEN, L. & DICK, W. A. 2009. Performance and Mechanism of Alkali-Activated Complex Binders of High-Ca Fly Ash and Other Ca-Bearing Materials. *2009 World of Coal Ash (WOCA) Conference* Lexington, KY, USA.

HAMEED, A., RAWDHAN, R. & AL-MISHHADANI, S. 2017a. Effect of Various Factors on the Manufacturing of Geopolymer Mortar. *Archives of Science,* 1**,** 1-8.

HAMEED, A., RAWDHAN, R. & AL-MISHHADANI, S. 2017b. Effect of various factors on the manufacturing of geopolymer mortar. *Archives of Science,* 1**,** 1-8.

HASAN, S. T. 2019. *What is Cement? History- Chemistry- Industries* [Online]. Civil Engineering. Available: https://civiltoday.com/civil-engineering-materials/cement/81-cement-definition-and-full-details [Accessed 02 April 2019].

HASSAN, A., RASHID, Y., MOURAD, A.-H. I., ISMAIL, N. & LAGHARI, M. S. 2019. Thermal and structural characterization of geopolymer-coated polyurethane foam—phase change material capsules/geopolymer concrete composites. *Materials,* 12**,** 796.

HAWILEH, R. A., ABDALLA, J. A., FARDMANESH, F., SHAHSANA, P. & KHALILI, A. 2017. Performance of reinforced concrete beams cast with different percentages of GGBS replacement to cement. *Archives of Civil and Mechanical Engineering,* 17**,** 511-519.

HE, J., JIE, Y., ZHANG, J., YU, Y. & ZHANG, G. 2013. Synthesis and characterization of red mud and rice husk ash-based geopolymer composites. *Cement and Concrete Composites,* 37**,** 108-118.

HE, J., ZHANG, J., YU, Y. & ZHANG, G. 2012. The strength and microstructure of two geopolymers derived from metakaolin and red mud-fly ash admixture: a comparative study. *Construction and building materials,* 30**,** 80-91.

HE, P., WANG, M., FU, S., JIA, D., YAN, S., YUAN, J., XU, J., WANG, P. & ZHOU, Y. 2016. Effects of Si/Al ratio on the structure and properties of metakaolin based geopolymer. *Ceramics international,* 42**,** 14416-14422.

HEAH, C. Y., KAMARUDIN, H., AL BAKRI, A. M., BINHUSSAIN, M., LUQMAN, M., NIZAR, I. K., RUZAIDI, C. & LIEW, Y. 2011. Effect of curing profile on kaolin-based geopolymers. *Physics Procedia,* 22**,** 305-311.

HEAH, C. Y., KAMARUDIN, H., MUSTAFA AL BAKRI, A. M., BNHUSSAIN, M., LUQMAN, M., KHAIRUL NIZAR, I., RUZAIDI, C. M. & LIEW, Y. M. 2012. Study on solids-to-liquid and alkaline activator ratios on kaolin-based geopolymers. *Construction and Building Materials,* 35**,** 912-922.

HUNGER, M. & BROUWERS, H. 2009. Flow analysis of water–powder mixtures: Application to specific surface area and shape factor. *Cement and Concrete Composites,* 31**,** 39-59.

HUSEIENA, G. F., ISMAILA, M., TAHIRB, M., MIRZAC, J., HUSSEINA, A., KHALIDA, N. H. & SARBINI, N. N. 2018. Effect of Binder to Fine Aggregate Content on Performance of Sustainable Alkali Activated Mortars Incorporating Solid Waste Materials. *CHEMICAL ENGINEERING TRANSACTIONS,* 63**,** 667-672.

JAFER, H., ATHERTON, W., SADIQUE, M., RUDDOCK, F. & LOFFILL, E. 2018a. Stabilisation of soft soil using binary blending of high calcium fly ash and palm oil fuel ash. *Applied Clay Science,* 152**,** 323-332.

JAFER, H. M., ATHERTON, W., SADIQUE, M., RUDDOCK, F. & LOFFILL, E. 2018b. Development of a new ternary blended cementitious binder produced from waste materials for use in soft soil stabilisation. *Journal of Cleaner Production,* 172**,** 516-528.

JINDAL, B. B. 2018. Feasibility study of ambient cured geopolymer concrete–A review. *Advances in concrete construction,* 6**,** 387.

JOEL, M. & EDEH, J. E. 2013. Effect of Curing Condition on Some Properties of Cement Stabilized Lateritic Interlocking Bricks. *Advanced Materials Research,* 824**,** 37-43.

JOGLEKAR, S. N., KHARKAR, R. A., MANDAVGANE, S. A. & KULKARNI, B. D. 2018. Sustainability assessment of brick work for low-cost housing: A comparison between waste based bricks and burnt clay bricks. *Sustainable Cities and Society,* 37**,** 396-406.

KADHIM, A., SADIQUE, M., AL-MUFTI, R. & HASHIM, K. 2020. Long-term performance of novel high-calcium one-part alkali-activated cement developed from thermally activated lime kiln dust. *Journal of Building Engineering***,** 101766.

KANI, E. N. & ALLAHVERDI, A. 2009. Effects of curing time and temperature on strength development of inorganic polymeric binder based on natural pozzolan. *Journal of materials science,* 44**,** 3088-3097.

KANI, E. N., ALLAHVERDI, A. & PROVIS, J. L. 2012. Efflorescence control in geopolymer binders based on natural pozzolan. *Cement and Concrete Composites,* 34**,** 25-33.

KELLY, B. 2020. *RE: Prices of alkali activators.*

KHALE, D. & CHAUDHARY, R. 2007. Mechanism of geopolymerization and factors influencing its development: a review. *Journal of materials science,* 42**,** 729-746.

KHAN, M. Z. N., SHAIKH, F. U. A., HAO, Y. & HAO, H. 2018. Effects of Curing Conditions and Sand-to-Binder Ratios on Compressive Strength Development of Fly Ash Geopolymer. *Journal of Materials in Civil Engineering,* 30**,** 04017267-1- 04017267-12.

KIM, B.-J., YI, C. & KANG, K.-I. 2015. Microwave curing of alkali-activated binder using hwangtoh without calcination. *Construction and Building Materials,* 98**,** 465-475.

KOŇÁKOVÁ, D., VEJMELKOVÁ, E. & ČERNÝ, R. Thermal properties of selected sandstones. Advances in modern mechanical engineering: Proceedings of the 4th International Conference on Fluid Mechanics and Heat & Mass Transfer (FLUIDSHEAT'13), Dubrovnik, Croatia, 25–27 June 2013., 2013. 100-104.

KONG, D. L. Y., SANJAYAN, J. G. & SAGOE-CRENTSIL, K. 2007a. Comparative performance of geopolymers made with metakaolin and fly ash after exposure to elevated temperatures. *Cement and Concrete Research,* 37**,** 1583-1589.

KONG, D. L. Y., SANJAYAN, J. G. & SAGOE-CRENTSIL, K. 2007b. Factors affecting the performance of metakaolin geopolymers exposed to elevated temperatures. *Journal of Materials Science,* 43**,** 824-831.

LAMPRIS, C., LUPO, R. & CHEESEMAN, C. R. 2009. Geopolymerisation of silt generated from construction and demolition waste washing plants. *Waste Manag,* 29**,** 368-73.

LEITÃO, D., BARBOSA, J., SOARES, E., MIRANDA, T., CRISTELO, N. & BRIGA-SÁ, A. 2017. Thermal performance assessment of masonry made of ICEB's stabilised with alkali-activated fly ash. *Energy and Buildings,* 139**,** 44-52.

LEMOUGNA, P. N., NZEUKOU, A., AZIWO, B., TCHAMBA, A., WANG, K.-T., MELO, U. C. & CUI, X.-M. 2020. Effect of slag on the improvement of setting time and compressive strength of low

reactive volcanic ash geopolymers synthetized at room temperature. *Materials Chemistry and Physics,* 239**,** 122077.

LIU, D., DUAN, Y.-Y., YANG, Z. & YU, H.-T. 2014. A new route for unburned carbon concentration measurements eliminating mineral content and coal rank effects. *Scientific reports,* 4**,** 4567.

LIU, M. Y. J., ALENGARAM, U. J., SANTHANAM, M., JUMAAT, M. Z. & MO, K. H. 2016. Microstructural investigations of palm oil fuel ash and fly ash based binders in lightweight aggregate foamed geopolymer concrete. *Construction and Building Materials,* 120**,** 112-122.

LLOYD, R. R., PROVIS, J. L. & VAN DEVENTER, J. S. J. 2008. Microscopy and microanalysis of inorganic polymer cements. 2: the gel binder. *Journal of Materials Science,* 44**,** 620-631.

LOZANO-MIRALLES, J. A., HERMOSO-ORZÁEZ, M. J., MARTÍNEZ-GARCÍA, C. & ROJAS-SOLA, J. I. 2018. Comparative study on the environmental impact of traditional clay bricks mixed with organic waste using life cycle analysis. *Sustainability,* 10**,** 2917.

LUPO, R. & CHEESEMAN, C. 2008. New technologies to allow beneficial reuse of silt from construction and demolition waste recycling washing plant. London: Imperial College London.

LUUKKONEN, T., ABDOLLAHNEJAD, Z., YLINIEMI, J., KINNUNEN, P. & ILLIKAINEN, M. 2018. One-part alkali-activated materials: A review. *Cement and Concrete Research,* 103**,** 21-34.

MARCELINO-SADABA, S., KINUTHIA, J., OTI, J. & SECO MENESES, A. 2017. Challenges in Life Cycle Assessment (LCA) of stabilised clay-based construction materials. *Applied Clay Science,* 144**,** 121-130.

MATHEWS, R. 2020. *The Economics Of The Brick Cycle and Its Effects on Firm and Industry Structure* [Online]. Brickbat. Available: http://www.brickbat.co.uk/brickproduction.htm [Accessed 12 October 2020].

MCLELLAN, B. C., WILLIAMS, R. P., LAY, J., VAN RIESSEN, A. & CORDER, G. D. 2011. Costs and carbon emissions for geopolymer pastes in comparison to ordinary portland cement. *Journal of Cleaner Production,* 19**,** 1080-1090.

MEHDIPOUR, I. & KHAYAT, K. H. 2017. Effect of particle-size distribution and specific surface area of different binder systems on packing density and flow characteristics of cement paste. *Cement and Concrete Composites,* 78**,** 120-131.

MESSINA, F., FERONE, C., MOLINO, A., ROVIELLO, G., COLANGELO, F., MOLINO, B. & CIOFFI, R. 2017. Synergistic recycling of calcined clayey sediments and water potabilization sludge as geopolymer precursors: Upscaling from binders to precast paving cement-free bricks. *Construction and Building Materials,* 133**,** 14-26.

MIRANDA, T., SILVA, R. A., OLIVEIRA, D. V., LEITÃO, D., CRISTELO, N., OLIVEIRA, J. & SOARES, E. 2017. ICEBs stabilised with alkali-activated fly ash as a renewed approach for green building: Exploitation of the masonry mechanical performance. *Construction and Building Materials,* 155**,** 65-78.

MOHSEN, H. & MOSTAFA, N. Y. 2010. Investigating the Possibility of Utilizing Low Kaolinitic Clays in Production of Geopolymer Bricks. *Ceramics,* 54**,** 160-168.

MOLINO, B., DE VINCENZO, A., FERONE, C., MESSINA, F., COLANGELO, F. & CIOFFI, R. 2014. Recycling of Clay Sediments for Geopolymer Binder Production. A New Perspective for Reservoir Management in the Framework of Italian Legislation: The Occhito Reservoir Case Study. *Materials (Basel),* 7**,** 5603-5616.

MORAES, J., FONT, A., SORIANO, L., AKASAKI, J., TASHIMA, M., MONZÓ, J., BORRACHERO, M. & PAYÁ, J. 2018. New use of sugar cane straw ash in alkali-activated materials: a silica source for the preparation of the alkaline activator. *Construction and Building Materials,* 171**,** 611-621.

MUÑOZ VELASCO, P., MORALES ORTÍZ, M. P., MENDÍVIL GIRÓ, M. A. & MUÑOZ VELASCO, L. 2014. Fired clay bricks manufactured by adding wastes as sustainable construction material – A review. *Construction and Building Materials,* 63**,** 97-107.

MURMU, A. L. & PATEL, A. 2018. Towards sustainable bricks production: An overview. *Construction and Building Materials,* 165**,** 112-125.

NAGARAJ, H. B., SRAVAN, M. V., ARUN, T. G. & JAGADISH, K. S. 2014. Role of lime with cement in long-term strength of Compressed Stabilized Earth Blocks. *International Journal of Sustainable Built Environment,* 3**,** 54-61.

NAGRAL, M. R., OSTWAL, T. & CHITAWADAGI, M. V. 2014. Effect of curing temperature and curing hours on the properties of geo-polymer concrete. *International Journal of Computational Engineering Research,* 4**,** 1-11.

NATH, S. & KUMAR, S. 2013. Influence of iron making slags on strength and microstructure of fly ash geopolymer. *Construction and Building Materials,* 38**,** 924-930.

NEMATOLLAHI, B., SANJAYAN, J., QIU, J. & YANG, E.-H. 2017. Micromechanics-based investigation of a sustainable ambient temperature cured one-part strain hardening geopolymer composite. *Construction and Building Materials,* 131**,** 552-563.

NG, C., ALENGARAM, U. J., WONG, L. S., MO, K. H., JUMAAT, M. Z. & RAMESH, S. 2018. A review on microstructural study and compressive strength of geopolymer mortar, paste and concrete. *Construction and Building Materials,* 186**,** 550-576.

NSHIMIYIMANA, P., MIRAUCOURT, D., MESSAN, A. & COURARD, L. 2018. Calcium Carbide Residue and Rice Husk Ash for improving the Compressive Strength of Compressed Earth Blocks. *MRS Advances***,** 1-6.

O'ROURKE, B., MCNALLY, C. & RICHARDSON, M. G. 2009. Development of calcium sulfate–ggbs–Portland cement binders. *Construction and Building Materials,* 23**,** 340-346.

ORION, T., VIJAY, D. M., MENON, P. A. & SHAHANAS, F. 2011. *Environmental Pollution From Brick Making Operations and Their Effect on Workers* [Online]. Available: https://businessimpactenvironment.wordpress.com/2011/10/03/environmental-pollution-from-brick-making-operations-and-their-effect-on-workers/ [Accessed].

OTI, J. E., KINUTHIA, J. M. & BAI, J. 2009. Unfired clay bricks: from laboratory to industrial production. *Proceedings of the Institution of Civil Engineers,* 162**,** 229-237.

OTI, J. E., KINUTHIA, J. M. & ROBINSON, R. B. 2014. The development of unfired clay building material using Brick Dust Waste and Mercia mudstone clay. *Applied Clay Science,* 102**,** 148-154.

PALOMO, A., GRUTZECK, M. & BLANCO, M. 1999. Alkali-activated fly ashes: a cement for the future. *Cement and concrete research,* 29**,** 1323-1329.

PERERA, D., UCHIDA, O., VANCE, E. & FINNIE, K. 2007. Influence of curing schedule on the integrity of geopolymers. *Journal of materials science,* 42**,** 3099-3106.

PERERA, D. S., UCHIDA, O., VANCE, E. R. & FINNIE, K. S. 2006. Influence of curing schedule on the integrity of geopolymers. *Journal of Materials Science,* 42**,** 3099-3106.

PEYS, A., RAHIER, H. & PONTIKES, Y. 2016. Potassium-rich biomass ashes as activators in metakaolin-based inorganic polymers. *Applied Clay Science,* 119**,** 401-409.

PHETCHUAY, C., HORPIBULSUK, S., SUKSIRIPATTANAPONG, C., CHINKULKIJNIWAT, A., ARULRAJAH, A. & DISFANI, M. M. 2014. Calcium carbide residue: Alkaline activator for clay–fly ash geopolymer. *Construction and Building Materials,* 69**,** 285-294.

PHUMMIPHAN, I., HORPIBULSUK, S., RACHAN, R., ARULRAJAH, A., SHEN, S. L. & CHINDAPRASIRT, P. 2018. High calcium fly ash geopolymer stabilized lateritic soil and granulated blast furnace slag blends as a pavement base material. *J Hazard Mater,* 341**,** 257-267.

POINOT, T., LARACY, M. E., APONTE, C., JENNINGS, H. M., OCHSENDORF, J. A. & OLIVETTI, E. A. 2018. Beneficial use of boiler ash in alkali-activated bricks. *Resources, Conservation and Recycling,* 128**,** 1-10.

POOWANCUM, A. & HORPIBULSUK, S. 2015. Development of Low Cost Geopolymer from Calcined Sedimentary Clay. *1st International Conference on Calcined Clays for Sustainable Concrete.* Lausanne, Switzerland,: Springer.

PPC AGGREGATE. 2020. *RE: Price of Sand* Type to SHUBBAR, A.

PRÉTOT, S., COLLET, F. & GARNIER, C. 2014. Life cycle assessment of a hemp concrete wall: Impact of thickness and coating. *Building and Environment,* 72**,** 223-231.

PROVIS, J. L., DUXSON, P. & VAN DEVENTER, J. S. 2010. The role of particle technology in developing sustainable construction materials. *Advanced Powder Technology,* 21**,** 2-7.

PROVIS, J. L., MYERS, R. J., WHITE, C. E., ROSE, V. & S.J. VAN DEVENTER, J. 2012. X-ray microtomography shows pore structure and tortuosity in alkali-activated binders. *Cement and Concrete Research,* 42**,** 855-864.

PUERTAS, F., TORRES-CARRASCO, M. & ALONSO, M. 2015. Reuse of urban and industrial waste glass as a novel activator for alkali-activated slag cement pastes: a case study. *Handbook of alkali-activated cements, mortars and concretes.* Elsevier.

QIAN, W., RAO, F., SONG, S. & LEÓN-PATIÑO, C. A. 2017. Geothermal clay-based geopolymer binders: Synthesis and microstructural characterization. *Applied Clay Science,* 146**,** 223-229.

RAHMAT, M. N., NORSALISMA, I. & KINUTHIA, J. M. 2016. Strength and environmental evaluation of stabilised Clay-PFA eco-friendly bricks. *Construction and Building Materials,* 125**,** 964-973.

RAKHIMOVA, N. R. & RAKHIMOV, R. Z. 2015. Alkali-activated cements and mortars based on blast furnace slag and red clay brick waste. *Materials & Design,* 85**,** 324-331.

RAMESH, T., PRAKASH, R. & SHUKLA, K. 2012. Life cycle energy analysis of a residential building with different envelopes and climates in Indian context. *Applied Energy,* 89**,** 193-202.

REEVES, G. M., SIMS, I. & CRIPPS, J. C. 2006. *Clay Materials Used in Construction,* London Geological Society Special Publications, 21.

REIG, L., TASHIMA, M. M., BORRACHERO, M. V., MONZÓ, J., CHEESEMAN, C. R. & PAYÁ, J. 2013. Properties and microstructure of alkali-activated red clay brick waste. *Construction and Building Materials,* 43**,** 98-106.

ROBAYO-SALAZAR, R. A., MEJÍA-ARCILA, J. M. & MEJÍA DE GUTIÉRREZ, R. 2017a. Eco-efficient alkali-activated cement based on red clay brick wastes suitable for the manufacturing of building materials. *Journal of Cleaner Production,* 166**,** 242-252.

ROBAYO-SALAZAR, R. A., RIVERA, J. F. & MEJÍA DE GUTIÉRREZ, R. 2017b. Alkali-activated building materials made with recycled construction and demolition wastes. *Construction and Building Materials,* 149**,** 130-138.

ROBAYO, R. A., MULFORD, A., MUNERA, J. & MEJÍA DE GUTIÉRREZ, R. 2016. Alternative cements based on alkali-activated red clay brick waste. *Construction and Building Materials,* 128**,** 163-169.

ROSSEN, J. & SCRIVENER, K. 2017. Optimization of SEM-EDS to determine the C–A–S–H composition in matured cement paste samples. *Materials Characterization,* 123**,** 294-306.

ROWLES, M. & O'CONNOR, B. 2003. Chemical optimisation of the compressive strength of aluminosilicate geopolymers synthesised by sodium silicate activation of metakaolinite. *Journal of materials chemistry,* 13**,** 1161-1165.

ROWLESA, M. & O'CONNOR, B. 2003. Chemical optimisation of the compressive strength of aluminosilicate geopolymers synthesised by sodium silicate activation of metakaolinite *Journal of Materials Chemistry,* 13**,** 1161-1165.

SADIQUE, M., AL-NAGEIM, H., ATHERTON, W., SETON, L. & DEMPSTER, N. 2013. Mechano-chemical activation of high-Ca fly ash by cement free blending and gypsum aided grinding. *Construction and Building Materials,* 43**,** 480-489.

SAIDI, M., CHERIF, A. S., ZEGHMATI, B. & SEDIKI, E. 2018. Stabilization effects on the thermal conductivity and sorption behavior of earth bricks. *Construction and Building Materials,* 167**,** 566-577.

SASUI, S., KIM, G., NAM, J., KOYAMA, T. & CHANSOMSAK, S. 2020. Strength and Microstructure of Class-C Fly Ash and GGBS Blend Geopolymer Activated in NaOH & NaOH+ Na2SiO3. *Materials,* 13**,** 59.

SAVJANI, P. 2020. *RE: Price of GGBS.* Type to SHUBBAR, A.

SCRIVENER, K., BAZZONI, A., MOTA, B. & ROSSEN, J. E. 2016. *A Practical Guide to Microstructural Analysis of Cementitious Materials,* Boca Raton, Florida, United States. , CRC Press.

SECO, A., URMENETA, P., PRIETO, E., MARCELINO, S., GARCÍA, B. & MIQUELEIZ, L. 2017. Estimated and real durability of unfired clay bricks: Determining factors and representativeness of the laboratory tests. *Construction and Building Materials,* 131**,** 600-605.

SEKHAR, D. C. & NAYAK, S. 2018. Utilization of granulated blast furnace slag and cement in the manufacture of compressed stabilized earth blocks. *Construction and Building Materials,* 166**,** 531-536.

SIDDIQUA, S. & BARRETO, P. N. M. 2018. Chemical stabilization of rammed earth using calcium carbide residue and fly ash. *Construction and Building Materials,* 169**,** 364-371.

SILVA, R. A., SOARES, E., OLIVEIRA, D. V., MIRANDA, T., CRISTELO, N. M. & LEITÃO, D. 2015. Mechanical characterisation of dry-stack masonry made of CEBs stabilised with alkaline activation. *Construction and Building Materials,* 75**,** 349-358.

SINGH, B., ISHWARYA, G., GUPTA, M. & BHATTACHARYYA, S. K. 2015. Geopolymer concrete: A review of some recent developments. *Construction and Building Materials,* 85**,** 78-90.

SITTON, J. D., ZEINALI, Y., HEIDARIAN, W. H. & STORY, B. A. 2018. Effect of mix design on compressed earth block strength. *Construction and Building Materials,* 158**,** 124-131.

SIVRIKAYA, O., KıYıLDı, K. R. & KARACA, Z. 2013. Recycling waste from natural stone processing plants to stabilise clayey soil. *Environmental Earth Sciences,* 71**,** 4397-4407.

SKINDER, B. M., SHEIKH, A. Q., PANDIT, A. K. & GANAI, B. A. 2014. Brick kiln emissions and its environmental impact: A. *Journal of Ecology and the Natural Environment,* 6**,** 1-11.

SLATY, F., KHOURY, H., RAHIER, H. & WASTIELS, J. 2015. Durability of alkali activated cement produced from kaolinitic clay. *Applied Clay Science,* 104**,** 229-237.

SLATY, F., KHOURY, H., WASTIELS, J. & RAHIER, H. 2013. Characterization of alkali activated kaolinitic clay. *Applied Clay Science,* 75-76**,** 120-125.

SMITH, A. S., BINGEL, P. & BOWN, A. 2016. Sustainability of masonry in construction. *Sustainability of Construction Materials.*

SORE, O. S., MESSAN, A., PRUD'HOMME, E., ESCADEILLAS, G. & TSOBNANG, F. 2018. Stabilization of compressed earth blocks (CEBs) by geopolymer binder based on local materials from Burkina Faso. *Construction and Building Materials,* 165**,** 333-345.

STATISTA. 2019. *Annual production of bricks in Great Britain (GB) from 2013 to 2018* [Online]. United Kingdom (Great Britain); Department for Business, Innovation and Skills Available: https://www.statista.com/statistics/472894/annual-brick-production-great-britain/ [Accessed 01/09/2019 2019].

SUKMAK, P., HORPIBULSUK, S., SHEN, S.-L., CHINDAPRASIRT, P. & SUKSIRIPATTANAPONG, C. 2013. Factors influencing strength development in clay–fly ash geopolymer. *Construction and Building Materials,* 47**,** 1125-1136.

SUNIL KUMAR, C. P., PARVATHI, S. & RUDRAMOORTHY, R. 2016. Impact Categories through Life Cycle Assessment of Coal-fired Brick. *Procedia Technology,* 24**,** 531-537.

TAALLAH, B. & GUETTALA, A. 2016. The mechanical and physical properties of compressed earth block stabilized with lime and filled with untreated and alkali-treated date palm fibers. *Construction and Building Materials,* 104**,** 52-62.

TENNAKOON, C., SAGOE-CRENTSIL, K., SAN NICOLAS, R. & SANJAYAN, J. G. 2015. Characteristics of Australian brown coal fly ash blended geopolymers. *Construction and Building Materials,* 101**,** 396-409.

TRAVIS PERKINS. 2019. *Wienerberger Terca Class B Engineering Brick Red 215mm x 102.5mm x 65mm (Pack of 504)* [Online]. Travis Perkins. Available: https://www.travisperkins.co.uk/engineering-bricks/wienerberger-terca-class-b-engineering-brick-red-215mm-x-102-5mm-x-65mm-pack-of-504/p/870923 [Accessed 04 October 2020].

TURNER, L. K. & COLLINS, F. G. 2013. Carbon dioxide equivalent (CO2-e) emissions: A comparison between geopolymer and OPC cement concrete. *Construction and Building Materials,* 43**,** 125-130.

TURTLE, L., PEARSON, B., RICHARDSON, J., TSAGATAKIS, I. & RUDDY, M. 2019. Local and Regional Carbon Dioxide Emissions Estimates for 2005–2017 for the UK.

UNITED UTILITIES. 2020. *Metered business customers* [Online]. United Utilities. Available: https://www.unitedutilities.com/Business-services/business-charges-2017-2018/metered-business-customers/ [Accessed 11 October 2020].

VAN DEVENTER, J. S., PROVIS, J. L., DUXSON, P. & LUKEY, G. C. 2007. Reaction mechanisms in the geopolymeric conversion of inorganic waste to useful products. *J Hazard Mater,* 139**,** 506-13.

VAN RIESSEN, A., JAMIESON, E., KEALLEY, C. S., HART, R. D. & WILLIAMS, R. P. 2013. Bayer-geopolymers: An exploration of synergy between the alumina and geopolymer industries. *Cement and Concrete Composites,* 41**,** 29-33.

WANG, H., LI, H. & YAN, F. 2005. Synthesis and mechanical properties of metakaolinite-based geopolymer. *Colloids and Surfaces A: Physicochemical and Engineering Aspects,* 268**,** 1-6.

WATTIMENA, O. K., ANTONI & HARDJITO, D. A review on the effect of fly ash characteristics and their variations on the synthesis of fly ash based geopolymer. AIP Conference Proceedings, 2017. AIP Publishing LLC, 020041.

XU, H., ANNIE, S. J. & DEVENTER, V. 2002. Geopolymerisation of multiple minerals. *Minerals Engineering* 15**,** 1131-1139.

XU, H. & VAN DEVENTER, J. S. J. 2002. Geopolymerisation of multiple minerals. *Minerals Engineering* 15**,** 1131-1139.

YIP, C. K. & VAN DEVENTER, J. S. J. 2003. Microanalysis of calcium silicate hydrate gel formed within a geopolymeric binder. *Journal of Materials Science,* 38**,** 3851– 3860.

YUN-MING, L., HEAH, C.-Y., MOHD MUSTAFA, A. B. & KAMARUDIN, H. 2016. Structure and properties of clay-based geopolymer cements: A review. *Progress in Materials Science,* 83**,** 595-629.

YUNSHENG, Z., WEI, S., QIANLI, C. & LIN, C. 2007. Synthesis and heavy metal immobilization behaviors of slag based geopolymer. *J Hazard Mater,* 143**,** 206-13.

ZHANG, L. 2013. Production of bricks from waste materials – A review. *Construction and Building Materials,* 47**,** 643-655.

ZHANG, L., AHMARI, S. & ZHANG, J. 2011. Synthesis and characterization of fly ash modified mine tailings-based geopolymers. *Construction and Building Materials,* 25**,** 3773-3781.

ZHANG, L., GUSTAVSEN, A., JELLE, B. P., YANG, L., GAO, T. & WANG, Y. 2017. Thermal conductivity of cement stabilized earth blocks. *Construction and Building Materials,* 151**,** 504-511.

ZHANG, Y. S., SUN, W. & LI, Z. J. 2005. Hydration process of potassium polysialate (K-PSDS) geopolymer cement. *Advances in Cement Research,* 17**,** 23-28.

ZHANG, Z., WONG, Y. C., ARULRAJAH, A. & HORPIBULSUK, S. 2018. A review of studies on bricks using alternative materials and approaches. *Construction and Building Materials,* 188**,** 1101-1118.

ZUHUA, Z., XIAO, Y., HUAJUN, Z. & YUE, C. 2009. Role of water in the synthesis of calcined kaolin-based geopolymer. *Applied Clay Science,* 43**,** 218-223.

# APPENDIX A: PATENT APPLICATION

Intellectual Property Office

Concept House
Cardiff Road, Newport
South Wales
NP10 8QQ
United Kingdom

Telephone +44 (0)1633 814000

Website https://www.gov.uk/ipo

**Electronic Filing Receipt**

Appleyard Lees IP LLP
15 Clare Road
Halifax
Yorkshire
United Kingdom
HX1 2HY

Your Ref. P36715GB1/KLH

11 March 2020

PATENT APPLICATION NUMBER 2003555.6

We have received your request for grant of a patent and recorded its details as follows:

| | | |
|---|---|---|
| Filing date(*) | 11 March 2020 | |
| Earliest priority date (if any) | | |
| Applicant(s) / contact point | Liverpool John Moores University | |
| Application fee paid | Yes | |
| Description (number of pages or reference) | 24 | |
| Certified copy of referenced application | Not applicable | |
| If description not filed | Not applicable | |
| Claims (number of pages) | 2 | |
| Drawings (number of pages) | 8 | |
| Abstract (number of pages) | 1 | |
| Statement of inventorship (Form 7) | No, file by 12 July 2021 | |
| Request for search (Form 9A) | Yes | |
| Request for examination (Form 10) | None | |
| Priority Documents | None | |
| Other Attachments Received | Pre-conversion archive | P36715GB1 - Pre-conversion Archive - Spec and Figs.zip |
| | PDAS Registration Form | PDASRegistration.pdf |